APSD-011-83

APPLICATION OF DIRECT MEASUREMENTS OF OPTICAL PARAMETERS TO THE ESTIMATION OF LAKE WATER QUALITY INDICATORS

by

R.P. Bukata, J.E. Bruton and J.H. Jerome

Environmental Spectro-Optics Section

Aquatic Physics and Systems Division

National Water Research Institute

Canada Centre for Inland Waters

Burlington, Ontario L7R 4A6

NWRI UM NS No. 84-28

Executive Summary

The colour of water has often been considered as an indicator of water quality. This hypothesis is often further quantified through use of a Secchi Disc estimate of water transparency and has formed the basis for remote airborne or satellite measurements that have been proposed to represent a measure of water quality.

This report examines the basic properties of scattering and absorption of water in terms of three indicators often used as a measure of water quality: concentrations of chlorophyll a, suspended minerals, and dissolved organic carbon and relates these properties to measurable subsurface irradiance reflectance (volume reflectance). The wavelength dependency of each of the water quality indicators is examined and the interactive influence on the total volume reflectance calculated.

The theoretical considerations indicate that no single wavelength or simple multiple of wavelengths can be used with significant sensitivity to relate the water quality indicators to volume reflectance. If a comprehensive analysis of the entire visible spectrum is considered, the suspended minerals and dissolved organic carbon concentrations may be specified to within a factor of two. In inland lake waters, the specification of chlorophyll a concentrations may be extremely hazardous, and in the presence of significant concentrations of suspended minerals and/or dissolved organic carbon, chlorophyll a cannot be accurately quantified.

Empirical comparisons of measurements of chlorophyll a, suspended minerals and dissolved organic carbon coincident with measurements of volume reflectance in Lake Ontario were used to validate the theoretical model. In general, reasonable agreements were obtained with the exception of chlorophyll a where the measured concentrations were generally less than those calculated from the model. Empirical adjustments were able to improve the agreement but

indicate that relationships may be non-constant. This problem may relate, at least in part, to the standard methods of measuring chlorophyll a and to the relationship of chlorophyll a to phytoplankton biomass.

The report provides a thorough examination of the basis and potential of optical measurements to the general area of water quality using the primary property of volume reflectance. This must relate to any airborne or satellite observations.

Résumé à l'intention de la Direction

Bien souvent, la couleur de l'eau est considérée comme un indice de qualité. La couleur, qui est souvent chiffrée par mesure de la transparence à l'aide du disque de Secchi, constitue la base des mesures faites par avion et par satellite, qui ont été proposées pour évaluer la qualité de l'eau.

Ce rapport examine les propriétés fondamentales de dispersion et d'absorption de l'eau, en termes de trois indices qui servent souvent à évaluer la qualité, soit la concentration de la chlorophylle a, la teneur en substances minérales en suspension et la teneur en carbone organique dissous, et les relie à la réflexion de l'éclairement énergétique sous la surface (réflexion volumique).

Selon la théorie, aucune longueur d'onde ou bande de longueurs d'onde est, à elle seule, suffisamment sensible pour évaluer la qualité de l'eau à partir de la réflexion volumique. Si on envisage l'analyse globale de tout le spectre visible, il peut être possible de déterminer à un ou deux facteurs près la concentration des substances minérales en suspension et la concentration du carbone organique dissous. Dans les eaux lacustres, la détermination de la concentration de la chlorophylle a peut être extrêmement difficile et, en présence de concentrations élevées de substances minérales en suspension et/ou de carbone organique dissous, il n'est pas possible de mesurer avec précision la concentration de la chlorophylle a.

On a utilisé des comparaisons empiriques de la concentration de la chlorophylle a, de la concentration de substances minérales en suspension et de la concentration du carbone organique dissous mesurées en même temps que la réflexion volumique dans le lac Ontario en vue de valider le modèle théorique. En général, les résultats concordaient bien, à l'exception de la concentration de la chlorophylle a qui était généralement inférieure à celles calculées à partir du modèle. Des ajustements empiriques ont permis d'améliorer la concordance, mais ont indiqué que les relations ne sont peut-être pas constantes. Ce problème découle, du moins en partie, des méthodes utilisées pour déterminer la concentration de la chlorophylle a et de la relation entre la chlorophylle a et la biomasse phytoplanctonique.

Le rapport examine en profondeur la théorie à la base des mesures optiques et le potentiel de ces méthodes dans le domaine général de l'évaluation de la qualité de l'eau par mesure de la propriété primaire de la réflexion volumique. Ces mesures doivent être reliées à toutes observations faites par avion ou par satellite.

ABSTRACT

This report deals with an evaluation of the utilization of direct measurements of optical parameters as a means of estimating the water quality indicators (concentrations of chlorophyll *a*, suspended mineral, and dissolved organic carbon) that define natural lake waters. The analyses and discussions presented are based on the results of a coordinated optical/water quality study of a complex inland lake (Lake Ontario), and consequently represent a possible "worst-case" approach to the problem since a body of water such as Lake Ontario will understandably present a very severe test of such optical modelling.

The report is not intended as a short course in lake optics although the necessary mathematical theory is briefly presented, as is a Glossary of technical terminology utilized in the text. The key linkages between measured optical properties and water quality indicators are the specific absorption and scattering properties (cross-sections) of the various aquatic components as a function of observed wavelengths. Considerable discussion is presented concerning not only the techniques utilized to estimate such optical cross-sections, but also the departures from constancy of such cross-sections for Lake Ontario waters (and waters on a more global scale) and the restrictions that such departures from constancy impose upon water quality prediction.

In its most simplistic form the method of utilizing optical parameters to estimate water quality considered in this report may be stated as follows: a direct measurement of the subsurface irradiance reflectance (volume reflectance) spectrum is obtained in the 400-700 nm (visible) range. Values of the wavelength dependencies of the optical cross-sections of chlorophyll, suspended mineral and dissolved organic carbon are then utilized in conjunction with appropriate optimization methodology to estimate those concentrations of chlorophyll, suspended mineral, and dissolved organic carbon that will generate a subsurface irradiance reflectance spectrum that most closely simulates the directly measured spectrum.

To illustrate the impact on the observed subsurface irradiance reflectance spectrum of varying the concentrations of the three principal organic and inorganic components, the report includes numerous examples of calculated optical spectra for water masses of distinctly dissimilar water quality.

The utilization of a volume reflectance measurement at a single wavelength is all but eliminated by this report as a means of estimating water quality indicators for multi-component waters. The utilization of the entire volume reflectance spectrum as a means of estimating water quality indicators, however, appears to be considerably more promising. Despite the severe limitations on predictive capabilities resulting from the non-constancies of the optical

cross-sections, this work has realized acceptable success in estimating suspended mineral and dissolved organic carbon concentrations in Lake Ontario. This appears to auger well for the utilization of such predictive methodology in less optically complex inland waters. Reliable predictive capabilities for chlorophyll concentrations continue to be much more elusive.

The model development and application presented here can, by no means, be regarded as definitive, representing as it does, the current level of understanding and state-of-the-art of such aquatic studies. However, comparable work is continuing at numerous optically-oriented research institutions on a worldwide basis.

RESUME

Le présent rapport concerne une évaluation de l'utilisation de mesures directes des paramètres optiques pour l'estimation des indicateurs de la qualité de l'eau (concentrations de chlorophylle a, minéraux en suspension et carbone organique dissous) qui définissent les eaux de lacs naturels. Les analyses et discussions présentées sont basées sur les résultats d'une étude de la qualité des eaux d'un lac intérieur complexe (le lac Ontario) faisant appel à des méthodes optiques et, par conséquent, constituent peut-être un cas extrême, puisqu'une masse d'eau comme le lac Ontario mé sérieusement à l'épreuve, on le comprendra, un modèle optique de ce genre.

Le rapport n'est pas censé être un cours intensif d'optique des lacs, bien que l'appareil mathématique connexe fasse l'objet d'une courte description et qu'un glossaire des termes techniques utilisés dans le texte soit fourni. Les relations-clés entre les caractéristiques optiques mesurées et les indicateurs de la qualité de l'eau sont l'absorption et la dispersion spécifiques ("profils") des diverses composantes de l'eau en fonction des longueurs d'onde observées. L'auteur aborde en détail non seulement les méthodes utilisées pour l'estimation de ces "profils" optiques, mais aussi la non-uniformité de ces profils pour les eaux du lac Ontario (et à une échelle plus vaste) et les limites que cette non-uniformité impose aux prédictions relatives à la qualité des eaux.

Dans sa forme la plus simpliste, la méthode de l'utilisation de paramètres optiques pour l'estimation de la qualité des eaux, présentée dans ce rapport, peut être décrite de la manière suivante : une mesure directe du spectre du facteur de réflexion de l'éclairement énergétique sous la surface (facteur de réflexion volumique) est faite dans la gamme de 400 à 700 mm (lumière visible). Les longueurs d'ondes privilégiées dans les profils optiques de la chlorophylle, des minéraux en suspension et du carbone organique dissous sont ensuite utilisées, dans le cadre de méthodes d'optimisation appropriées, pour déterminer les concentrations de chlorophylle, de minéraux en suspension et de carbone organique dissous qui produiront un spectre du facteur de réflexion de l'éclairement énergétique sous la surface, qui ressemble le plus possible au spectre mesuré directement.

Pour montrer l'impact, sur le spectre observé du facteur de réflexion de l'éclairement énergétique sous la surface, de la variation des concentrations des trois principaux éléments organiques et inorganiques, le rapport contient nombre d'exemples de spectres optiques calculés pour des masses d'eau de qualités très diverses.

L'utilisation de la mesure d'un facteur de réflexion volumique à une seule longueur d'onde pour l'estimation des indicateurs de la qualité des eaux à plusieurs composantes, est pratiquement rejeté par l'auteur du rapport. Toutefois, l'utilisation du spectre entier du facteur de réflexion volumique pour l'estimation des indicateurs de la qualité des eaux semble beaucoup plus prometteuse. Malgré les restrictions importantes imposées aux possibilités prévisionnelles par la non-uniformité des

profils optiques, ces travaux ont obtenu un succès acceptable dans l'estimation des concentrations de minéraux en suspension et de carbone organique dissous dans le lac Ontario. Cela est de bonne augure pour l'application future de telles méthodes de prédiction à des eaux intérieures moins complexes du point de vue optique. Les possibilités de prédiction exacte des concentrations de chlorophylle continuent d'être insaisissables.

La modélisation décrite ici ne peut certes pas être considérée comme définitive; elle ne constitue que le niveau actuel de la compréhension des problèmes et représente la pointe des études aquatiques de ce genre. Cependant des travaux comparables se poursuivent dans de nombreux établissements de recherches optiques dans le monde.

INTRODUCTORY THEORY

The combined processes of scattering and absorption control the manner in which impinging radiation propagates through a natural water mass. The nature and magnitude of the scattering and absorption processes depend, in turn, upon the nature and concentrations of the suspended and dissolved organic and inorganic materials distributed within the water column, as well as the nature and radiance distribution of the impinging radiation. Since water masses display both spatial and temporal variations in their organic and inorganic compositions, it logically follows that they will be characterized by related variabilities in their observed interactions with the impinging radiation field. Consequently, studies of the optical properties of water masses must contend with two broad categories of optical properties. The <u>inherent</u> optical properties of a water mass are those properties which are totally independent of the spatial distribution of the impinging radiation, while the so-called <u>apparent</u> optical properties of a water mass are those properties which are dependent upon the spatial distribution of impinging radiation.

Apparent optical properties of a water mass include:

Irradiance reflectance (volume reflectance) R, and

Irradiance attenuation coefficient K

Inherent optical properties of a water mass include:

total attenuation coefficient c

absorption coefficient a

scattering albedo ω_o

scattering coefficient b

forwardscattering probability F

backscattering probability B

volume scattering function $\beta(\Theta)$

Appendix I contains a glossary providing a technical definition of the terms used in this report.

Since the electromagnetic frequency spectrum comprises many orders of magnitude, and since water quality is a highly subjective term encompassing a myriad of species and subspecies of organic and inorganic materials, a comprehensive document relating optical behaviour to water quality is beyond the scope of current capabilities. Consequently, this work will consider as its terms of reference an electromagnetic spectrum restricted to the visible wavelengths (400 to 700 nm) and the quality of a water mass to be defined in terms of its chlorophyll a, suspended mineral, and dissolved organic carbon concentrations.

The inherent optical properties b and B are mathematically defined in terms of appropriate integrations of the volume scattering function $\beta(\Theta)$. Consequently, direct measurements of the inherent optical properties of natural waters require sophisticated instrumentation capable of determining the entire volume scattering function $\beta(\Theta)$ in order to separate the scattering coefficient b and the absorption coefficient a from the total attenuation coefficient c ($c = a+b$). It is considerably easier, however, to perform *in situ* measurements of the apparent optical properties of the water column. The total attenuation coefficient c is readily obtained from transmissometry, and the apparent optical properties R and K are readily determined from upwelling and downwelling spectrometric measurements. Consequently a widely-used approach to the general area of ocean and lake optics has been to determine the general relationships between the inherent and apparent optical properties though the development of models based upon suitable simulations of the radiative transfer equations. Two such models have been proposed by Gordon *et al.* (1975) using a Monte Carlo simulation and Di Toro (1978) using a combination of an exponential and a quasi-single scattering approximation. Although both radiative transfer simulations have been utilized at the National Water Research Institute, the remainder of this report will consider only the Gordon *et al.* (1975) simulation.

From Gordon et al. (1975), curve fitting to the Monte Carlo calculations results in the equations

$$\omega_o F = \sum_{n=0}^{N} k'_n(\tau) \left[\frac{K(\tau)}{c(\tau)D_d(\tau)}\right]^n \qquad (1)$$

and

$$\frac{\omega_o B}{1-\omega_o F} = \sum_{n=0}^{N} r'_n(\tau) \left[R(\tau)\right]^n \qquad (2)$$

where $\omega_o = \frac{b}{c} \equiv$ scattering albedo

$F \equiv$ forwardscattering probability

$B \equiv$ backscattering probability = 1-F

$K(\tau) \equiv$ irradiance attenuation coefficient at depth τ for downwelling irradiance

$R(\tau) \equiv$ irradiance reflectance (volume reflectance) at depth τ for downwelling irradiance

$D_d(\tau) \equiv$ distribution function at depth τ for downwelling irradiance

$c(\tau) \equiv$ total attenuation coefficient at depth τ

$k'_n(\tau)$ and $r'_n(\tau)$ are the sets of appropriate coefficients for the expansions of equations (1) and (2)

Gordon et al. (1975) have determined two sets of values for the coefficients $r'_n(\tau)$, one set appropriate for conditions of solar incidence angles $\lesssim 20°$, and one set appropriate for solar incidence angles $\gtrsim 30°$ as measured in the water column. The set of coefficients $k'_n(\tau)$ is independent of sun angle.

Equations (1) and (2) then enable the apparent optical properties $K(\tau)$, $R(\tau)$ and the inherent optical property $c(\tau)$ (determined from in situ lake measurements) to be utilized in the determination of the inherent optical properties, ω_b, a, b, F, and B. The implicit wavelength dependence of equations (1) and (2) has been omitted for simplicity.

The inherent optical properties are themselves interrelated ($c = a+b$) and display additive properties which are dependent upon the presence of scattering and absorption centres within the water column.

$$
\begin{aligned}
a(\lambda) &= \sum_{i=1}^{n} x_i a_i(\lambda) \\
b(\lambda) &= \sum_{i=1}^{n} x_i b_i(\lambda) \\
(Bb)(\lambda) &= \sum_{i=1}^{n} x_i (Bb)_i(\lambda)
\end{aligned}
\qquad (3)
$$

where $(Bb)(\lambda)$ ≡ backscatter coefficient at wavelength λ, the product of B and b

x_i ≡ concentration of the ith component of the water mass in question

$a_i(\lambda)$ ≡ absorption at wavelength λ for a unit concentration of component i

$b_i(\lambda)$ ≡ scattering at wavelength λ for a unit concentration of component i

$(Bb)_i(\lambda)$ ≡ backscattering at wavelength λ for a unit concentration of component i

Since $a_i(\lambda)$, $b_i(\lambda)$ and $(Bb)_i(\lambda)$ represent the optical behaviour (in terms of absorption and scattering) of the water column per unit concentration of component matter, they will be referred to as the optical cross-sections of the water mass in subsequent discussions. The determination of these optical cross-sections clearly provides the linkages between the inherent optical properties of a water mass and its water quality parameters. Obviously, the definitive optical model should consider the cross-sections of every species and sub-species of aquatic components present in natural water masses, as well as possible temporal, shape, and size dependencies of each. Such a model is clearly unattainable. The present work considers that at any instant of time a natural water mass may be taken to be defined by a homogeneous combination of pure water, unique suspended organic material (taken to be represented by the chlorophyll a concentration

corrected for phaeophytin contamination), unique suspended inorganic material (taken to be represented by the suspended mineral concentration SM), dissolved organic material (represented by dissolved organic carbon DOC) and a non-living organic component NLO, determined in the following manner:

$$\frac{NLO}{78} = \frac{SO}{78} - \frac{Chl_{cor}}{Chl_{unc}} \cdot \frac{POC}{24} \qquad (4)$$

where SO = measured value of total suspended organic material concentration

Chl_{unc} = measured value of chlorophyll *a* uncorrected for phaeophytin contamination

Chl_{cor} = measured value of chlorophyll *a* corrected for phaeophytin contamination

POC = measured value of particulate organic carbon concentration

The units in equation (4) have been normalized on the assumption (Burns, 1980) that the average organic component may be represented by the molecular formula $C_2H_6O_3$ (and, therefore, by a molecular weight of 78 a.u.). Equation (4), however, does not take into account the contribution from the living zooplankton population.

For such a five component optical model (SM, Chl *a*, DOC, NLO, plus pure water), equation set (3) may be written

$$a(\lambda) = a_w(\lambda) + x\, a_{Chl}(\lambda) + y\, a_{SM}(\lambda) + z\, a_{DOC}(\lambda) + u\, a_{NLO}(\lambda)$$

$$b(\lambda) = b_w(\lambda) + x\, b_{Chl}(\lambda) + y\, b_{SM}(\lambda) + u\, b_{NLO}(\lambda) \qquad (5)$$

$$(Bb)(\lambda) = (Bb)_w(\lambda) + x(Bb)_{Chl}(\lambda) + y(Bb)_{SM}(\lambda) + u(Bb)_{NLO}(\lambda)$$

where the subscripts w, Chl, SM, DOC, and NLO refer to the pure water, unique organic, unique inorganic, dissolved organic, and unique non-living organic components of the water column, respectively; x, y, z, and u are the concentrations of chlorophyll *a* (corrected for phaeophytin contamination), suspended mineral, dissolved organic carbon, and non-living organic material, respectively; and the components of a (a_{Chl}, a_{SM}, a_{DOC}, a_{NLO}), b(b_{Chl}, b_{SM}, b_{NLO}), and Bb[$(Bb)_{Chl}$, $(Bb)_{SM}$, $(Bb)_{NLO}$] are the optical cross-sections.

To obtain values for the cross-sections, a coordinated spectro-optical program was conducted in western Lake Ontario (the entire program was a joint venture between NWRI, CCRS and MONITEQ Ltd., and included an airborne remote sensing and atmospheric study component in addition to the *in situ*/theoretical optical program

discussed in this report). Logistical details of the multi-stage Lake Ontario experiment are presented elsewhere [Jain et al. (1980); Zwick et al. (1980); Bukata et al. (1981a, 1981b)]. Suffice to say that coordinated collections of water samples (which were laboratory analysed for water quality parameters) occurred in conjunction with in situ determinations of transmission profiles (using a modified Martek multiband XMS transmissometer), and spectral irradiance profiles and spectral volume reflectance (using a Techtum QSM 2500 scanning Quanta spectrometer) in the upper 10 m of water. Details of the numerical determinations of the optical cross-sections are given in Bukata et al (1981a). However, the flow diagram of Figure 1 outlines the basic steps taken. The in situ transmissometer and spectrometer data were used to determine the inherent optical property $c(\lambda, \tau)$ and the apparent optical properties $K(\lambda, \tau)$ and $R(\lambda, \tau)$. The Gordon et al. (1975) model (equations (1) and (2)) was utilized [see Bukata et al. (1979)] to determine the inherent optical properties a, b, ω_b, F, and B. Multiple regression techniques applied to the determined values of a, b, and (Bb) and the measured values of water quality parameters (equation set (5)) yielded the desired optical cross-sections for the five-component model.

It was discovered, however, at least for Lake Ontario, that only a slight loss in generality occurred when a 4-component optical model which neglected the contribution of NLO was considered. This was due, in part, to the fact that the NLO component was rarely a

dominant factor in the optical behaviour of Lake Ontario [the numerical value of NLO concentration (in gm^{-3}) rarely exceeded 10% of the numerical value of chlorophyll a concentration (in mgm^{-3})]. However, the use of a 4-component model necessitated the use of Chl a_{unc} (i.e. chlorophyll a concentration uncorrected for phaeophytin contamination). Consequently, the remainder of this report will deal with a four-component optical model (pure water, chlorophyll a with phaeophytin, suspended mineral and dissolved organic carbon). In such a model, equation set (5) becomes:

$$\begin{aligned} a(\lambda) &= a_w(\lambda) + xa_{Chl}(\lambda) + ya_{SM}(\lambda) + za_{DOC}(\lambda) \\ b(\lambda) &= b_w(\lambda) + xb_{Chl}(\lambda) + yb_{SM}(\lambda) \\ (Bb)(\lambda) &= (Bb)_w(\lambda) + x(Bb)_{Chl}(\lambda) + y(Bb)_{SM}(\lambda) \end{aligned} \qquad (6)$$

where it is noted that the subscript Chl now refers to Chl a_{unc} and x refers to the concentration of Chl a_{unc}.

OPTICAL CROSS-SECTIONS FOR LAKE ONTARIO

The cross-sections for the four-component optical model (pure water, SM, Chl a_{unc}, DOC) are illustrated in Figures 2 and 3 as a function of visible wavelength. Figure 2 illustrates the $a_i(\lambda)$ values and Figure 3 illustrates the $b_i(\lambda)$ values for Lake Ontario waters. The values of $a_w(\lambda)$ and $b_w(\lambda)$ were taken from the work of Hulburt (1945). Once these optical cross-sections are known, a volume

reflectance spectrum $R_v(\lambda)$ may be generated for water masses comprised of varying amounts of chlorophyll a (uncorrected for phaeophytin contamination), suspended mineral, and dissolved organic carbon, utilizing the Gordon et al. (1975) Monte Carlo simulation model. In principle, therefore, in situ measured volume reflectance spectra could be compared to a catalog of existing volume reflectance spectra for water masses comprised of known component concentrations. Such an inter-comparison, however, is subject to the following stipulations:

a) The natural waters under consideration must be appropriately defined by a four-component optical model. Clearly, the more optically complex a water mass becomes (i.e. the greater the number of components which significantly alter its optical behaviour), the less reliable will be the use of the current model in providing lake water quality indicators.

b) The optical cross-sections must be known. Further, they must be confidently assumed to be relatively invariant, or at least insignificantly varying during the measurement time interval. Such conditions are satisfied at some locations and time periods, and not at others. For example, the optical cross-sections determined in western Lake Ontario have been shown to possess, to a large degree, a lake-wide applicability (Bukata et al. (1981c)) throughout most of the field season. However, as yet unpublished work appears to indicate

that Lake Ontario waters may require an independent set of optical cross-sections during the autumn months (due possibly to a change in the indigenous chlorophyll-bearing biota).

c) The water mass is considered to be homogeneous. The current model does not include possible layering effects.

d) No provision is incorporated for chemical impurities. Small concentrations of such chemicals (by comparison to the concentrations of Chl, SM, and DOC) produce negligible absorption and scattering effects and their detection is beyond current in situ optical techniques.

SUBSURFACE IRRADIANCE REFLECTANCE SPECTRA

From Gordon et al. (1975), the irradiance reflectance (also referred to as the volume reflectance) $R(0,\lambda)$ just beneath the free-surface layer is given by

$$R(0,\lambda) = \sum_{n=0}^{N} r_n(0) \left[\frac{Bb(\lambda)}{a(\lambda) + Bb(\lambda)}\right]^n \qquad (7)$$

where all terms are as previously defined. $r_n(0)$ are the expansion coefficients, taken in this work as those appropriate for solar incidence angles $\lesssim 20°$ as measured within the water column. Further, n is

taken as 3. Using the additive properties of $a(\lambda)$ and $Bb(\lambda)$ displayed in equation set (6) for the four-component water mass representation, and using the optical cross-sections illustrated in Figures 2 and 3, it is clear that point-by-point subsurface irradiance reflectance spectra may be generated for selected values of x, y, and z, i.e. for a variety of water masses displaying varying concentrations of chlorophyll a (uncorrected for phaeophytin contamination), suspended minerals, and dissolved organic carbon.

Figure 4 illustrates a family of subsurface irradiance reflectance spectra (at 20 nm increments from 410 to 690 nm) calculated in this manner for varying chlorophyll a concentrations in a water mass for which the suspended mineral and dissolved organic carbon concentrations are kept fixed at zero (i.e. for a 2-component model of the water mass, viz. chlorophyll and pure water). Clearly, water masses with small concentrations of chlorophyll a display a pronounced volume reflectance in the blue region of the spectrum and minimal volume reflectance in the red. Increasing the chlorophyll concentration in such a water mass (i.e. a water mass comprised solely of pure water and chlorophyll) tends to decrease the volume reflectance at the blue wavelengths while increasing the volume reflectance at the red wavelengths at a more rapid rate. For chlorophyll concentrations $> \sim 1$ to 2 mgm^{-3} the irradiance reflectance spectra are characterized by well-defined blue minima and green maxima. Of particular note is the pivotal role played by the 505 nm wavelength, indicating that in

such waters (i.e. pure water and chlorophyll) the volume reflectance at 505 nm is independent of the chlorophyll concentration, i.e. $\frac{\partial R(0,505)}{\partial Chl} = 0$. By integrating equation (7) with respect to chlorophyll, it may be shown that the volume reflectance will be independent of chlorophyll at that value of λ for which $\frac{Bb_{Chl}}{a_{Chl}} = \frac{Bb_w}{a_w}$, i.e. at that value of λ for which the backscatter to absorption ratio of chlorophyll is equal to the backscatter to absorption ratio of pure water. An equilibrium is established, therefore, between the optical properties of each of the two aquatic components.

The effect of the insertion of a small fixed concentration of suspended mineral (0.10 gm^{-3}) into the water mass (i.e. a three-component representation) is shown in the family of subsurface irradiance reflectance spectra illustrated in Figure 5. In such a water mass (0.10 gm^{-3} SM, zero DOC) the rate at which the volume reflectance in the blue region is depressed by the addition of chlorophyll is more nearly equal to the rate of elevation of the volume reflectance in the red. The pivotal wavelength at which $\frac{\partial R(0,\lambda)}{\partial Chl} = 0$ has shifted to ~ 570 nm. For such a three component water mass representation (pure water, chlorophyll, and suspended mineral), the volume reflectance will be independent of chlorophyll concentration at that wavelength for which $\frac{Bb_{Chl}}{a_{Chl}} = \frac{Bb_w + Bb_{SM}C_{SM}}{a_w + a_{SM}C_{SM}}$. An equilibrium is thus established between the optical properties of chlorophyll and the

combined optical properties of the remaining two aquatic components.

In a similar manner, Figures 6-12 represent the family of subsurface irradiance reflectance spectra for varying chlorophyll concentrations, a fixed concentration of zero DOC, and fixed suspended mineral concentrations of 0.2, 0.5, 1.0, 2.0, 5.0, 10.0, and 20.0 gm^{-3} respectively. Note that the pivotal wavelength at which $\frac{\partial R(0,\lambda)}{\partial Chl} = 0$ rapidly moves beyond 690 nm as the suspended mineral concentration increases.

Even though the dramatic impact upon the subsurface irradiance reflectance spectrum of adding suspended mineral concentrations to a lake containing chlorophyll may be readily appreciated from a consideration of Figures 4-12, Figure 13 illustrates the evaluation of subsurface irradiance reflectance spectra resulting from a systematic increase of suspended mineral concentration in a lake containing zero DOC and a small, fixed amount of chlorophyll. Similarly, Figure 14 illustrates the effect of varying suspended mineral concentrations in a lake containing zero DOC and a large, fixed amount of chlorophyll. As logically expected, large concentrations of suspended mineral (say $> \sim 0.5\ gm^{-3}$) drastically curtail the spectral sensitivity of the volume reflectance to changes in chlorophyll concentrations.

Clearly, therefore, a wide range of subsurface irradiance reflectance spectra may be anticipated for a three component (pure water, chlorophyll, suspended mineral) representation of a water mass. The addition of a fourth component (DOC) to the lake system will also significantly alter the irradiance reflectance spectrum observed just beneath the air-water interface, particularly at the lower visible wavelengths (see Figure 2). This impact is readily seen in Figure 15 for the family of volume reflectance spectra (for varying DOC concentrations) for a water mass with a small fixed suspended mineral concentration of 0.05 gm^{-3} and a fixed chlorophyll *a* concentration of 1.00 mgm^{-3}. It is evident that for relatively clear waters (i.e. waters characterized by small concentrations of suspended mineral and small to moderate concentrations of chlorophyll), the systematic addition of DOC results in a rapid depression of the subsurface irradiance reflectance at wavelengths $< \sim 600$ nm (i.e. the blue and green region of the visible spectrum), and a comparatively minimal depression of the subsurface irradiance reflectance at wavelengths $> \sim 600$ nm (i.e. in the red region of the visible spectrum).

Figure 16 illustrates the impact of DOC on a water mass characterized by a large fixed concentration of Chl *a* (10.0 mgm^{-3}) and a small fixed concentration of suspended mineral (0.05 gm^{-3}), while Figure 17 illustrates the impact of DOC on a water mass characterized by a small fixed concentration of Chl *a* (0.05 mgm^{-3}) and a large fixed

concentration of suspended mineral (10.0 gm^{-3}). For the water masses depicted in Figures 16 and 17, it is clear that:

a) The water mass containing high concentrations of suspended minerals displays volume reflectance spectra which are an order of magnitude higher than the water mass containing high concentrations of chlorophyll.

b) The effect of DOC is more noticeable in water masses containing high chlorophyll and low suspended mineral concentrations than in water masses containing low chlorophyll and high suspended mineral concentrations.

c) For all water masses, the maximum impact of DOC will be registered in the low wavelength (blue) portion of the visible spectrum, while the minimum impact of DOC will be registered in the high wavelength (red) portion of the visible spectrum.

Although local values of DOC may vary both spatially and temporally throughout inland aquatic systems, it has been observed (Bukata et al. 1981a) that a not unreasonable typical value for the dissolved organic carbon concentration for the lower Great Lakes is ~ 2.0 g carbon m^{-3}. Figures 18 and 19 illustrate the anticipated changes in subsurface irradiance reflectance spectra resulting from

changes in chlorophyll and suspended mineral concentrations, respectively, in a lake characterized by a fixed DOC concentration of 2.0 g carbon m^{-3}. Figure 18 illustrates the family of volume reflectance spectra resulting from varying the chlorophyll concentrations in a water mass containing no suspended mineral concentration, while Figure 19 illustrates the family of volume reflectance spectra resulting from varying the suspended mineral concentrations in a water mass containing virtually no chlorophyll (a small fixed concentration of 0.05 mgm^{-3})

Certain similarities between Figures 18 and 19 are immediately apparent. Increasing either the suspended mineral or chlorophyll concentration in a water mass containing 2.0 g carbon m^{-3} DOC results in more rapid volume reflectance increases in the red end of the spectrum than in the blue, with the basic shape of the spectrum of chlorophyll in the absence of suspended mineral becoming very similar to the basic shape of the spectrum of suspended mineral in the absence of chlorophyll. Clearly, large concentrations of suspended mineral result in volume reflectance values an order of magnitude greater than those resulting from large concentrations of chlorophyll. Similarly, small concentrations of suspended mineral result in volume reflectance values an order of magnitude greater than those resulting from small concentrations of chlorophyll. However, as seen from Figures 18 and 19, for natural water masses containing 2.0 g carbon m^{-3} DOC, comparable volume reflectance values are observed for water masses

containing large concentrations of chlorophyll (and no suspended mineral) and for water masses containing relatively small concentrations of suspended mineral (and no chlorophyll).

The effects on observed subsurface irradiance reflectance spectra of increasing the suspended mineral concentration in a lake containing a fixed DOC concentration of 2.0 g carbon m^{-3} and a large fixed chlorophyll a concentration of 10.0 mgm^{-3} are illustrated in Figure 20.

Figure 21 attempts to illustrate the interactive effects on the volume reflectance spectra of varying both the chlorophyll and suspended mineral in a lake containing 2.0 g carbon m^{-3} DOC. Figure 22 illustrates the comparable situation in a lake containing 10.0 g carbon m^{-3} DOC.

Clearly, the examples of subsurface irradiance reflectance spectra presented in this section serve to illustrate the impact that variations in the water quality parameters (chlorophyll, suspended mineral, dissolved organic carbon) will have on the *in situ* measurements of such optical spectra, and consequently underline the care that must be taken in deconvolving optical complexities when measured volume reflectance spectra are used to estimate the water quality parameters.

It is equally clear that the examples of subsurface irradiance reflectance spectra presented in this report are inexhaustive, and by no means cover the myriad of spectra possible for lakes as complex as Lake Ontario. Consequently, Table I contains a numerical listing of the 15 point (20 nm increments from 410 to 690 nm) absorption and backscatter cross-section spectra utilized in this report. The interested reader may directly utilize the data in Table I together with equations 6 and 7 to generate the anticipated subsurface irradiance reflectance (volume reflectance) for any desired water mass.

SUBSURFACE IRRADIANCE REFLECTANCE AT A SINGLE WAVELENGTH

To this point, this report has dealt with subsurface irradiance reflectance spectra (410 to 690 nm), and thus assumes an operational capability of determining such an in situ spectrum. Much optical research, however, is conducted with single band subsurface irradiance meters. This section evaluates the possible application of such single band devices in estimating the water quality parameters from a single measurement of volume reflectance at one wavelength. Since the visible spectrum may be conveniently divided into blue, green, and red components, a single wavelength from each of the blue (450 nm), green (570 nm), and red (650 nm) will be utilized as the basis for ensuing discussions.

From the absorption cross-section versus wavelength curves of Figure 2, it is evident that the influence of dissolved organic carbon (DOC) on subsurface irradiance reflectance is most pronounced in the blue region of the visible spectrum and least pronounced in the red region of the spectrum. Consequently, a natural water mass may be approximated, to some extent, by a three component model (viz. pure water, chlorophyll, and suspended mineral) at red wavelengths. It might be anticipated, therefore, that estimations of chlorophyll and/or suspended mineral concentrations from a single wavelength measurement of subsurface irradiance reflectance, if possible at all, might display the highest probability of success if the single wavelength selected were in the red portion of the spectrum. That such an anticipation is, in fact, realized, will emerge from the following discussion.

Figure 23 illustrates the family of relationships that exist between the subsurface irradiance reflectance at 450 nm (blue) and the chlorophyll concentration for a water mass in which the DOC concentration is kept fixed at 2.0 g carbon m^{-3} (a not unreasonable average value for a large number of natural water bodies) and the suspended mineral concentration is allowed to vary between 0 and 10 gm^{-3}. Clearly, the subsurface irradiance reflectance at 450 nm (blue) is highly insensitive to change of suspended mineral. Similar relationships between the subsurface irradiance reflectance in the blue and chlorophyll concentrations emerge from a consideration of other DOC

concentrations, emphasizing the futility of attempting to estimate chlorophyll concentrations from a single subsurface irradiance reflectance at 450 nm.

In a similar manner, Figure 24 illustrates the situations that arise when the subsurface irradiance reflectance at 570 nm (green) is utilized in an attempt to estimate chlorophyll concentration from a single wavelength measurement. Even though the subsurface irradiance reflectance in the green displays a reasonable sensitivity for a water mass which contains no suspended mineral component, this sensitivity rapidly evaporates once even a trace (< 0.10 gm^{-3} of suspended mineral) is present in the aquatic system.

Figure 25 (similar to Figures 23 and 24), likewise eliminates a single subsurface irradiance measurement at 650 nm (red) as a means of estimating chlorophyll concentrations, although the sensitivity of the subsurface irradiance reflectance for very clear (in terms of suspended mineral concentrations) water masses is slightly higher for the red wavelength than for the green wavelength.

It is evident from Figures 23 to 25, therefore, that reliable estimates of chlorophyll concentrations cannot result from single wavelength measurements of the subsurface irradiance reflectance (volume reflectance).

Figure 26 illustrates the family of relationships that exist between the subsurface irradiance reflectance at 450 nm (blue) and the suspended mineral concentration for a water mass in which the DOC concentration is kept fixed at 2.0 g carbon m^{-3} and the chlorophyll concentration is allowed to vary from 0.05 mgm^{-3} to 20.0 mgm^{-3}. A somewhat promising sensitivity of subsurface irradiance reflectance at the blue wavelength to changes in suspended mineral concentration (coupled with the relative insensitivity of this subsurface irradiance reflectance to changes in chlorophyll concentration as indicated in Figure 24) appears to be suggested by Figure 26. However, as indicated earlier, the maximum impact of DOC manifests in the blue region of the spectrum. This impact is illustrated in Figure 27 wherein the observable range of subsurface irradiance reflectance values at 450 nm (blue) is plotted as a function of suspended mineral concentration for a water body which may display a range of DOC concentrations between 0 and 5 g carbon m^{-3} and a range of chlorophyll *a* concentrations between 0.05 and 20.0 mgm^{-3}. The sensitivity of the volume reflectance in the blue to changes in suspended mineral concentration quickly loses its initial attractiveness.

The sensitivity of the subsurface irradiance reflectance at 570 nm (green) to changes in suspended mineral concentration for a water mass containing a fixed DOC concentration of 2.0 g carbon m^{-3} is shown in Figure 28 for several values of chlorophyll concentration. The impact of the presence of chlorophyll on the measured subsurface

irradiance reflectance at green wavelengths for small suspended mineral concentrations is clearly more pronounced than the corresponding impact of the presence of chlorophyll on the measured subsurface irradiance reflectance at blue wavelengths. However, the volume reflectance at green wavelengths is less sensitive to changes in DOC concentrations than is the volume reflectance at blue wavelengths. Figure 29 (similar to Figure 27) illustrates the observable range of subsurface irradiance reflectance values at 570 nm (green) plotted as a function of suspended mineral concentration for a water body which may display a range of DOC concentrations between 0 and 5 g carbon m^{-3} and a range of chlorophyll concentrations between 0.05 and 20.0 mgm^{-3}. While the response of the subsurface irradiance reflectance at 570 nm (green) to changes in suspended mineral concentration will not satisfactorily allow a reliable estimation of suspended mineral concentration from a volume reflectance measurement at a single wavelength in the green region of the spectrum, Figure 29 (for green volume reflectance), nonetheless, displays an obvious improvement in sensitivity over Figure 27 (for blue volume reflectance).

The sensitivity of the subsurface irradiance reflectance at 650 nm (red) to changes in suspended mineral concentration for a water mass containing a fixed DOC concentration of 2.0 g carbon m^{-3} is shown in Figure 30 for several values of chlorophyll concentration. The very large impact of the presence of chlorophyll on the volume reflectance at red wavelengths observed in water masses containing small

concentrations of suspended mineral is an obvious feature of Figure 30. However, when the minimal impact of DOC concentrations on the volume reflectance observable in the red region of the spectrum is also considered, the sensitivity curve of Figure 31 may be constructed. Comparable to Figures 27 and 29, Figure 31 illustrates the observable ranges of subsurface irradiance reflectance values at 650 nm (red) plotted as a function of suspended mineral concentration for a water body which may display a range of DOC concentrations between 0 and 5 g carbon m^{-3} and a range of chlorophyll concentrations between 0.05 and 20.0 mgm^{-3}. Clearly, a reasonable sensitivity to suspended mineral concentration may be ascribed to the subsurface irradiance reflectance at 650 nm (red), particularly for suspended mineral concentrations $> \sim 0.10$ gm^{-3}, and consequently a single volume reflectance measurement at red wavelengths does appear to possess some capability of estimating suspended mineral concentrations in most natural lake waters.

The asymptotic nature of Figure 31 is also quite apparent. As seen from equation (7), R(0,650) asymptotically approaches the approximate value $\frac{1}{3} \circ \frac{Bb(650)}{a(650) + Bb(650)}$ which would render determinations of suspended mineral concentrations $> \sim 40$ gm^{-3} very hazardous. However, in the general range $0.10\ gm^{-3} < C_{SM} < 40\ gm^{-3}$, a single volume reflectance measurement at 650 nm may provide a reasonable estimate of suspended mineral concentration despite the competing

optical activity resulting from the simultaneous presence of chlorophyll and dissolved organic material within the water mass.

The sensitivity of the subsurface irradiance reflectance at 650 nm is further improved if such single wavelength in situ optical measurements are performed within natural waters which do not display an excessive amount of biological activity (oceans, oligotrophic and mesotrophic lakes and rivers, etc.). Figure 32 illustrates the observable ranges of subsurface irradiance reflectance values at 650 nm plotted as a function of suspended mineral concentration for a water body in which the chlorophyll concentration range is restricted to $0.05 \leq C_{Chl} \leq 5.0$ mg m^{-3}. The increased sensitivity becomes readily apparent.

In summary, therefore, the optical complexities of inland water bodies present overwhelming obstacles to the use of single wavelength measurements of subsurface irradiance reflectance (volume reflectance) as a means of providing water quality indicators. It is totally unfeasible to attempt a reliable estimate of the chlorophyll concentration from such single wavelength in situ measurements, irrespective of what wavelength is considered. Similarly, the blue and green region of the visible spectrum are inappropriate wavelength bands with which to attempt an estimation of suspended mineral concentrations (due, in large part, to the interference from dissolved organic material). Despite severe restrictions resulting from the

optical interference of chlorophyll concentrations (particularly at low suspended mineral concentrations), however, single wavelength subsurface irradiance measurements in the red region of the visible spectrum do possess some applicability to the estimation of small to moderate concentrations of suspended mineral.

Therefore, if direct measurements of subsurface irradiance reflectance, do, in fact, possess an application to the determination of water quality indicators, it is evident that the entire subsurface irradiance reflectance spectrum must be considered.

RELATIONSHIPS AMONG OPTICAL AND WATER QUALITY PARAMETERS

This section will attempt to define, in mathematical terms, the interrelationships between the volume reflectance and the water quality parameters. That is, it investigates the effect on observed volume reflectance spectra of varying chlorophyll, suspended mineral, and dissolved organic carbon concentrations simultaneously. The resulting equations will illustrate the difficulties encountered in attempting a mathematical determination of the water quality parameters from direct measurements of the volume reflectance (subsurface irradiance reflectance) spectrum, and illustrate the need for a multivariate optimization technique for the extraction of water quality information from such optical spectra. Consequently, the reader may

choose to ignore the discussions presented in this section and proceed directly to the next section with no loss of continuity.

Consider a homogeneous water mass comprised of concentrations of water, chlorophyll, suspended mineral, and dissolved organic carbon given by C_w, C_{Chl}, C_{SM}, and C_{DOC}, respectively. The volume reflectance at wavelength λ, $R(\lambda)$ will be a function of these concentrations and the optical cross-sections, viz.,

$$R(\lambda) = f(C_w a_w,\ C_{Chl} a_{Chl},\ C_{SM} a_{SM},\ C_{DOC} a_{DOC},\ C_w (Bb)_w,\ C_{Chl} (Bb)_{Chl},\ C_{SM} (Bb)_{SM}) \qquad (8)$$

where the wavelength dependence of the optical cross-sections has been dropped for simplicity of notation.

The rate of change of volume reflectance with wavelength (i.e. the slope of the measured volume reflectance spectrum at wavelength λ) $\frac{dR(\lambda)}{d\lambda}$, is therefore defined as:

$$\frac{dR(\lambda)}{d\lambda} = \frac{\partial R}{\partial a_w} \cdot \frac{\partial a_w}{\partial \lambda} + C_{Chl} \frac{\partial R}{\partial a_{Chl}} \cdot \frac{\partial a_{Chl}}{\partial \lambda}$$

$$+ C_{SM} \frac{\partial R}{\partial a_{SM}} \cdot \frac{\partial a_{SM}}{\partial \lambda} + C_{DOC} \frac{\partial R}{\partial a_{DOC}} \cdot \frac{\partial a_{DOC}}{\partial \lambda}$$

$$+ \frac{\partial R}{\partial (Bb)_w} \cdot \frac{\partial (Bb)_w}{\partial \lambda} + C_{Chl} \frac{\partial R}{\partial (Bb)_{Chl}} \cdot \frac{\partial (Bb)_{Chl}}{\partial \lambda}$$

$$+ C_{SM} \frac{\partial R}{\partial (Bb)_{SM}} \cdot \frac{\partial (Bb)_{SM}}{\partial \lambda} \qquad (9)$$

where C_w has been set to 1, and the partial derivatives of the optical cross-sections (which are a function of λ) are defined by the shapes of the curves illustrated in Figures 2 and 3 (with the exception of Figure 3 in which each point would be multiplied by its appropriate $B(\lambda)$).

From equation (7), the volume reflectance $R(\lambda)$ is given by:

$$R(\lambda) = \sum_{n=0}^{3} r_n \left[\frac{(Bb)(\lambda)}{a(\lambda) + (Bb)(\lambda)} \right]^n$$

$$= \sum_{n=0}^{3} r_n \left[\frac{u(\lambda)}{v(\lambda)}\right]^n \qquad (10)$$

where $u(\lambda) = (Bb)_w + C_{Chl}(Bb)_{Chl} + C_{SM}(Bb)_{SM}$

and $v(\lambda) = a_w + C_{Chl}a_{Chl} + C_{SM}a_{SM} + C_{DOC}a_{DOC}$

$+ (Bb)_w + C_{Chl}(Bb)_{Chl} + C_{SM}(Bb)_{SM}$

Partially differentiating equation (10) with respect to each of the optical cross-sections yields:

$$\frac{\partial R}{\partial a_w} = -\frac{Nu}{v^2}$$

$$\frac{\partial R}{\partial a_{Chl}} = -\frac{N\,C_{Chl}\,u}{v^2}$$

$$\frac{\partial R}{\partial a_{SM}} = -\frac{N\,C_{SM}\,u}{v^2}$$

$$\frac{\partial R}{\partial a_{DOC}} = -\frac{N\,C_{DOC}\,u}{v^2} \qquad (11)$$

$$\frac{\partial R}{\partial (Bb)_w} = \frac{N(v-u)}{v^2}$$

$$\frac{\partial R}{\partial (Bb)Chl} = \frac{N\,C_{Chl}\,(v-u)}{v^2}$$

$$\frac{\partial R}{\partial (Bb)_{SM}} = \frac{N\,C_{SM}\,(v-u)}{v^2}$$

where $N = r_1 + 2r_2\frac{u}{v} + 3r_3\frac{u^2}{v^2}$

and r_1, r_2, and r_3 are the coefficients of expansion from equation (7).

Substituting equation set (11) into equation (9) yields:

$$\frac{dR(\lambda)}{d\lambda} = -\frac{Nu}{v^2}\left[\frac{\partial a_w}{\partial\lambda} + C_{Chl}{}^2\,\frac{\partial a_{Chl}}{\partial\lambda}\right.$$

$$\left. + C_{SM}{}^2\,\frac{\partial a_{SM}}{\partial\lambda} + C_{DOC}{}^2\,\frac{\partial a_{DOC}}{\partial\lambda}\right]$$

$$+\frac{N(v-u)}{v^2}\left[\frac{\partial(Bb)_w}{\partial\lambda} + C_{Chl}{}^2\,\frac{\partial(Bb)_{Chl}}{\partial\lambda}\right.$$

$$\left. + C_{SM}{}^2\,\frac{\partial(Bb)_{SM}}{\partial\lambda}\right] \qquad (12)$$

where u, v, and N are functions of C_{Chl}, C_{SM} and C_{DOC} as defined above.

Equation (12) then relates the slope of a directly measured subsurface irradiance reflectance spectrum at wavelength λ to the concentrations of chlorophyll, suspended mineral, and dissolved organic carbon generating that observed spectrum. Very obvious difficulties exist in attempting to apply equation (12) (say, at three discrete values of λ) to estimate, from three simultaneous equations, the

values of C_{Chl}, C_{SM} and C_{DOC} describing the water mass. From the nature of the wavelength dependencies of the optical cross-sections, it is clear that not only are judicious choices of λ's required, but so are very accurate determinations of the slopes. Further, very accurate values of $\frac{dR(\lambda)}{d\lambda}$ are also mandatory, and as is evident, these slope values may be very small numerically (in addition to being either positive or negative). Further, the values of N, v and u are themselves functions of C_{Chl}, C_{SM}, and C_{DOC} (the very parameters being sought). This latter problem, however, may be overcome, at least in principle. Since $u(\lambda) = (Bb)(\lambda)$ and $v(\lambda) = a(\lambda) + (Bb)(\lambda)$, a determination of the bulk inherent properties $(Bb)(\lambda)$ (total backscattering coefficient) and $a(\lambda)$ (total absorption coefficient) in the manner described in the earlier sections of this report can provide the required values of u, v, and N.

Clearly, therefore, equation (12) provides, in principle, the capability of providing three equations (at three judiciously selected wavelengths) which may be simultaneously solved for the water quality indicators C_{Chl}, C_{SM}, and C_{Chl}. However, the severe onus placed upon precisely determining small values of slopes in both measured and available optical parameter spectra would adversely impact the reliability and reproducibility of such a mathematical calculation. The need to determine $a(\lambda)$ and $(Bb)(\lambda)$ along with each *in situ* measurement of the subsurface irradiance spectrum further renders the use of equation (12) unattractive. Ideally, a method of

extracting the desired water quality indicators from a single measurement of the volume reflectance spectrum should be sought and utilized. Such a method is described in the next section.

MULTIVARIATE OPTIMIZATION TECHNIQUE FOR THE EXTRACTION OF WATER QUALITY PARAMETERS FROM MEASURED SUBSURFACE IRRADIANCE REFLECTANCE SPECTRA

The fundamental problem to be solved is as follows: Given a directly measured subsurface irradiance reflectance spectrum $R(0,\lambda)$, which may be mathematically defined by equation (7) (i.e. $R(0,\lambda)$ as an expanded function of $a(\lambda)$ and $Bb(\lambda)$ which are themselves functions of the optical cross-sections and the concentrations of chlorophyll, suspended mineral, and DOC), find those values of chlorophyll, suspended mineral, and DOC which generate a subsurface irradiance reflectance spectrum most closely resembling the measured spectrum.

Clearly, a multivariate optimization technique appropriate for estimating "best fit" concentrations of chlorophyll, suspended mineral and dissolved organic carbon should also have application to the solution of an inverse problem, viz: Given directly measured subsurface irradiance spectra and the corresponding concentrations of chlorophyll, suspended mineral, and dissolved organic carbon which contribute to the observation of such spectra, find those values of absorption and scattering cross-sections (as a function of λ) which

generate a subsurface irradiance reflectance most closely resembling the measured spectrum.

This section details the nature of the multivariate optimization technique utilized by the Environmental Optics Section of the National Water Research Institute in a) attempting an extraction of water quality indicators from *in situ* measurements of the subsurface irradiance reflectance spectra in the range 400 to 700 nm and b) attempting a determination of the optical cross-sections from *in situ* measurements of the subsurface irradiance reflectance and water quality measurements performed in concert with the optical measurements.

Some of the mathematical difficulties associated with attempting an analytical solution of equation (7) have been outlined in the preceding section. However, numerical techniques exist which can circumvent such complexities.

Rewriting equation (7) in vector form yields:

$$R(0,\underline{a}(\lambda),\underline{Bb}(\lambda),\underline{C}) = \sum_{n=0}^{3} r_n(0)\left[1+(\underline{a}(\lambda)\cdot\underline{C})/(\underline{Bb}(\lambda)\cdot\underline{C})\right]^{-n} \quad (13)$$

where

$$\underline{a}(\lambda) = (a_w(\lambda),\ a_{Chl}(\lambda),\ a_{SM}(\lambda),\ a_{DOC}(\lambda))$$

$$\underline{Bb}(\lambda) = (Bb_w(\lambda),\ Bb_{Chl}(\lambda),\ Bb_{SM}(\lambda),\ 0)$$

$$\underline{C} = (1,\ C_{Chl},\ C_{SM},\ C_{DOC})$$

Given a measured spectrum $\{S_i\}$ consisting of a set of irradiance reflectances at discrete values of λ (e.g. the fifteen point spectrum from 410 to 690 nm in 20 nm increments) the weighted residuals between the measured and theoretical volume reflectances $R(0,\underline{a}_i,\underline{Bb}_i,\underline{C})$ can be written as

$$g_i(C) = [S_i - R(0,\underline{a}_i,\underline{Bb}_i,C)]/R(0,\underline{a}_i,\underline{Bb}_i,C) \qquad (14)$$

Here it is assumed that the absorption and backscatter vector functions $\underline{a}$ and $\underline{Bb}$ are known for the homogeneous water mass under consideration, and it is desired to find (at the wavelengths corresponding to $\{S_i\}$) the multidimensional least squares solution by minimizing over $\underline{C}$ the function

$$f(\underline{C}) = \sum_i g_i^2(\underline{C}) \qquad (15)$$

The value of the concentration vector $\underline{C}$ for which $f(\underline{C})$ is the minimum will then be accepted as defining the parameter concentrations for the water mass which produced the measured subsurface irradiance reflectance spectrum $\{S_i\}$.

The subroutine ZXSSQ (one of the routines available in the International Mathematical and Statistical Library (IMSL, 1980)) is a Levenberg (1944)-Marquardt (1963) finite difference algorithm

appropriate to such multivariate non-linear least squares optimization applications. Given a suitable initial value $\underline{C}_o$ the algorithm will systematically determine a local minimum of $f(\underline{C})$. This value of $f(\underline{C})$ may not, however, be the smallest achievable over the valid range of $\underline{C}$. Consequently, numerous starting points $\{\underline{C}_{oj}\}$ are chosen and the algorithm allowed to determine the corresponding minima $\{f_j(\underline{C})\}$. The $\underline{C}$ associated with the minimum $f_j(\underline{C})$ of this set is then selected as the appropriate solution. There is no guarantee, however, that any particular starting point $\underline{C}_{oj}$ will result in the algorithm successfully finding any minimum for $f(\underline{C})$ since the algorithm may diverge. Furthermore, a $\underline{C}$ may be found which although mathematically satisfactory is physically meaningless (e.g. negative concentrations). In order to obviate such difficulties, suggestions in the IMSL program notes were implemented in which constraints are placed on $\underline{C}$ such that

$$C_{iMIN} \leq C_i \leq C_{iMAX} \qquad \text{for } i = 2,3,4$$

where the subscript i refers to the ith component of the water mass (e.g. $C_2 = C_{Chl}$, $C_3 = C_{SM}$ and $C_4 = C_{DOC}$), and a transformation from the constrained $\underline{C}$ space to an unconstrained $\underline{W}$ space ($-\infty < W_i < +\infty$) is effected using the error function relationship

$$C_i = C_{iMIN} + (C_{iMAX} - C_{iMIN})\,(1 + \text{erf}\,(W_i))/2 \qquad (16)$$

The Levenberg-Marquardt algorithm may also be utilized in a similar manner to extract the parameter cross-sections from a set of volume reflectance and concentration measurements. For this application equation (7) can be rewritten as:

$$R(0,\underline{C}(\underline{u}),\underline{X}) = \sum_{n=0}^{3} r_n(0) \left[1 + (\underline{C}(\underline{u}) \cdot \underline{X})/(\underline{C}'(\underline{u}) \cdot \underline{X})\right]^{-n} \qquad (17)$$

where $\underline{X} = (a_w, a_{Chl}, a_{SM}, a_{DOC}, Bb_w, Bb_{Chl}, Bb_{SM}, 0)$

$\underline{C}(\underline{u}) = (1, C_{Chl}(\underline{u}), C_{SM}(\underline{u}), C_{DOC}(\underline{u}), 0, 0, 0, 0)$

$\underline{C}'(\underline{u}) = (0, 0, 0, 0, 1, C_{Chl}(\underline{u}), C_{SM}(\underline{u}), C_{DOC}(\underline{u}))$

Here $\underline{u}$ is the vector defining the geographical position of the concentration vector $\underline{C}(\underline{u})$, and $\underline{C}'(\underline{u})$ is merely a rotation of $\underline{C}(\underline{u})$ in the multidimensional space.

Given a set of volume reflectance data $\{S_j\}$ at a wavelength λ_i and the corresponding concentration data $\{\underline{C}_j\}$ at a number, j, of stations for which we assume the cross-sections are invariant, the weighted residuals $g_j(\underline{X})$ can be formed

$$g_j(\underline{X}) = [S_j - R(0,\underline{C}_j,\underline{X})]/R(0,\underline{C}_j,\underline{X}) \qquad (18)$$

and the least squares solution is again found by minimizing over $\underline{X}$ the function

$$f(\underline{X}) = \sum_j g_j^2(\underline{X}) \tag{19}$$

As before, appropriate constraints are placed on $\underline{X}$

$$X_{iMIN} \leq X_i \leq X_{iMAX} \qquad \text{for } i = 1,2,\ldots,7$$

(e.g. $X_1 = a_w$, $X_2 = a_{Chl}$ ..... $X_7 = Bb_{SM}$)

and the algorithm is allowed to operate in $\underline{W}$ space according to the error function transformation

$$X_i = X_{iMIN} + (X_{iMAX} - X_{iMIN})(1 + \text{erf } (W_i))/2 \tag{20}$$

The resulting least squares solution for $\underline{X}$ is, of course, applicable only to the specific wavelength of the $\{S_j\}$ used and the same procedure must be repeated substituting the $\{S_j\}$ corresponding to each wavelength at which $\underline{X}$ is desired. In this way it is possible to determine the entire cross-section spectrum $\underline{X}(\lambda)$.

Although a similar Levenberg-Marquardt procedure is utilized in each instance, the determination of $\underline{X}$ is intrinsically more complex

than the determination of $\underline{C}$ since the number of dimensions defining $\underline{X}$ space is double the number of dimensions defining $\underline{C}$ space. A fifteen point volume reflectance spectrum from a single station is adequate to enable the extraction of the three variable components of $\underline{C}$ for that station. However, data from considerably more than fifteen stations are necessary to extract the seven variable components of $\underline{X}$ and yet successfully avoid divergence of the algorithm. In the absence of a sufficient number of stations, the dimensionality of the $\underline{X}$ extraction must be reduced by supplying fixed cross-section values for some of the $\underline{X}$ components (e.g. the absorption and backscatter cross-section spectra of pure water can be used for a_w and Bb_w).

An additional complication which may arise in the determination of the cross-section spectrum $\underline{X}(\lambda)$ will occur at wavelengths where the absorption and/or backscatter cross-section of a component decreases to such an extent that the component's contribution to the volume reflectance becomes comparable in magnitude to the uncertainties in the measured data. The Levenberg-Marquardt algorithm will then be incapable of unambiguously determining the cross-section for that component and will instead yield one of the constraint boundaries X_{iMIN} or X_{iMAX}. This also results in the determined cross-sections of the other components being unreliable at these wavelengths. Such gaps in the spectrum of $\underline{X}(\lambda)$ may be filled by interpolation or extrapolation utilizing the successfully calculated portions of the $\underline{X}(\lambda)$ spectrum.

Thus, the concentration vector $\underline{C}$ may be efficiently extracted from a given measured volume reflectance spectrum, and in a similar manner the cross-section spectrum $\underline{X}(\lambda)$ may be determined from volume reflectance and concentration data.

APPLICATION OF WATER QUALITY MODEL TO THE ESTIMATION OF CHLOROPHYLL, SUSPENDED MINERAL, AND DISSOLVED ORGANIC CARBON CONCENTRATIONS IN LAKE ONTARIO

An independent data set of water quality parameters and subsurface irradiance reflectance spectra was obtained in western Lake Ontario also during the 1979 field season. Using the directly measured optical spectra, the optical cross-sections (for the four-component model) depicted in Figures 2 and 3, and the Levenberg-Marquardt multivariate optimization technique discussed in the preceding section, concentrations of suspended mineral, dissolved organic carbon, and chlorophyll a (uncorrected for phaeophytin contamination) were predicted and these values compared to the values obtained from laboratory analyses of water samples collected at the same time the optical spectra were measured.

Figure 33 illustrates the comparison between predicted and directly measured suspended mineral concentrations so obtained. The cone of predictability, defined by the dotted lines, represents a predictability to within a factor of two about the line of exact predictability, i.e. a predictability uncertainty of $\pm \log 2$.

Figures 34 and 35 illustrate in a corresponding manner, the comparison between predicted and directly measured dissolved organic carbon and chlorophyll a concentrations, respectively.

It is seen from Figures 33-35 that:

a) the four-component water quality model and the optical cross-sections of Figures 2 and 3 yield excellent predictive capabilities for suspended mineral concentrations and possibly acceptable predictive capabilities for dissolved organic carbon concentrations.

b) predictive capabilities of the four-component water quality model and the optical cross-sections of Figures 2 and 3 appear to be virtually non-existent for chlorophyll a concentrations.

Clearly, from Figure 35 (which is characterized by a dramatic underprediction of the chlorophyll a concentration) it is seen that near-zero values of chlorophyll a concentrations appear to not only satisfy the Levenberg-Marquardt optimization process, but also to not interfere with the prediction of reasonable values of both suspended mineral and dissolved organic carbon concentrations. This suggests three salient possibilities: i) that subsurface volume reflectance spectra directly measured in Lake Ontario may be satisfactorily simulated (in general) by varying only concentrations of suspended mineral and dissolved organic carbon, ii) (which is actually

a variation of i)) that the optical cross-sections of chlorophyll *a* are less effective in determining the optical properties of inland lakes (particularly for small concentrations of chlorophyll) than are the optical properties of suspended mineral and dissolved organic carbon concentrations, and iii) the optical cross-sections for chlorophyll (taken from Figures 2 and 3 and determined for Lake Ontario from the first data set) are inappropriate for the second data set. In reality, all three suggested possibilities are indeed correct, as will be discussed below.

Suggestion i) is depicted in Figure 36. Therein are shown both the calculated "best fit" subsurface irradiance optical spectrum (joined points) and the experimentally measured subsurface irradiance reflectance spectrum (unjoined points) for a typical relatively nearshore station (within the Niagara plume) in western Lake Ontario. The predicted (calculated) water quality parameters resulting in the "best fit" spectrum are listed, along with the measured values of the water quality parameters at that station, and it is immediately seen that the Levenberg-Marquardt analyses supplied reasonable values of suspended mineral and DOC concentrations while predicting a zero concentration of chlorophyll *a*.

The presence of chlorophyll in the water mass in this instance actually diminishes the ability of the water quality model to simulate the experimentally measured subsurface irradiance reflectance

spectrum at this station. This is seen from Figure 37 wherein two calculated optical spectra (for the cross-sections of Figures 2 and 3) are compared to the actually measured optical spectrum. The solid line depicts the predicted optical spectrum for a water mass possessing concentrations of chlorophyll a, suspended mineral and dissolved organic carbon close to those actually measured at the station (Chl a is taken as 5.0 mg per m^3; SM is taken as 5.0 g per m^3; DOC is taken as 2.0 g carbon per m^3). The dotted line depicts the predicted optical spectrum for a water mass possessing concentrations of chlorophyll a, suspended mineral, and dissolved organic carbon close to those predicted by the Levenberg-Marquardt optimization technique (Chl a is taken as zero; SM is taken as 5.0 g per m^3; DOC is taken as 3.0 g carbon per m^3). A distinct improvement in curve fitting is readily realized by the removal of chlorophyll from the aquatic system.

The general shape of the directly measured subsurface irradiance reflectance spectrum (i.e. a distinct peak in the green wavelength region) shown in Figure 36 is almost always observed in Lake Ontario throughout the field season for both nearshore stations and stations substantially off-shore. This is illustrated in Figure 38 wherein directly measured volume reflectance spectra are illustrated for both nearshore and midlake stations visited during May, July and September. Although the actual magnitudes of the observed irradiance reflectance (volume reflectance) may vary (a direct consequence of the spatial and temporal variabilities of the water quality parameters at

the stations), the pronounced peak at mid-wavelengths is a readily recognizable feature of each optical spectrum. Salient point ii) may be readily seen from a consideration of Figures 37 and 38 and Figures 18 and 19.

As evident from Figures 18 and 19, the addition of either suspended mineral or chlorophyll a (to a water mass containing ~ 2.0 g carbon per m^3) will produce a distinct maximum in the mid-wavelength region of the visible spectrum. Further, as seen from Figures 18 and 19 (and discussed earlier in this report) the effect of the relative concentrations of chlorophyll a and suspended mineral normally found in inland lakes will be such as to make the suspended mineral concentrations more effective than the chlorophyll concentrations in generating the "green" maximum in the measured volume reflectance spectrum.

Suggestion iii) was investigated by utilizing the Levenberg-Marquardt optimization method to obtain a new set of optical cross-sections for chlorophyll a (uncorrected for phaeophytin contamination). Optical and water quality data collected from the western Lake Ontario test sites during May and July 1979 were utilized. The Figures 2 and 3 cross-sections for suspended mineral and dissolved organic carbon were retained and the optimization technique was used to determine new values of a_{chl} and b_{chl} throughout the visible spectrum. For the second data set however, additional information

concerning the composition of the above surface impinging radiation was also available and therefore utilized. Since the coefficients $r_n(0)$ in equation (7) are functions of the incident radiance distribution (Gordon et al., 1975), (a direct consequence of the fact that volume reflectance is one of the apparent properties of a water mass) the measured volume reflectance will be influenced by both the solar zenith angle (time of day) and the diffuse fraction of the incident downwelling irradiance. This will be true irrespective of changes in the concentrations of the suspended and dissolved constituents of the water mass (see also discussions in Jerome et al., 1982).

Figure 39 (adapted from Table B.3.2 of Moniteq (1981)) presents the fraction of above-water downwelling irradiance that is diffuse for each of the months during which the independent data set was obtained. Figure 39 was then used to generate an appropriate set of $r_n(0)$ coefficients corresponding to each fraction, and these coefficients were inserted into equation (7) prior to the inverse Levenberg-Marquardt analysis.

The resulting Levenberg-Marquardt analysis yielded b_{Chl} values which were essentially in agreement with the b_{Chl} values obtained previously. The a_{Chl} values obtained, however, were significantly different from the a_{Chl} values previously obtained, as illustrated in Figure 40. While the two data sets agree reasonably well in the high wavelength red portion, the values of a_{Chl} obtained

from the second data set (optimization method) for $\lambda < \sim 600$ nm are consistently about a factor of two lower than the values of a_{Chl} obtained from the first data set (multiple regression method).

Utilizing the Levenberg-Marquardt optimized values of a_{Chl} (b_{Chl} and all other cross-section values as shown in Figures 2 and 3) and the directly measured subsurface irradiance reflectance spectra, the optimization technique (incorporating the incident radiance distribution dependence of $r_n(0)$) was once again used to estimate the water quality indicators that would generate "best fit" simulations to the observed volume reflectance spectra.

Figure 41 (directly comparable to Figure 36) illustrates the comparison between the directly measured subsurface irradiance reflectance spectrum (unjoined points) and the calculated "best fit" subsurface irradiance reflectance spectrum (joined points) resulting from the use of the modified values of a_{Chl}. It is seen that the Levenberg-Marquardt optimization technique, in addition to predicting acceptable values for suspended mineral and dissolved organic carbon concentrations for the station, also predicts an acceptable value for chlorophyll concentration.

Figures 42, 43 and 44 illustrate the comparison between the predicted and directly measured concentrations of suspended mineral, dissolved organic carbon, and chlorophyll a, respectively. These

figures may be directly compared to Figures 33-35, the only difference between the two sets of results being that Figures 42-44 were generated from the addition of an incident radiance distribution dependence of $r_n(0)$ and the use of the dotted curve (Figure 40) for the spectral dependence of a_{Chl}.

A consideration of Figures 42-44 indicates:

a) The predictive capabilities of the four-component optical model with respect to suspended mineral and dissolved organic carbon concentrations, while impacted to some extent by the utilization of the modified chlorophyll a absorption cross-sections, do not appear to be affected to any statistically significant degree.

b) A very noticeable improvement in the predictive capabilities of the four-component optical model for chlorophyll a concentrations, however, is certainly realized by the utilization of the modified chlorophyll a absorption cross-sections. The majority of the underpredicted chlorophyll a concentrations (Figure 44) were observed during the month of September. This is more clearly seen from Figure 45 which subdivides the information plotted in Figure 44 into the months (May, July, September) during which the volume reflectance measurements were taken.

DIFFICULTIES ASSOCIATED WITH CHLOROPHYLL PREDICTIONS

The physical principles upon which the multi-component optical models described in this report are based are, to within the limitations presented and current level of aquatic understanding, sound. The absorption and scattering properties of the suspended and dissolved materials comprising inland water masses will, along with the properties of the impinging above-surface irradiance, dictate the subsurface irradiance reflectance (volume reflectance) spectra that will be experimentally measured within those water masses. Water quality indicators (organic and inorganic components of natural water masses) exist as absorption and scattering centres throughout the water column. It logically follows, therefore, that (within limits of possible ambiguities) simulated volume reflectance spectra generated from known concentrations of water quality indicators could be mathematically compared to measured volume reflectance spectra as a means of estimating the in situ concentrations of those water quality indicators which have contributed to the observance of those spectra.

The critical ingredient to such predictive methodology, however, is a precise knowledge of the optical cross-sections (absorption and scattering on a per unit concentration basis) of the constituent materials of the water mass in question. While there is an increasing effort, on a worldwide scale, to obtain such precise information, the results of such efforts to date have been far from

universally applicable. Certainly there is general agreement as to the observed range of such cross-section values and the realization that such cross-sections will be not only geographically dependent and sub-species dependent, but also temporally dependent. Consequently, a major obstacle to such optical research has been an inherent inability to experimentally reproduce equivalent and/or reliably extrapolatable values for such critical parameters. Our own work in Lake Ontario directly reflects this frustration. Two independent coordinated optical/water quality data sets were obtained in western Lake Ontario during the 1979 field season. While similar wavelength spectra for the absorption and scattering cross-sections of suspended mineral and dissolved organic carbon and for the scattering cross-section of chlorophyll appear to be reasonably appropriate for both of the data sets, each of the data sets appears to require significantly dissimilar absorption cross-section spectra for chlorophyll (see Figure 40). Within these cross-section restraints, the four-component optical model possesses a water quality indicator predictability to within a factor of two. The value of such water quality predictability is, of course, a moot point and will not be discussed further here.

This observed uncertainty (i.e. the uncertainty as to an appropriate value for a specific species at a specific spatial location and/or temporal location within a biological growth cycle) is currently being observed by many workers. Recently, Morel and Bricaud (1981) have elegantly discussed the problems that originate from the

non-constancy of the absorption cross-section for chlorophyll a and have illustrated that large departures from constancy exist not only for several distinct species of chlorophyll-bearing cells, but also for variations (cell size, cell structure, cell stability, etc.) within the cells of the same species.

A typical representation of the vast discrepancies that exist among various determinations of a_{Chl} is shown in Figure 46 wherein are plotted not only the apparently conflicting results of the current work, but also the results of other workers. Several features are immediately evident from the limited data shown in Figure 46:

a) There is, in general, reasonable agreement concerning the absorption peak at the red end of the visible spectrum (although our earlier work (Bukata et al. 1981(a)) along with the work of other investigators concerning the NIMBUS-G satellite bands failed to extract a significant peak at these wavelengths)

b) Very large departures from constancy are observed at the blue end of the spectrum, as is the existence of a possible absorption peak near 450 nm. Notice that the absorption curve resulting from the first data set in Lake Ontario (Curve B) displays a distinct absorption peak in the blue, while the absorption curve resulting from the second data set in Lake Ontario (curve C) does not.

c) The various curves illustrated in Figure 46 display variable rising and falling slopes. As discussed earlier, such variable slopes may dramatically impact the shape of experimentally measured subsurface irradiance profiles.

d) The Lake Ontario curve C illustrated in the figure appears to be a lower-limit envelope to the plotted data. This is, in fact, not a valid conclusion since many other workers (data not shown) have obtained smaller values of a_{Chl} than comprise curve C, just as values of a_{Chl} larger than those comprising curve A' have likewise been observed.

The difficulties encountered in the prediction of chlorophyll a from optical measurements and methodologies may be readily appreciated from a consideration of Figure 46. These difficulties notwithstanding, however, the results of this investigation do appear somewhat encouraging. Lake Ontario displays a high degree of optical complexity, and while Lake Ontario may be very representative of optically complex waters, it is not necessarily representative of the majority of inland water masses. A four-component optical model (even with inherent uncertainties in the per unit absorption and scattering properties of the chlorophyll-bearing components) has been shown to possess the capability of predicting to within a factor of two simultaneous concentrations of chlorophyll, suspended mineral and dissolved organic carbon in Lake Ontario. It is certainly reasonable to conclude that such predictability might be dramatically improved for less optically complex waters.

APPENDIX I
Glossary of Terms

Quantity of Radiant Energy, Q. The quantity of energy transferred by radiation.

Q in joules (J)

Radiant Flux, ϕ. The rate of flow of radiant energy.

$$\phi = \frac{Q}{t} \text{ in watts (W)}$$

Radiant Intensity, I. The flux radiated from an element of surface per unit solid angle $\partial\omega$.

$$I = \frac{\partial\phi}{\partial\omega} \quad \text{in W sr}^{-1}$$

Radiance, L. The radiant flux per unit of solid angle $\partial\omega$ per unit of projected area $\partial A \cos\Theta$ where ∂A is the unit of surface area and Θ is the angle between the incident radiant flux and the normal to the surface area.

$$L = \frac{\partial^2\phi}{\partial A \cos\Theta \, \partial\omega} \quad \text{in W m}^{-2}\text{sr}^{-1}$$

Irradiance, E. The radiant flux per unit of area ∂A.

$$E = \frac{\partial\phi}{\partial A} \quad \text{in W m}^{-2}$$

Downwelling Irradiance, $E_d = \int_{\phi=0}^{2\pi} \int_{\Theta=0}^{\pi/2} L(\Theta,\phi) \cos\Theta \, \partial\omega$

Upwelling Irradiance, $E_u = \int_{\phi=0}^{2\pi} \int_{\Theta=\pi/2}^{\pi} L(\Theta,\phi) \cos\Theta \, \partial\omega$

where $\Theta = 0$ indicates the downward normal direction.

Absorption Coefficient, a. The fraction of radiant energy absorbed from a collimated beam per unit distance ∂x.

$$a = \frac{-(\partial\phi)\text{abs}}{\phi\partial x} \quad \text{in m}^{-1}$$

Scattering Coefficient, b. The fraction of radiant energy scattered from a collimated beam per unit distance ∂x.

$$b = \frac{-(\partial\phi)scat}{\phi\partial x} \quad \text{in } m^{-1}$$

Total Attenuation Coefficient, c. The fraction of radiant energy removed from a beam per unit distance ∂x due to the combined processes of both absorption and scattering.

$$c = -\left[\frac{(\partial\phi)_{abs} + (\partial\phi)_{scat}}{\phi\partial x}\right]$$

$$= a+b \qquad \text{in } m^{-1}$$

Scattering Albedo, ω_o. The number of scattering interactions expressed as a fraction of the total number of interactions.

$$\omega_o = \frac{b}{c}$$

Volume Scattering Function, $\beta(\theta)$. The scattered radiant intensity in a direction θ per unit scattering volume ∂V normalized to the incident irradiance E.

$$\beta(\theta) = \frac{\partial I(\theta)}{E\partial V} \quad \text{in } m^{-1}\ sr^{-1}$$

Appropriate integrations of $\beta(\theta)$ provide mathematical definitions of the scattering, forwardscattering, and backscattering coefficients.

Forwardscattering Probability, F. The ratio of the scattering into the foward hemisphere (i.e. the hemisphere ahead of the interaction) to the total scattering into all directions.

$$F = \frac{\int_{\phi=0}^{2\pi}\int_{\theta=0}^{\pi/2}\beta(\theta)\partial\omega}{\int_{\phi=0}^{2\pi}\int_{\theta=0}^{\pi}\beta(\theta)\partial\omega}$$

Backscattering Probability, B. The ratio of the scattering into the backward hemisphere (i.e. the hemisphere behind the interaction) to the total scattering into all directions.

$$B = \frac{\int_{\phi=0}^{2\pi}\int_{\theta=\pi/2}^{\pi}\beta(\theta)\partial\omega}{\int_{\phi=0}^{2\pi}\int_{\theta=0}^{\pi}\beta(\theta)\partial\omega}$$

Fowardscattering coefficient, $Fb = \int_{\phi=0}^{2\pi} \int_{\theta=0}^{\pi/2} \beta(\theta)\,\partial\omega$ in m^{-1}

Backscattering coefficient, $Bb = \int_{\phi=0}^{2\pi} \int_{\theta=\pi/2}^{\pi} \beta(\theta)\,\partial\omega$ in m^{-1}

Scattering coefficient, $b = \int_{\phi=0}^{2\pi} \int_{\theta=0}^{\pi} \beta(\theta)\,\partial\omega$ in m^{-1}

where $b = Fb + Bb$.

Volume Reflectance (Irradiance Ratio or Irradiance Reflectance, or Diffuse Reflectance), R. The ratio of the upwelling irradiance to the downwelling irradiance at any point.

$$R = \frac{E_u}{E_d}$$

Irradiance Attenuation Coefficient, K. The logarithmic depth-derivative of the downwelling irradiance at depth z.

$$K(z) = \frac{1}{E_d(z)} \left[\frac{\partial E_d(z)}{\partial z}\right] \text{ in } m^{-1}$$

Scalar Irradiance, E_0. The integral over all directions of the radiance distribution at a point.

$$E_0 = \int_{\phi=0}^{2\pi} \int_{\theta=0}^{\pi} L(\theta,\phi)\,\partial\omega \text{ in } W\,m^{-2}$$

Downwelling Scalar Irradiance, E_{0d}.

$$E_{0d} = \int_{\phi=0}^{2\pi} \int_{\theta=0}^{\pi/2} L(\theta,\phi)\,\partial\omega \text{ in } W\,m^{-2}$$

Downwelling Distribution Function, D_d. The ratio of the downwelling scalar irradiance at depth z to the downwelling irradiance at that depth.

$$D_d(z) = \frac{E_{0d}(z)}{E_d(z)}$$

Table I. Fifteen Point Absorption and Backscatter Cross Section Spectra Utilized with Equations 6 and 7 of this Report.

Wavelength (Nanometres)	a_w	a^1_{CHL}	a^2_{CHL}	a_{SM}	a_{DOC}	$(Bb)_w$	$(Bb)_{CHL}$	$(Bb)_{SM}$
410	.03800	.03780	.02428	.13350	.14500	.00229	.00136	.05240
430	.02600	.04050	.02188	.13510	.12100	.00186	.00125	.04992
450	.01700	.04100	.01938	.13090	.10000	.00152	.00119	.04816
470	.01700	.04020	.01817	.11680	.08290	.00128	.00116	.04760
490	.02100	.03550	.01586	.10340	.06880	.00108	.00117	.04736
510	.02600	.03040	.01341	.09220	.05700	.00091	.00120	.04712
530	.03000	.02360	.00855	.08340	.04800	.00077	.00125	.04680
550	.03700	.01900	.00584	.07370	.04010	.00066	.00128	.04688
570	.05700	.01730	.00550	.06380	.03330	.00058	.00127	.04696
590	.11200	.01500	.00296	.06110	.02790	.00050	.00124	.04616
610	.23600	.01250	.00518	.06740	.02340	.00044	.00125	.04408
630	.27400	.01200	.01814	.07660	.01950	.00038	.00122	.04160
650	.30300	.01600	.02231	.08350	.01620	.00033	.00116	.03920
670	.37000	.02600	.02721	.08730	.01520	.00030	.00109	.03680
690	.46300	.01300	.01716	.09270	.01050	.00026	.00099	.03408

a^1_{CHL} is the chlorophyll absorption cross-section represented by Curve B of Figure 46.

a^2_{CHL} is the chlorophyll absorption cross-section represented by Curve C of Figure 46.

REFERENCES

1. Bukata, R.P., Jerome, J.H., Bruton, J.E., and Jain, S.C. (1979), "Determination of Inherent Optical Properites of Lake Ontario Coastal Waters", Appl. Opt., 18, 3926-3932.

2. Bukata, R.P., Jerome, J.H., Bruton, J.E., Jain, S.C., and Zwick, H.H. (1981a), "Optical Water Quality Model of Lake Ontario. 1: Determination of the Optical Cross-Sections of Organic and Inorganic Particulates in Lake Ontario", Appl. Opt. 20, 1696-1703.

3. Bukata, R.P., Bruton, J.E., Jerome, J.H., Jain, S.C., and Zwick, H.H. (1981b), "Optical Water Quality Model of Lake Ontario. 2: Determination of Chlorophyll a and Suspended Mineral Concentrations of Natural Waters from Submersible and Low Altitude Optical Sensors", Appl. Opt., 20, 1704-1714.

4. Bukata, R.P., Jerome, J.H., and Bruton, J.E. (1981c), "Validation of a Five-Component Optical Model for Estimating Chlorophyll a and Suspended Mineral Concentrations in Lake Ontario", Appl. Opt., 20, 3472-3474.

5. Burns, N.M. (1980), Canada Centre for Inland Waters, private communication.

6. DiToro, D.M. (1978), "Optics of Turbid Estuarine Waters: Approximations and Applications", Water Research, 12, 1059-1068.

7. Doerffer, V.R. (1979), "The Distribution of Substances in the Elfe-Estuary Determined by Remote Sensing", Arch. Hydrobiol. 43, 119-224.

8. Gordon, H.R., Brown, O.B., and Jacobs, M.M. (1975), "Computed Relationships Between the Inherent and Apparent Optical Properties of a Flat Homogeneous Ocean", Appl. Opt. 14, 417-427.

9. Hulburt, E.O. (1945), "Optics of Distilled and Natural Water", J. Opt. Soc. Am., 35, 698-705.

10. IMSL (1980), The IMSL Library Reference Manual, Edition 8 (revised June 1980), International Mathematical and Statistical Libraries, Inc., Houston.

11. Jain, S.C., Zwick, H.H., McColl, W.D., Bukata, R.P., and Jerome, J.H. (1980), "Combined Coastal Zone Color Scanner (CZCS), Aircraft, and In-Situ Water Quality Remote Sensing Experiment in Lake Ontario", Proc. Soc. Photo-Op Instrum. Eng. 208, 178-188.

12. Jerome, J.H., Bruton, J.E., and Bukata, R.P. (1982), "Influence of Scattering Phenomena on the Solar Zenith Angle Dependence of In-Water Irradiance Levels", Appl. Opt., 21, 642-647.

13. Kiefer, D.A., Olson, R.J. and Wilson, W.H. (1979), "Reflectance Spectroscopy of Marine Phytoplankton: Part 1. Optical Properties as Related to Age and Growth Rate", Limnol. Oceanogr. 24, 664-672.

14. Levenberg, K. (1944), "A method for the Solution of Certain Non-linear Problems in Least Squares", Quant. Appl. Math. 2, 164-168.

15. Marquardt, D.W. (1963), "An Algorithm for Least-Squares Estimation of Nonlinear Parameters", J. SIAM, 11(2).

16. Moniteq Ltd. (1981), "Water Quality Remote Sensing Report, Appendices, DSS Contract number 19SQ.23413-8-1345, Table B.3.2, p 22.

17. Morel, A. and Bricaud, A. (1981), "Theoretical Results Concerning Light Absorption in a Discrete Medium, and Application to Specific Absorption of Phytoplankton", Deep Sea Res., 11, 1375-1393.

18. Morel, A. and Prieur, L. (1977), "Analysis of Variations in Ocean Color", Limnol. Oceanogr. 22, 709-722.

19. Yentsch, C.S. (1960), "The Influence of Phytoplankton Pigments on the Color of Sea Water", Deep Sea Res., 7, 1-9.

20. Zwick, H.H., Jain, S.C. and Bukata, R.P. (1980), "A Satellite/Airborne and In-Situ Water Quality Experiment in Lake Ontario", Proc. ISPRA Workshop on EURASEP Ocean Color Scanner Exp., 181-198.

FIGURE CAPTIONS

Figure 1. Flow diagram outlining the operations employed in the development of subsurface optical water quality methodology.

Figure 2. The calculated absorption cross-sections for chlorophyll *a* uncorrected for phaeophytin contamination (Chl a_{unc}), total suspended mineral (SM), and dissolved organic carbon (DOC). Also shown are the absorption coefficients for pure water.

Figure 3. The calculated scattering cross-sections for chlorophyll *a* uncorrected for phaeophytin contamination (Chl a_{unc}) and total suspended mineral (SM). Also shown are the scattering coefficients for pure water.

Figure 4. Subsurface irradiance reflectance spectra for various chlorophyll *a* concentrations in a water mass for which the suspended mineral and dissolved organic carbon concentrations are kept fixed at zero.

Figure 5. Subsurface irradiance reflectance spectra for various chlorophyll *a* concentrations in a water mass for which the dissolved organic carbon concentration is kept fixed at zero and the total suspended mineral concentration is kept fixed at 0.10 g m^{-3}.

Figure 6. Subsurface irradiance reflectance spectra for various chlorophyll *a* concentrations in a water mass for which the dissolved organic carbon concentration is kept fixed at zero and the total suspended mineral concentration is kept fixed at 0.20 g m^{-3}.

Figure 7. Subsurface irradiance reflectance spectra for various chlorophyll *a* concentrations in a water mass for which the dissolved organic carbon concentration is kept fixed at zero and the total suspended mineral concentration is kept fixed at 0.50 g m^{-3}.

Figure 8. Subsurface irradiance reflectance spectra for various chlorophyll *a* concentrations in a water mass for which the dissolved organic carbon concentration is kept fixed at zero and the total suspended mineral concentration is kept fixed at 1.0 g m^{-3}.

Figure 9. Subsurface irradiance reflectance spectra for various chlorophyll *a* concentrations in a water mass for which the dissolved organic carbon concentration is kept fixed at zero and the total suspended mineral concentration is kept fixed at 2.0 g m^{-3}.

Figure 10. Subsurface irradiance reflectance spectra for various chlorophyll *a* concentrations in a water mass for which the dissolved organic carbon concentration is kept fixed at zero and the total suspended mineral concentration is kept fixed at 5.0 g m^{-3}.

Figure 11. Subsurface irradiance reflectance spectra for various chlorophyll *a* concentrations in a water mass for which the dissolved organic carbon concentration is kept fixed at zero and the total suspended mineral concentration is kept fixed at 10.0 g m^{-3}.

Figure 12. Subsurface irradiance reflectance spectra for various chlorophyll *a* concentrations in a water mass for which the dissolved organic carbon concentration is kept fixed at zero and the total suspended mineral concentration is kept fixed at 20.0 g m^{-3}.

Figure 13. Subsurface irradiance reflectance spectra for various suspended mineral concentrations in a water mass containing a small fixed concentration of chlorophyll *a* and zero dissolved organic carbon.

Figure 14. Subsurface irradiance reflectance spectra for various suspended mineral concentrations in a water mass containing a large fixed concentration of chlorophyll *a* and zero dissolved organic carbon.

Figure 15. Subsurface irradiance reflectance spectra for various dissolved organic carbon concentration in a water mass for which the suspended mineral concentration is kept fixed at 0.05 g m^{-3} and the chlorophyll *a* concentration is kept fixed at 1.0 mg m^{-3}.

Figure 16. Subsurface irradiance reflectance spectra for various dissolved organic carbon concentrations in a water mass containing a large fixed concentration of chlorophyll *a* (10.0 mg m^{-3}) and a small fixed concentration of suspended mineral (0.05 gm^{-3}).

Figure 17. Subsurface irradiance reflectance spectra for various dissolved organic carbon concentrations in a water mass containing a small fixed concentration of chlorophyll *a* (0.05 mg m^{-3}) and a large fixed concentration of suspended mineral (10.0 gm^{-3}).

Figure 18. Subsurface irradiance reflectance spectra for various chlorophyll *a* concentrations in a water mass for which the dissolved organic carbon concentration is kept fixed at 2.0 g carbon m^{-3} and the total suspended mineral concentration is kept fixed at zero.

Figure 19. Subsurface irradiance reflectance spectra for various suspended mineral concentrations in a water mass for which the dissolved organic carbon concentration is kept fixed at 2.0 g carbon m^{-3} and the chlorophyll *a* concentration is kept fixed at 0.05 mg m^{-3}.

Figure 20. Subsurface irradiance reflectance spectra for various suspended mineral concentrations in a water mass for which the dissolved organic carbon concentration is kept fixed at 2.0 g carbon m^{-3} and the chlorophyll *a* concentration is kept fixed at 10.0 mg m^{-3}.

Figure 21. Subsurface irradiance reflectance spectra for various chlorophyll *a* and suspended mineral concentrations in a water mass for which the dissolved organic carbon concentration is kept fixed at 2.0 g carbon m^{-3}.

Figure 22. Subsurface irradiance reflectance spectra for various chlorophyll *a* and suspended mineral concentrations in a water mass for which the dissolved organic carbon concentration is kept fixed at 10.0 g carbon m^{-3}.

Figure 23. Relationship between subsurface irradiance reflectance at 450 nm (blue) and chlorophyll *a* concentration for a water mass in which the dissolved organic carbon concentration is kept fixed at 2.0 g carbon m^{-3} and the suspended $mineral_3$ concentration is allowed to vary between zero and 10 g m^{-3}.

Figure 24. Relationship between subsurface irradiance reflectance at 570 nm (green) and chlorophyll *a* concentration for a water mass in which the dissolved organic carbon concentration is kept fixed at 2.0 g carbon m^{-3} and the suspended mineral concentration is allowed to vary between zero and 10 g m^{-3}.

Figure 25. Relationship between subsurface irradiance reflectance at 650 nm (red) and chlorophyll *a* concentration for a water mass in which the dissolved organic carbon concentration is kept fixed at 2.0 g carbon m^{-3} and the suspended $mineral_3$ concentration is allowed to vary between zero and 10 g m^{-3}.

Figure 26. Relationship between subsurface irradiance reflectance at 450 nm (blue) and suspended mineral concentration for several discrete values of chlorophyll *a* concentration in a water mass for which the dissolved organic carbon concentration is kept fixed at 2.0 g carbon m^{-3}.

Figure 27. Relationship between subsurface irradiance reflectance at 450 nm (blue) and suspended mineral concentration for a water mass in which the dissolved organic carbon concentration is allowed to vary between zero and 5 g carbon m^{-3} and the chlorophyll a concentration is allowed to vary between 0.05 and 20.0 mg m^{-3}.

Figure 28. Relationship between subsurface irradiance reflectance at 570 nm (green) and suspended mineral concentration for several discrete values of chlorophyll a concentration in a water mass for which the dissolved organic carbon concentration is kept fixed at 2.0 g carbon m^{-3}.

Figure 29. Relationship between subsurface irradiance reflectance at 570 nm (green) and suspended mineral concentration for a water mass in which the dissolved organic carbon concentration is allowed to vary between zero and 5 g carbon m^{-3} and the chlorophyll a concentration is allowed to vary between 0.05 and 20.0 mg m^{-3}.

Figure 30. Relationship between subsurface irradiance reflectance at 650 nm (red) and suspended mineral concentration for several discrete values of chlorophyll a concentration in a water mass for which the dissolved organic carbon concentration is kept fixed at 2.0 g carbon m^{-3}.

Figure 31. Relationship between subsurface irradiance reflectance at 650 nm (red) and suspended mineral concentration for a water mass in which the dissolved organic carbon concentration is allowed to vary between zero and 5 g carbon m^{-3} and the chlorophyll a concentration is allowed to vary between 0.05 and 20.0 mg m^{-3}.

Figure 32. Relationship between subsurface irradiance reflectance at 650 nm (red) and suspended mineral concentration for a water mass in which the dissolved organic carbon concentration is allowed to vary between zero and 5 g carbon m^{-3} and the chlorophyll a concentration is allowed to vary between 0.05 and 5.0 mg m^{-3}.

Figure 33. Comparison between predicted and directly measured suspended mineral concentrations (using the cross-sections of Figures 2 and 3).

Figure 34. Comparison between predicted and directly measured dissolved organic carbon concentrations (using the cross-sections of Figures 2 and 3).

Figure 35. Comparison between predicted and directly measured chlorophyll a concentrations (using the cross-sections of Figures 2 and 3).

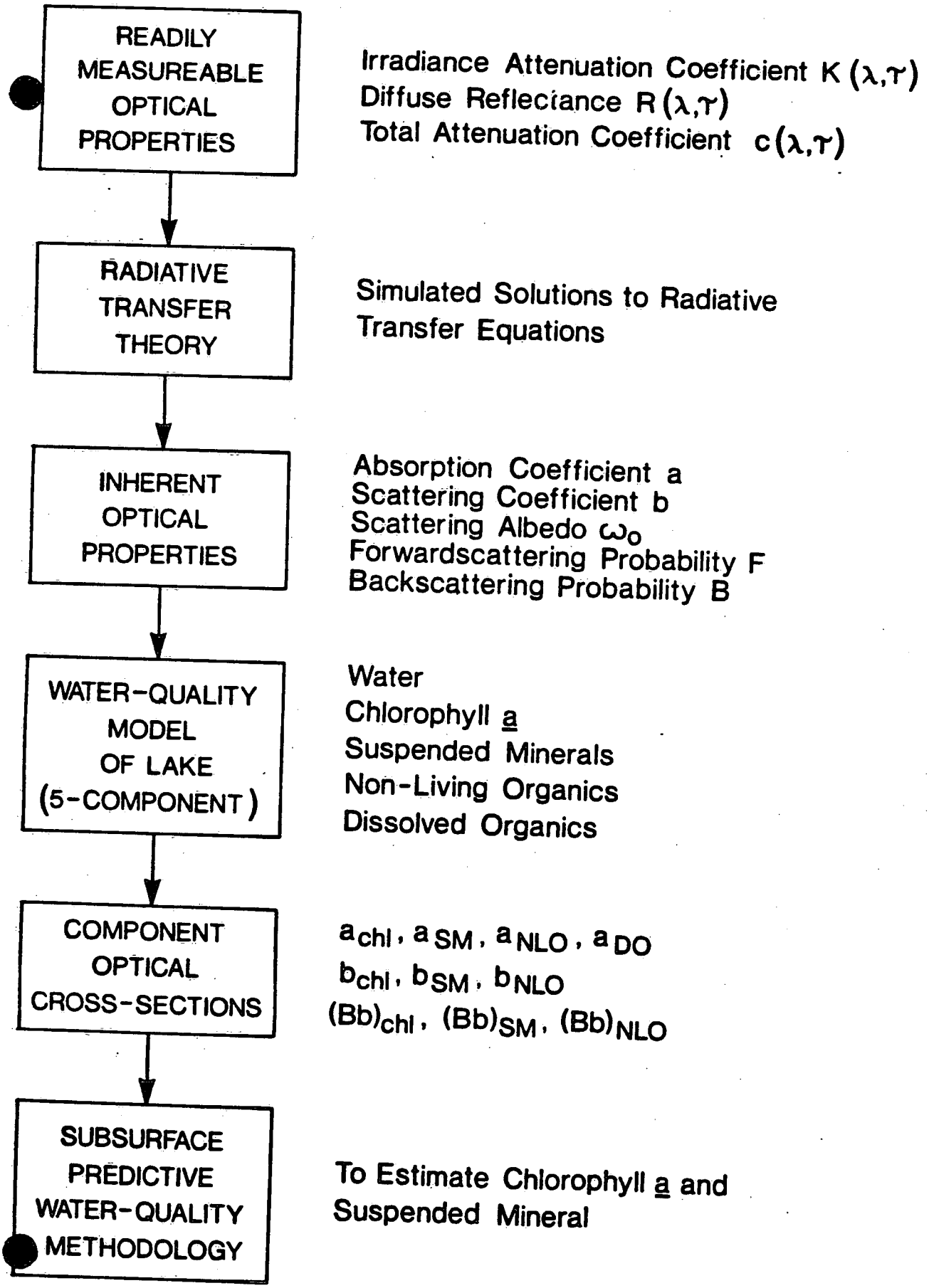
READILY MEASUREABLE OPTICAL PROPERTIES
Irradiance Attenuation Coefficient K (λ,τ)
Diffuse Reflectance R (λ,τ)
Total Attenuation Coefficient c (λ,τ)
RADIATIVE TRANSFER THEORY
Simulated Solutions to Radiative Transfer Equations
INHERENT OPTICAL PROPERTIES
Absorption Coefficient a
Scattering Coefficient b
Scattering Albedo ω0
Forwardscattering Probability F
Backscattering Probability B
WATER-QUALITY MODEL OF LAKE (5-COMPONENT)
Water
Chlorophyll a
Suspended Minerals
Non-Living Organics
Dissolved Organics
COMPONENT OPTICAL CROSS-SECTIONS
achl, aSM, aNLO, aDO
bchl, bSM, bNLO
(Bb)chl, (Bb)SM, (Bb)NLO
SUBSURFACE PREDICTIVE WATER-QUALITY METHODOLOGY
To Estimate Chlorophyll a and Suspended Mineral

FIG. 1

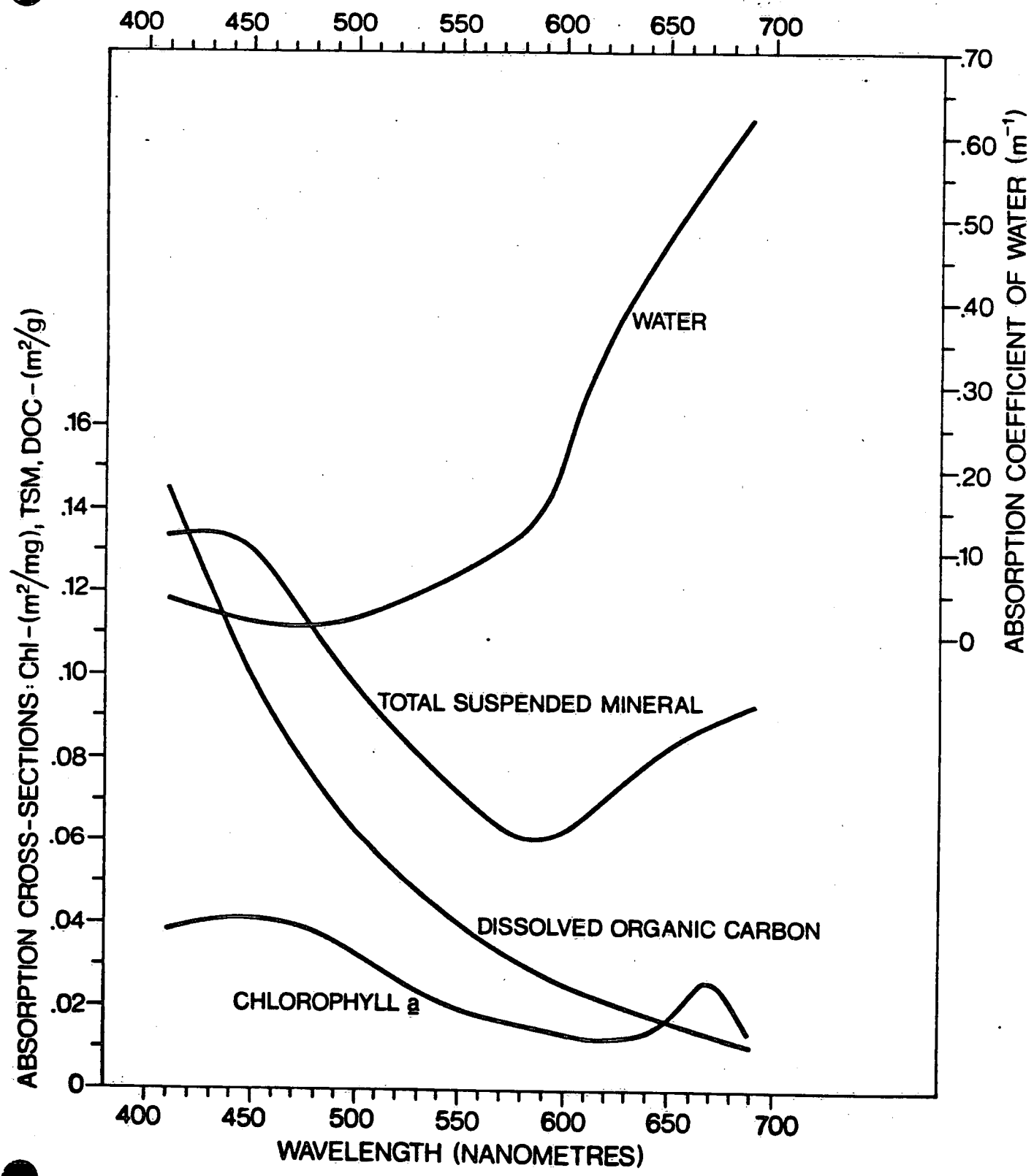
400
450
500
550
600
650
700
.70
.60
.50
.40
.30
.20
.10
0
ABSORPTION COEFFICIENT OF WATER (m^{-1})
WATER
.16
.14
.12
.10
.08
.06
.04
.02
0
ABSORPTION CROSS-SECTIONS: Chl-(m^2/mg), TSM, DOC-(m^2/g)
TOTAL SUSPENDED MINERAL
DISSOLVED ORGANIC CARBON
CHLOROPHYLL a
400
450
500
550
600
650
700
WAVELENGTH (NANOMETRES)

FIG. 2

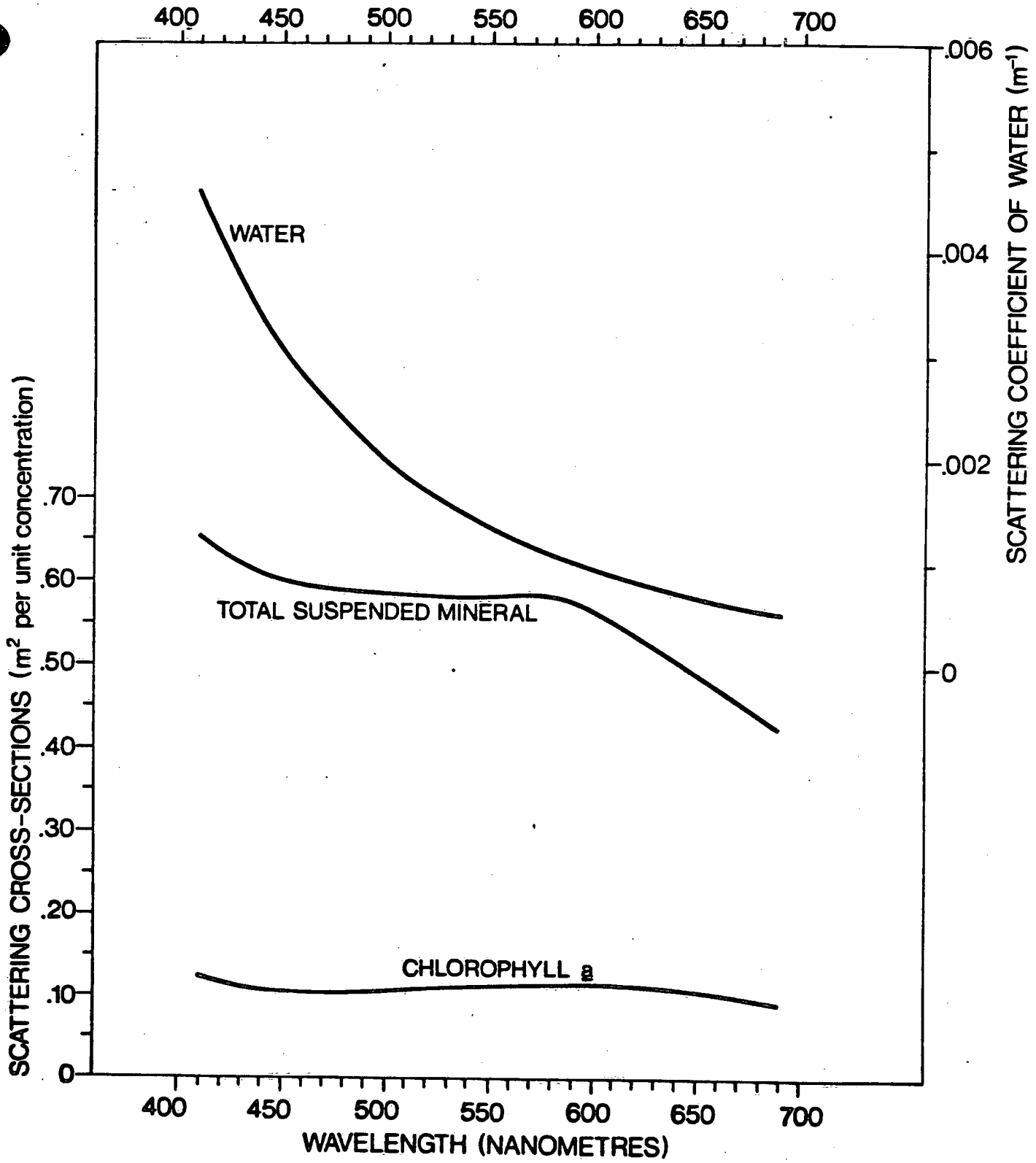
400
450
500
550
600
650
700
.006
.004
.002
0
WATER
TOTAL SUSPENDED MINERAL
CHLOROPHYLL a
SCATTERING COEFFICIENT OF WATER (m⁻¹)
SCATTERING CROSS-SECTIONS (m² per unit concentration)
.70
.60
.50
.40
.30
.20
.10
0
WAVELENGTH (NANOMETRES)

FIG. 3

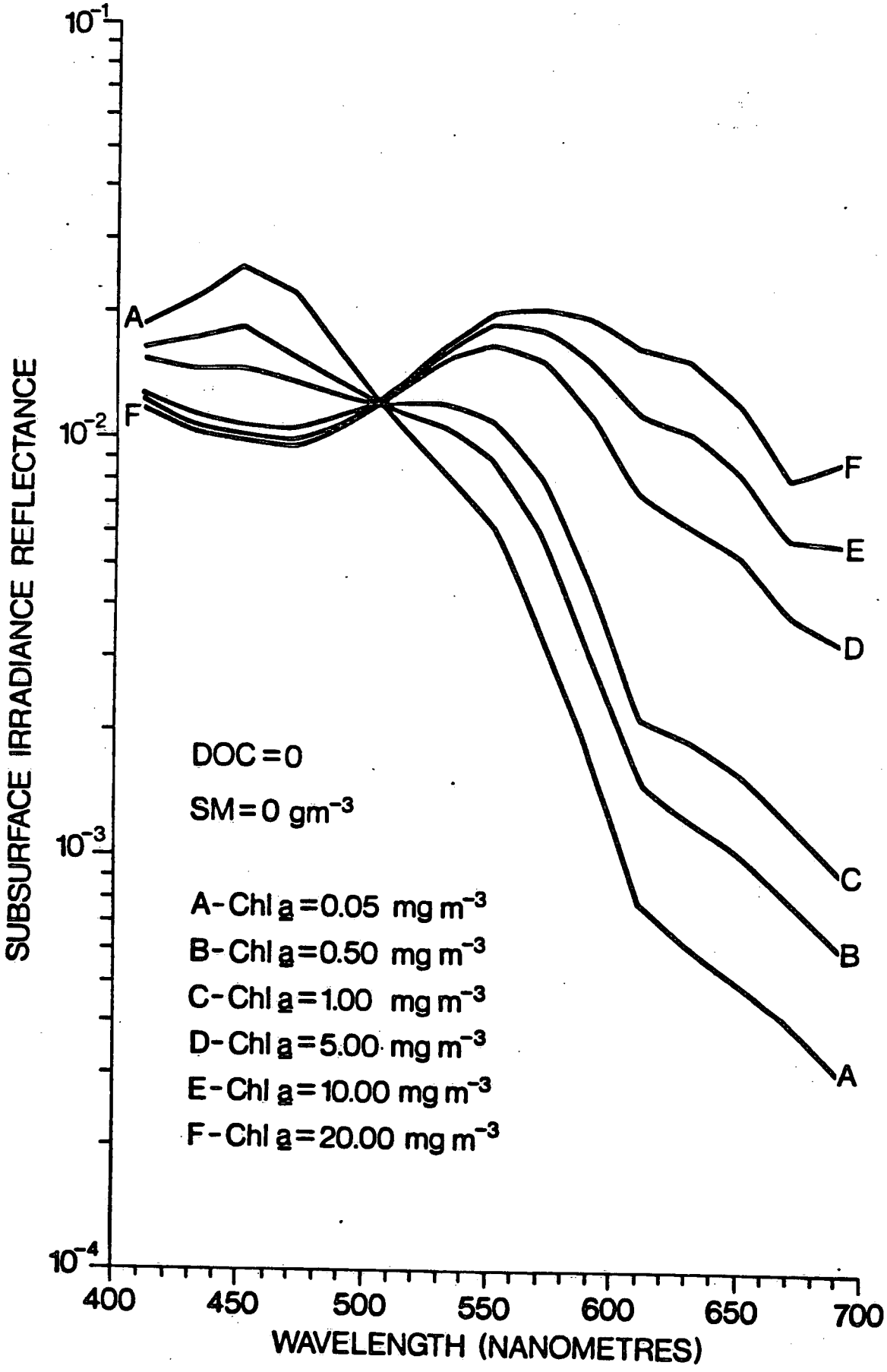
SUBSURFACE IRRADIANCE REFLECTANCE
10^{-1}
10^{-2}
10^{-3}
10^{-4}
400
450
500
550
600
650
700
WAVELENGTH (NANOMETRES)
A
F
F
E
D
C
B
A
DOC = 0
SM = 0 gm^{-3}
A - Chl a = 0.05 mg m^{-3}
B - Chl a = 0.50 mg m^{-3}
C - Chl a = 1.00 mg m^{-3}
D - Chl a = 5.00 mg m^{-3}
E - Chl a = 10.00 mg m^{-3}
F - Chl a = 20.00 mg m^{-3}

FIG. 4

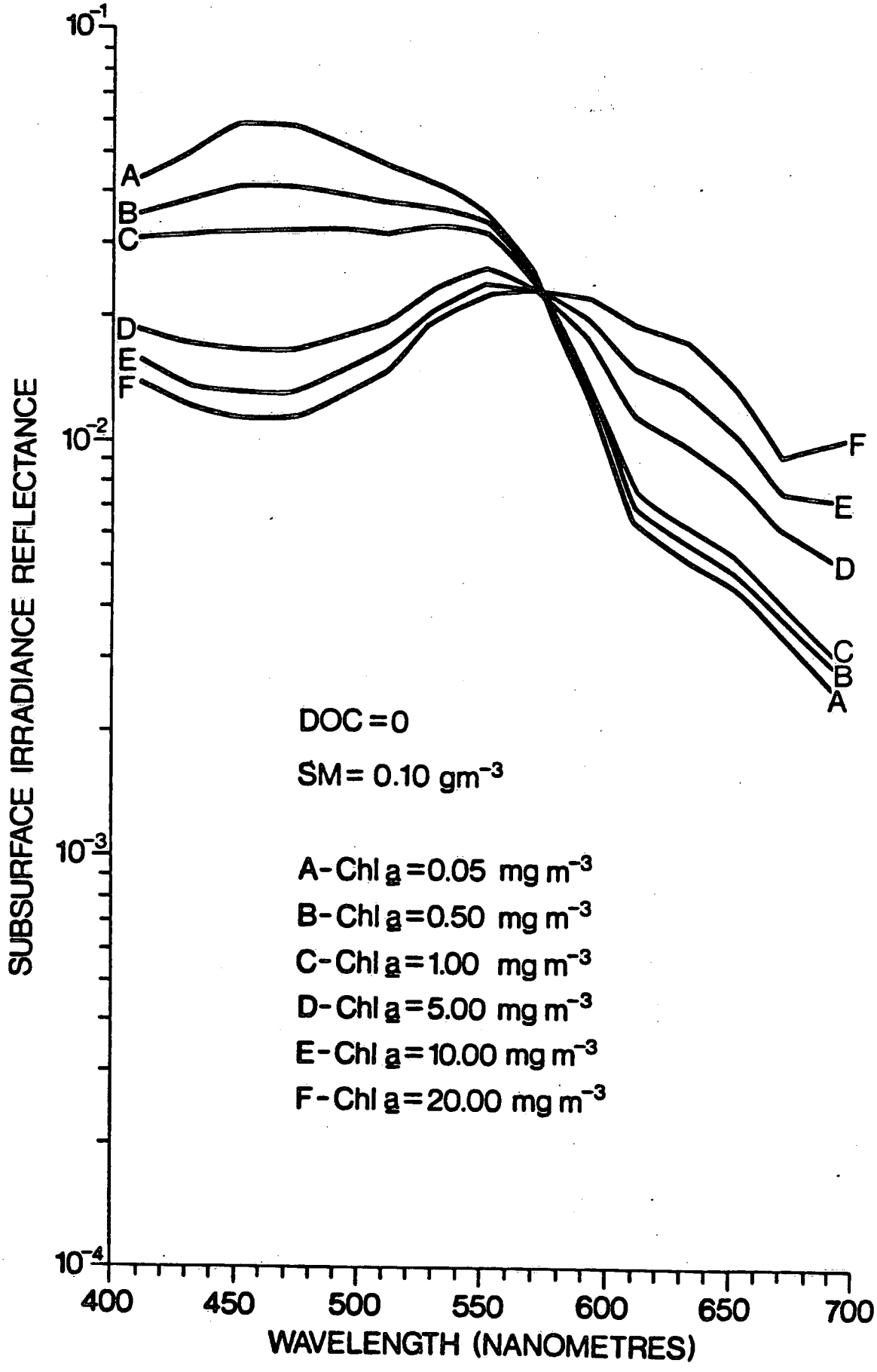
SUBSURFACE IRRADIANCE REFLECTANCE
10^{-1}
10^{-2}
10^{-3}
10^{-4}
A
B
C
D
E
F
DOC = 0
SM = 0.10 gm^{-3}
A - Chl a = 0.05 $mg\ m^{-3}$
B - Chl a = 0.50 $mg\ m^{-3}$
C - Chl a = 1.00 $mg\ m^{-3}$
D - Chl a = 5.00 $mg\ m^{-3}$
E - Chl a = 10.00 $mg\ m^{-3}$
F - Chl a = 20.00 $mg\ m^{-3}$
400
450
500
550
600
650
700
WAVELENGTH (NANOMETRES)

FIG. 5

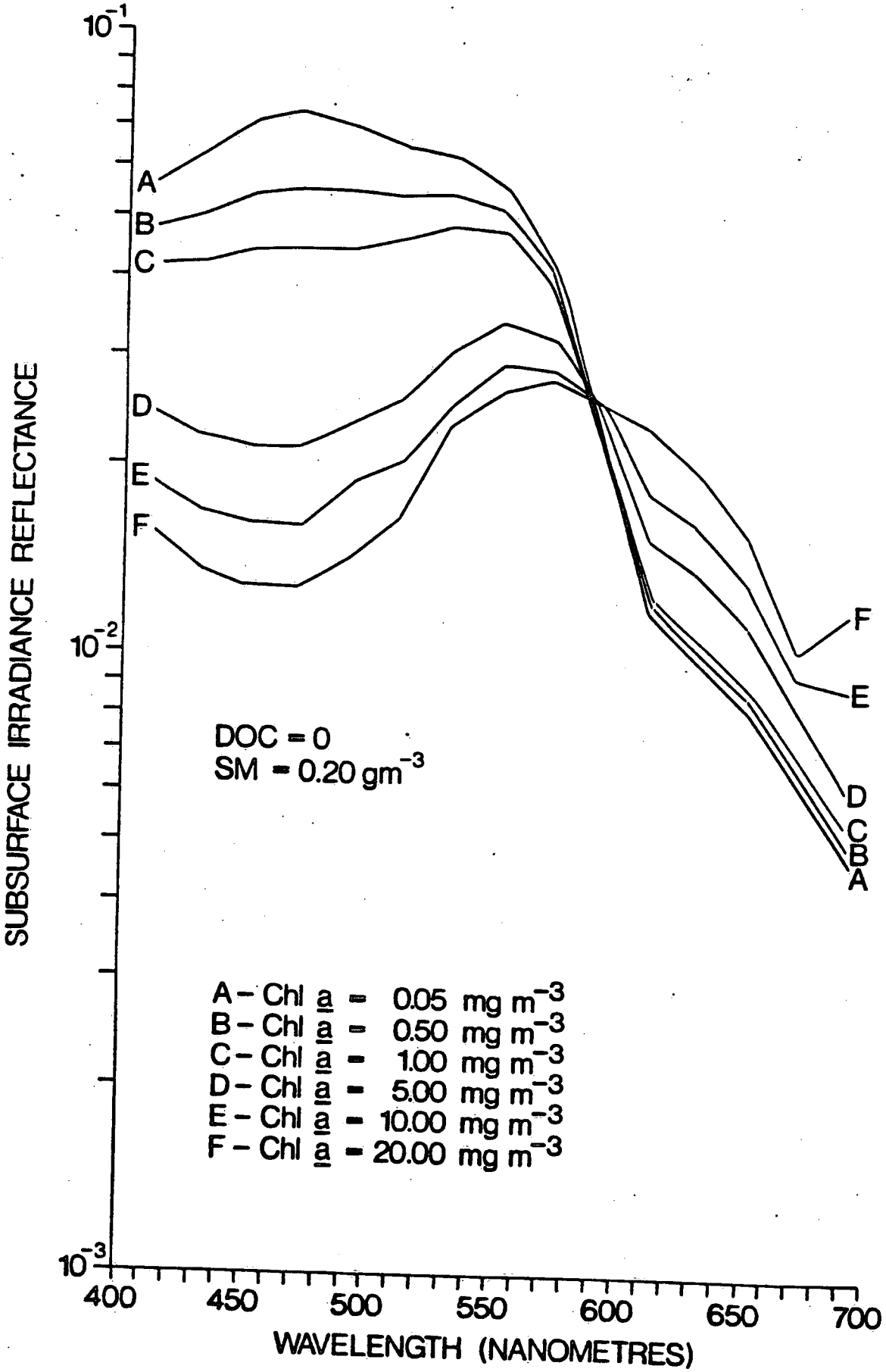
SUBSURFACE IRRADIANCE REFLECTANCE
10^{-1}
10^{-2}
10^{-3}
A
B
C
D
E
F
DOC = 0
SM = 0.20 gm^{-3}
A – Chl a = 0.05 mg m^{-3}
B – Chl a = 0.50 mg m^{-3}
C – Chl a = 1.00 mg m^{-3}
D – Chl a = 5.00 mg m^{-3}
E – Chl a = 10.00 mg m^{-3}
F – Chl a = 20.00 mg m^{-3}
400
450
500
550
600
650
700
WAVELENGTH (NANOMETRES)

FIG. 6

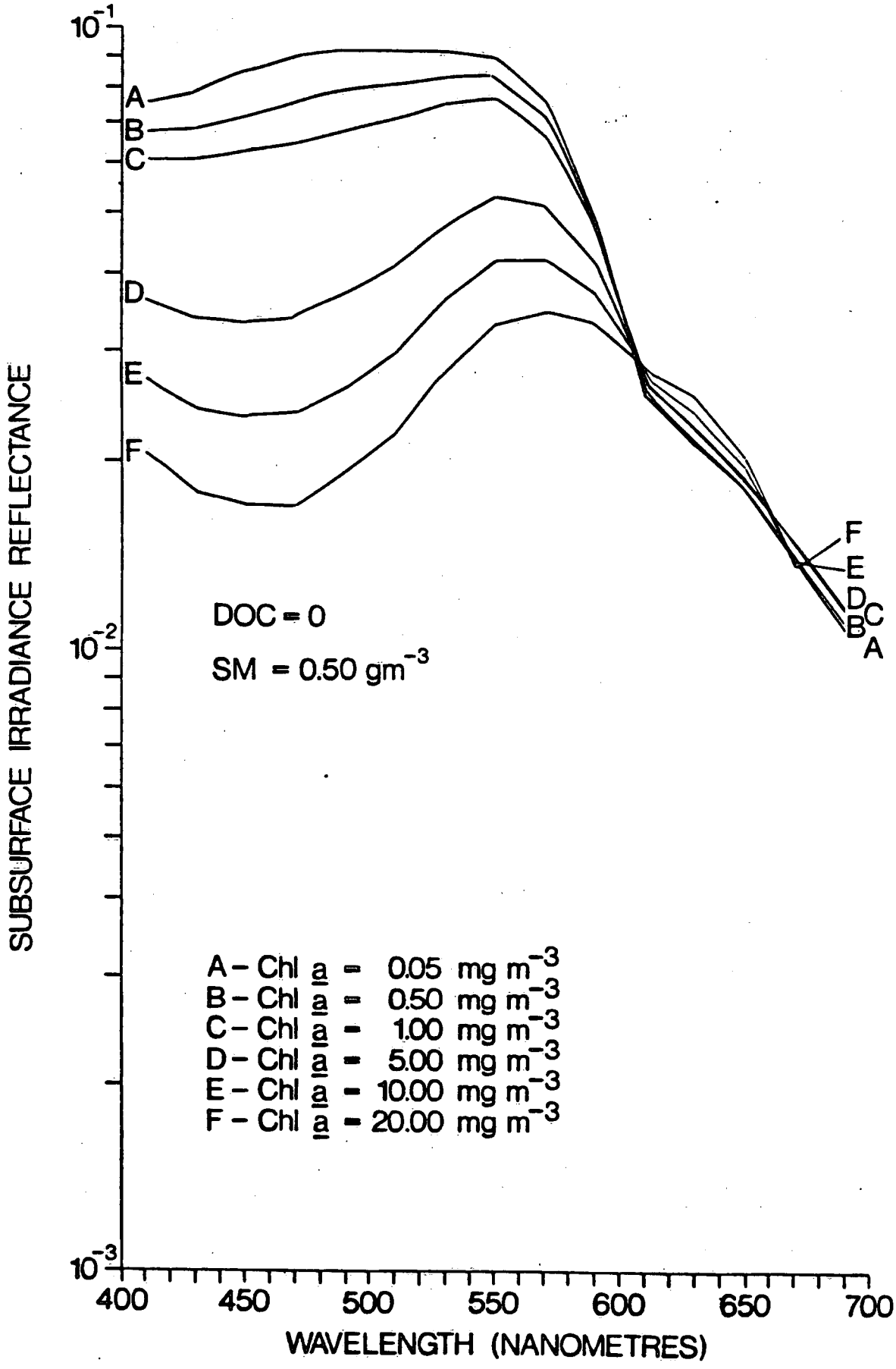
SUBSURFACE IRRADIANCE REFLECTANCE
10^{-1}
10^{-2}
10^{-3}
A
B
C
D
E
F
DOC = 0
SM = 0.50 gm^{-3}
A – Chl a = 0.05 mg m^{-3}
B – Chl a = 0.50 mg m^{-3}
C – Chl a = 1.00 mg m^{-3}
D – Chl a = 5.00 mg m^{-3}
E – Chl a = 10.00 mg m^{-3}
F – Chl a = 20.00 mg m^{-3}
400
450
500
550
600
650
700
WAVELENGTH (NANOMETRES)

FIG. 7

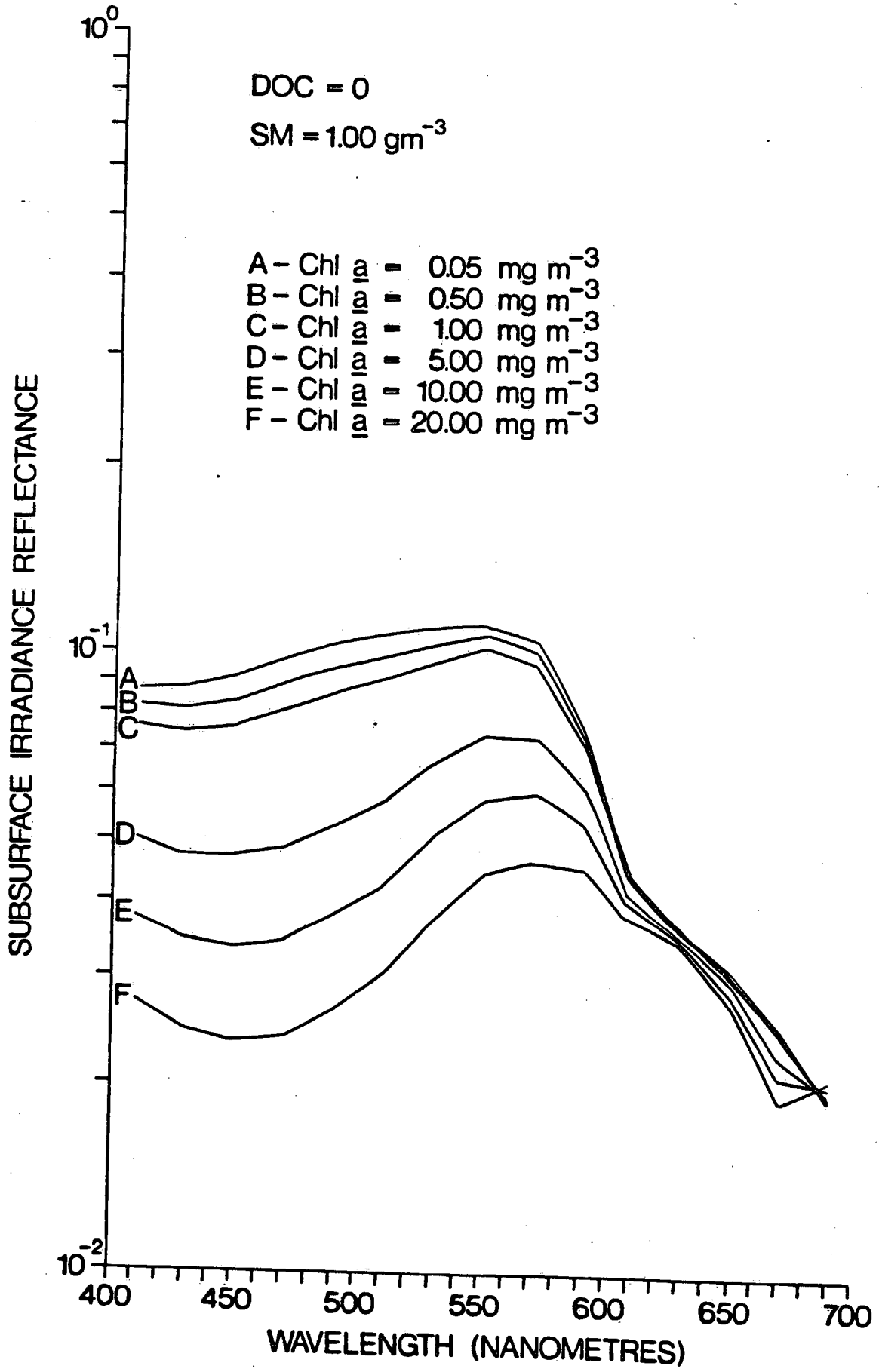
DOC = 0
SM = 1.00 gm^{-3}
A – Chl a = 0.05 mg m^{-3}
B – Chl a = 0.50 mg m^{-3}
C – Chl a = 1.00 mg m^{-3}
D – Chl a = 5.00 mg m^{-3}
E – Chl a = 10.00 mg m^{-3}
F – Chl a = 20.00 mg m^{-3}
SUBSURFACE IRRADIANCE REFLECTANCE
10^{0}
10^{-1}
10^{-2}
A
B
C
D
E
F
400
450
500
550
600
650
700
WAVELENGTH (NANOMETRES)

FIG. 8

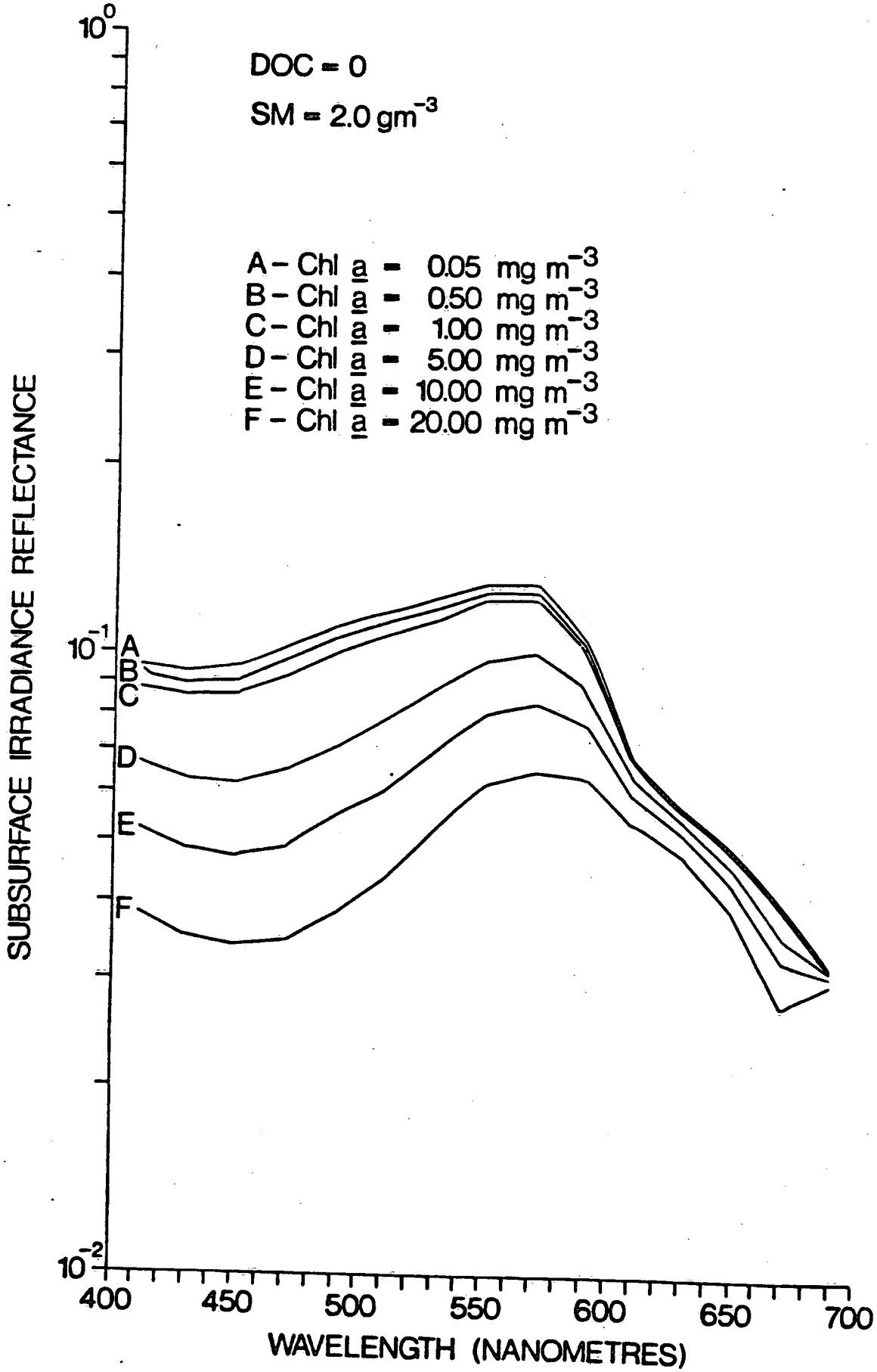
DOC = 0
SM = 2.0 gm^{-3}
A – Chl a = 0.05 mg m^{-3}
B – Chl a = 0.50 mg m^{-3}
C – Chl a = 1.00 mg m^{-3}
D – Chl a = 5.00 mg m^{-3}
E – Chl a = 10.00 mg m^{-3}
F – Chl a = 20.00 mg m^{-3}
SUBSURFACE IRRADIANCE REFLECTANCE
10^{0}
10^{-1}
10^{-2}
A
B
C
D
E
F
400
450
500
550
600
650
700
WAVELENGTH (NANOMETRES)

FIG. 9

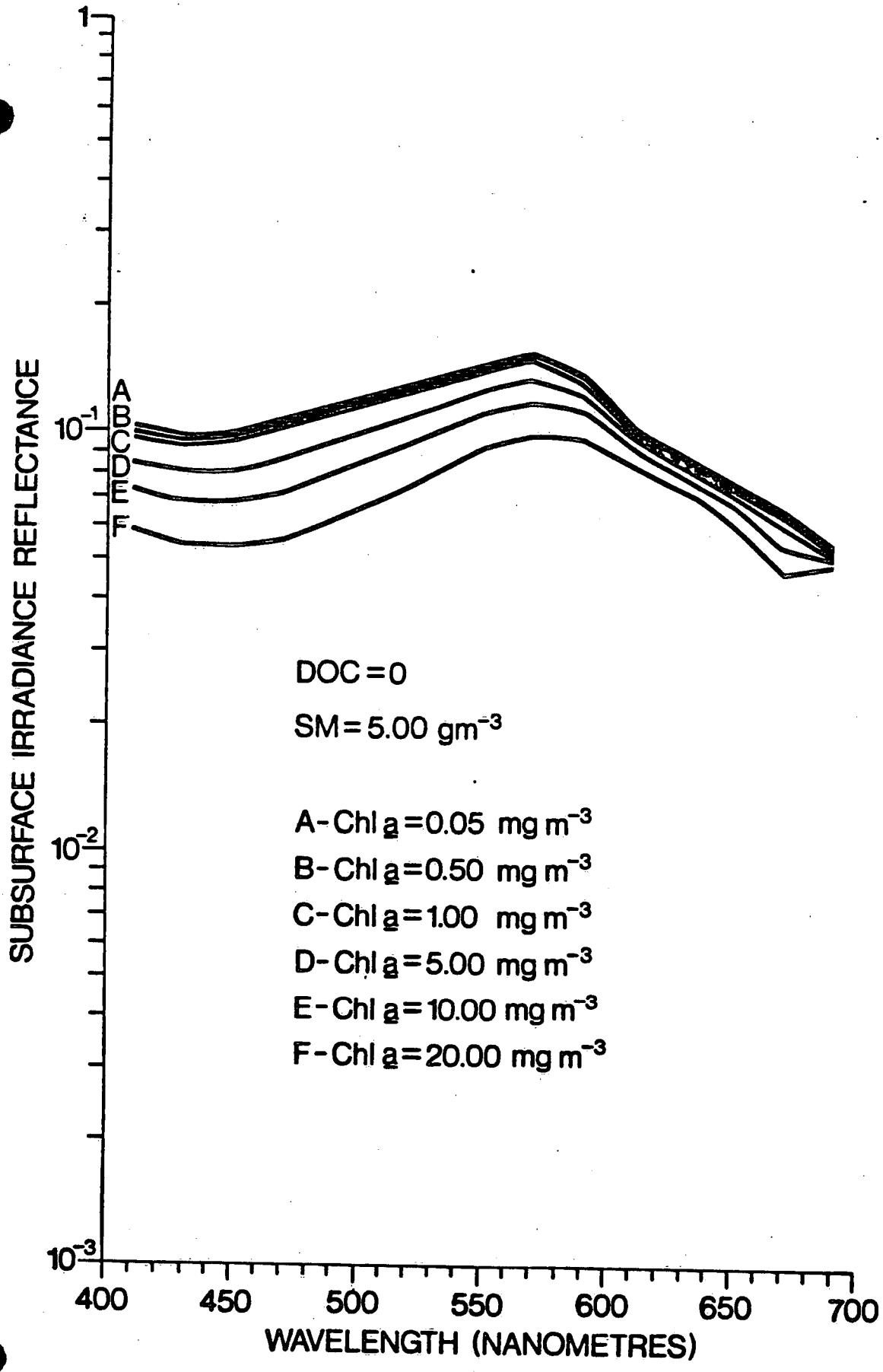
SUBSURFACE IRRADIANCE REFLECTANCE
1
10^{-1}
10^{-2}
10^{-3}
A
B
C
D
E
F
DOC = 0
SM = 5.00 gm^{-3}
A - Chl a = 0.05 $mg\ m^{-3}$
B - Chl a = 0.50 $mg\ m^{-3}$
C - Chl a = 1.00 $mg\ m^{-3}$
D - Chl a = 5.00 $mg\ m^{-3}$
E - Chl a = 10.00 $mg\ m^{-3}$
F - Chl a = 20.00 $mg\ m^{-3}$
400
450
500
550
600
650
700
WAVELENGTH (NANOMETRES)

FIG. 10

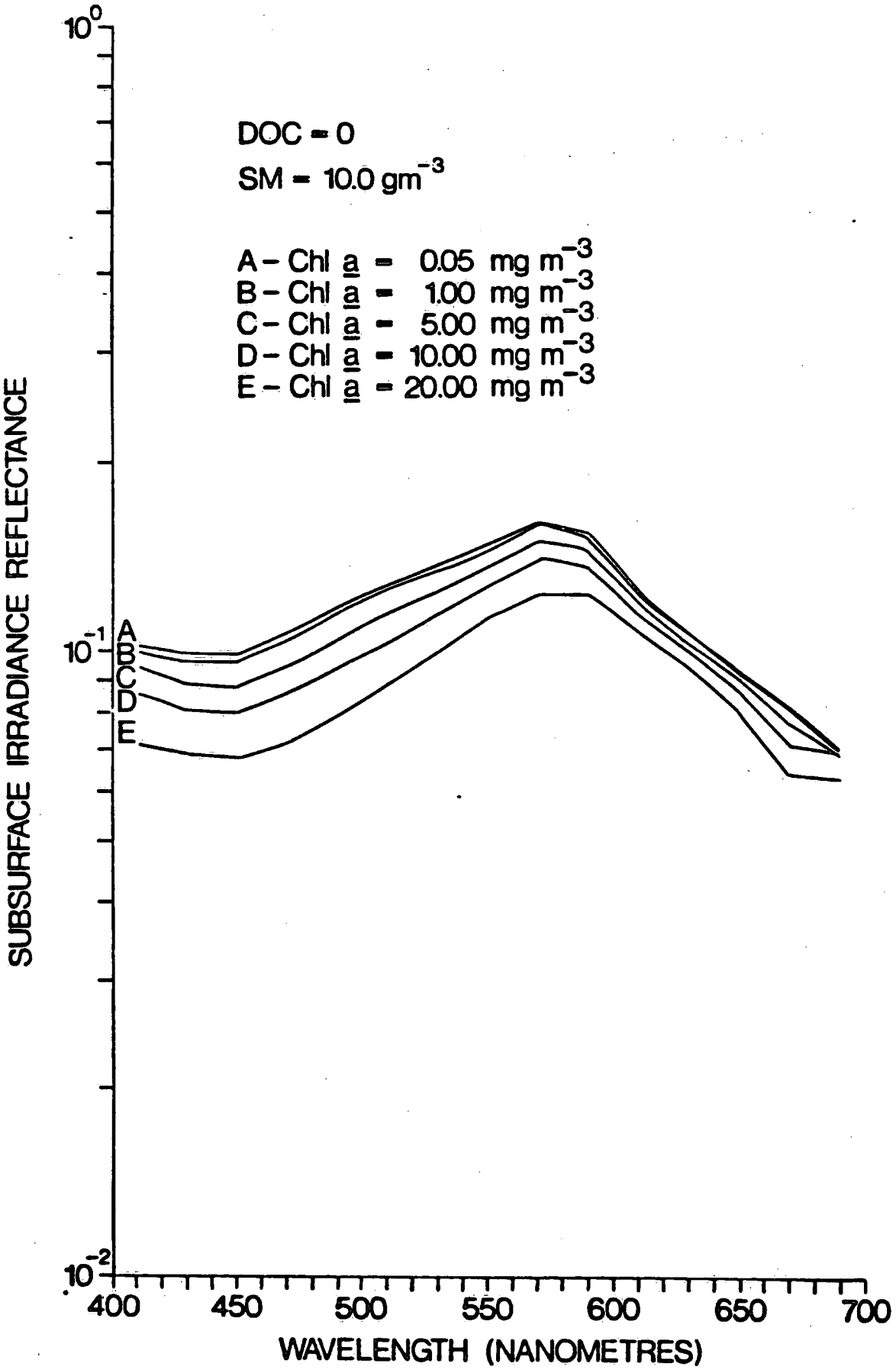
DOC = 0
SM = 10.0 gm^{-3}
A – Chl a = 0.05 mg m^{-3}
B – Chl a = 1.00 mg m^{-3}
C – Chl a = 5.00 mg m^{-3}
D – Chl a = 10.00 mg m^{-3}
E – Chl a = 20.00 mg m^{-3}
SUBSURFACE IRRADIANCE REFLECTANCE
10^{0}
10^{-1}
10^{-2}
A
B
C
D
E
400
450
500
550
600
650
700
WAVELENGTH (NANOMETRES)

FIG. 11

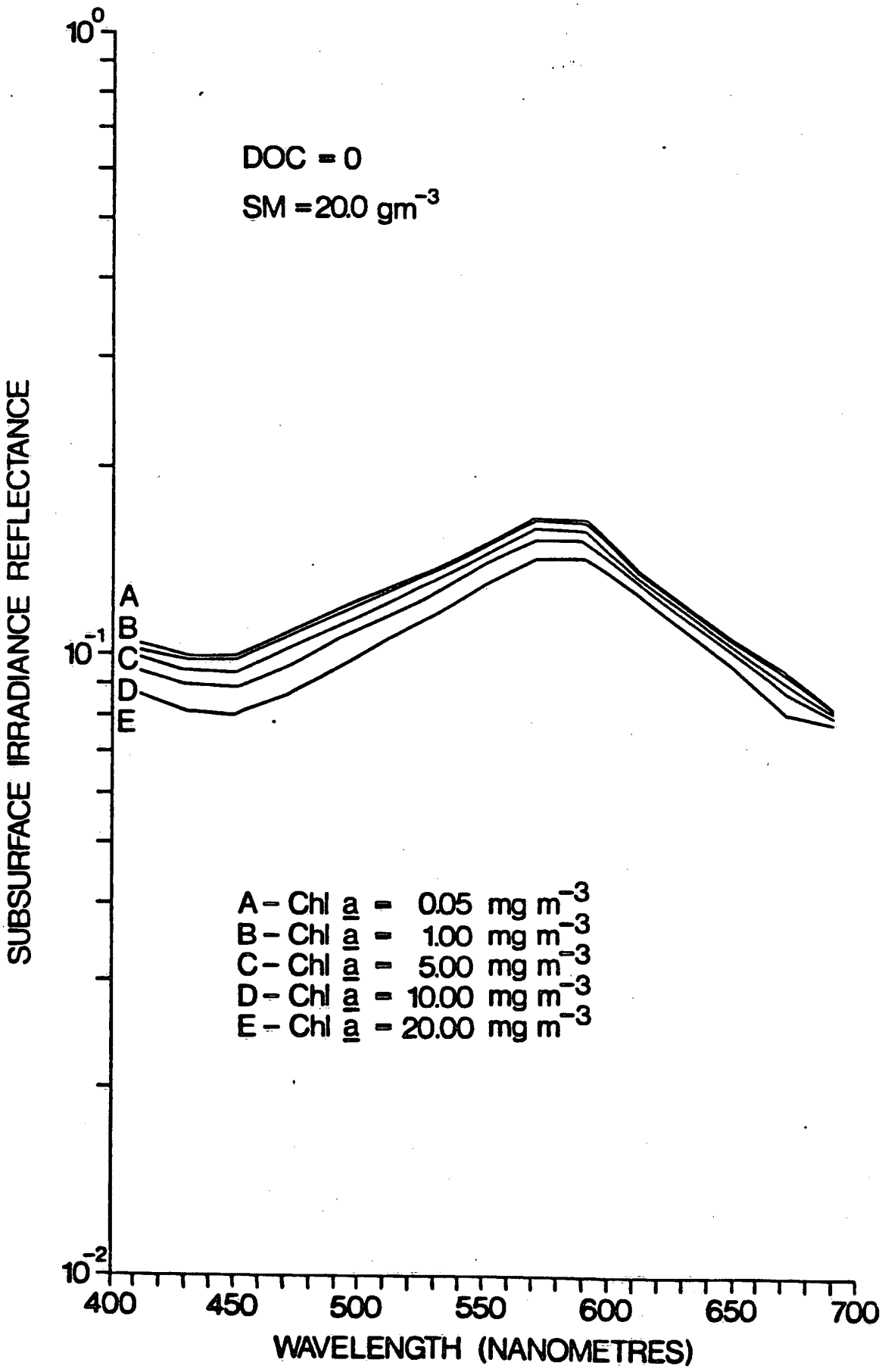
DOC = 0
SM = 20.0 gm^{-3}
SUBSURFACE IRRADIANCE REFLECTANCE
10^0
10^{-1}
10^{-2}
A
B
C
D
E
A – Chl a = 0.05 mg m^{-3}
B – Chl a = 1.00 mg m^{-3}
C – Chl a = 5.00 mg m^{-3}
D – Chl a = 10.00 mg m^{-3}
E – Chl a = 20.00 mg m^{-3}
400
450
500
550
600
650
700
WAVELENGTH (NANOMETRES)

FIG. 12

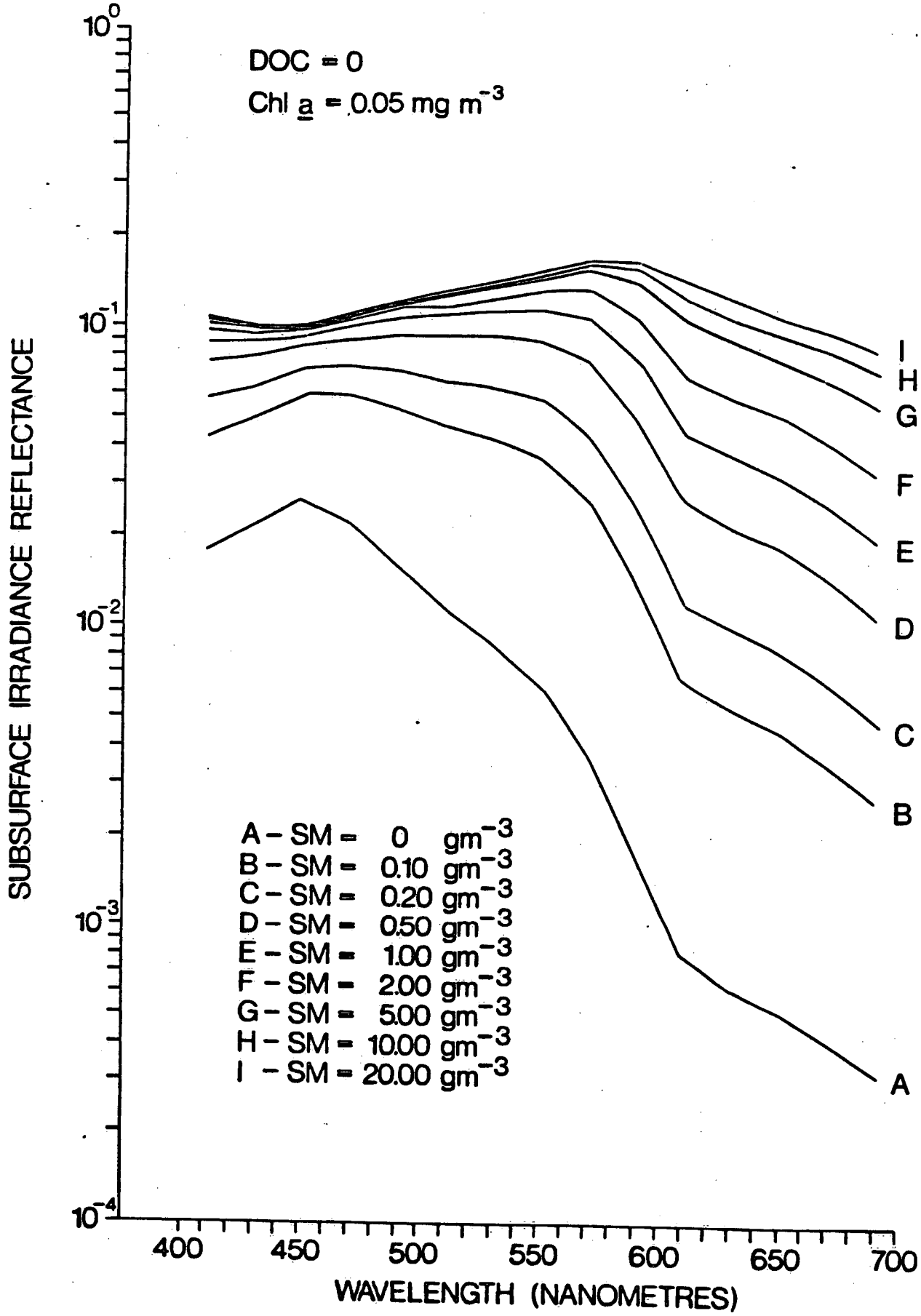
DOC = 0
Chl a = 0.05 mg m^{-3}
SUBSURFACE IRRADIANCE REFLECTANCE
10^{0}
10^{-1}
10^{-2}
10^{-3}
10^{-4}
A – SM = 0 gm^{-3}
B – SM = 0.10 gm^{-3}
C – SM = 0.20 gm^{-3}
D – SM = 0.50 gm^{-3}
E – SM = 1.00 gm^{-3}
F – SM = 2.00 gm^{-3}
G – SM = 5.00 gm^{-3}
H – SM = 10.00 gm^{-3}
I – SM = 20.00 gm^{-3}
A
B
C
D
E
F
G
H
I
400
450
500
550
600
650
700
WAVELENGTH (NANOMETRES)

FIG. 13

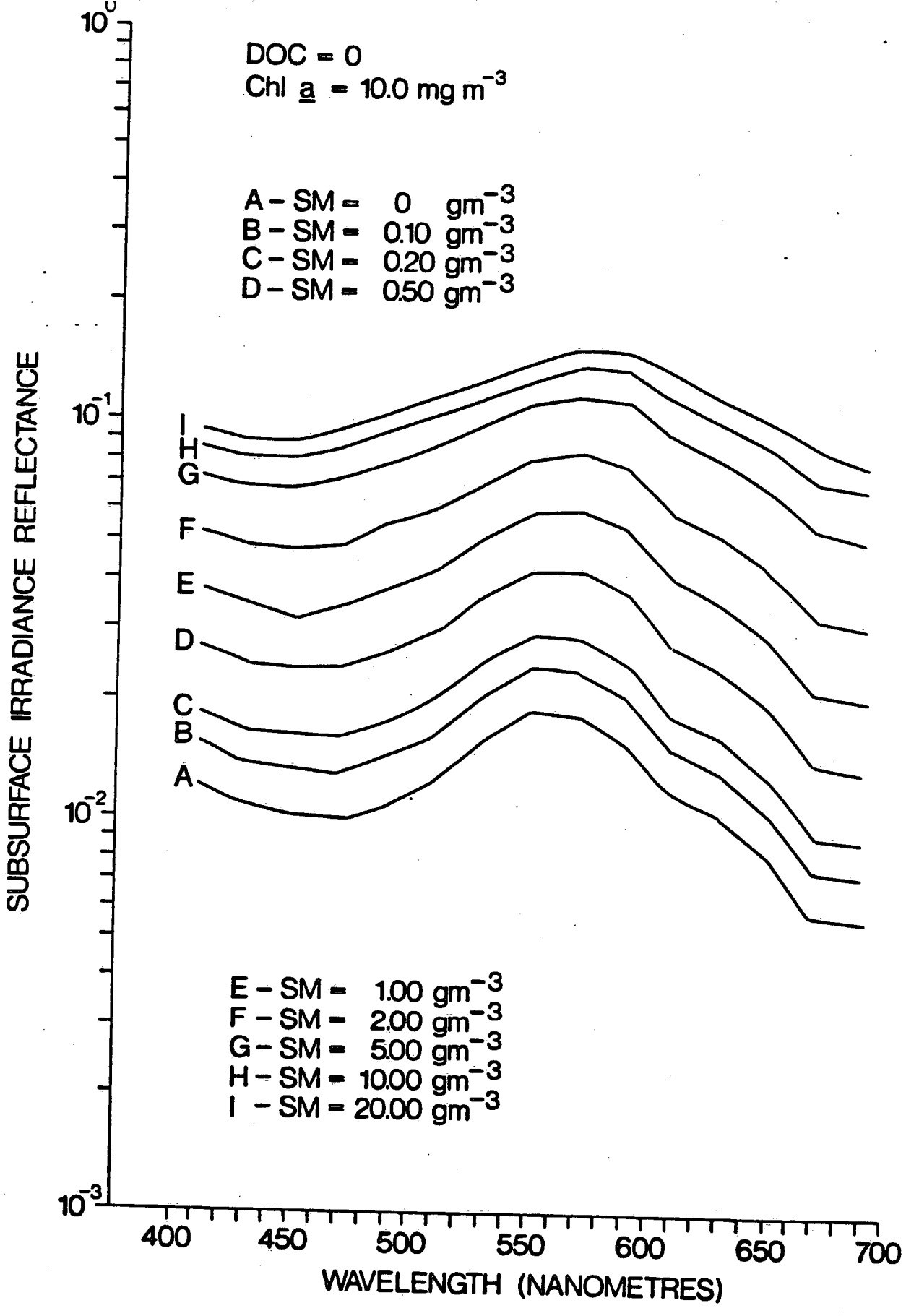
DOC = 0
Chl a = 10.0 mg m^{-3}
A – SM = 0 gm^{-3}
B – SM = 0.10 gm^{-3}
C – SM = 0.20 gm^{-3}
D – SM = 0.50 gm^{-3}
E – SM = 1.00 gm^{-3}
F – SM = 2.00 gm^{-3}
G – SM = 5.00 gm^{-3}
H – SM = 10.00 gm^{-3}
I – SM = 20.00 gm^{-3}
SUBSURFACE IRRADIANCE REFLECTANCE
10^{0}
10^{-1}
10^{-2}
10^{-3}
400
450
500
550
600
650
700
WAVELENGTH (NANOMETRES)

FIG. 14

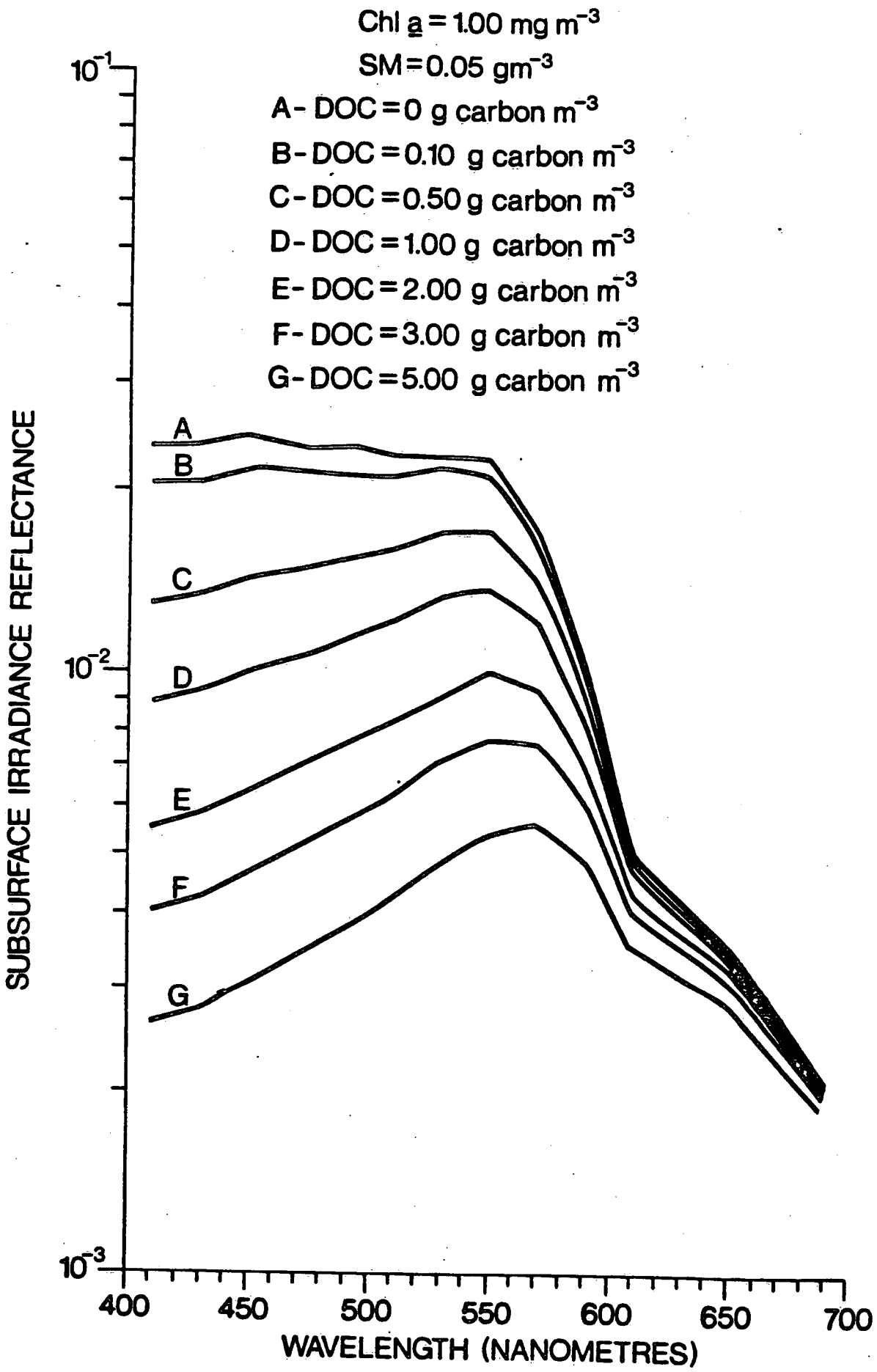
Chl a = 1.00 mg m^{-3}
SM = 0.05 gm^{-3}
A - DOC = 0 g carbon m^{-3}
B - DOC = 0.10 g carbon m^{-3}
C - DOC = 0.50 g carbon m^{-3}
D - DOC = 1.00 g carbon m^{-3}
E - DOC = 2.00 g carbon m^{-3}
F - DOC = 3.00 g carbon m^{-3}
G - DOC = 5.00 g carbon m^{-3}
SUBSURFACE IRRADIANCE REFLECTANCE
10^{-1}
10^{-2}
10^{-3}
A
B
C
D
E
F
G
400
450
500
550
600
650
700
WAVELENGTH (NANOMETRES)

FIG. 15

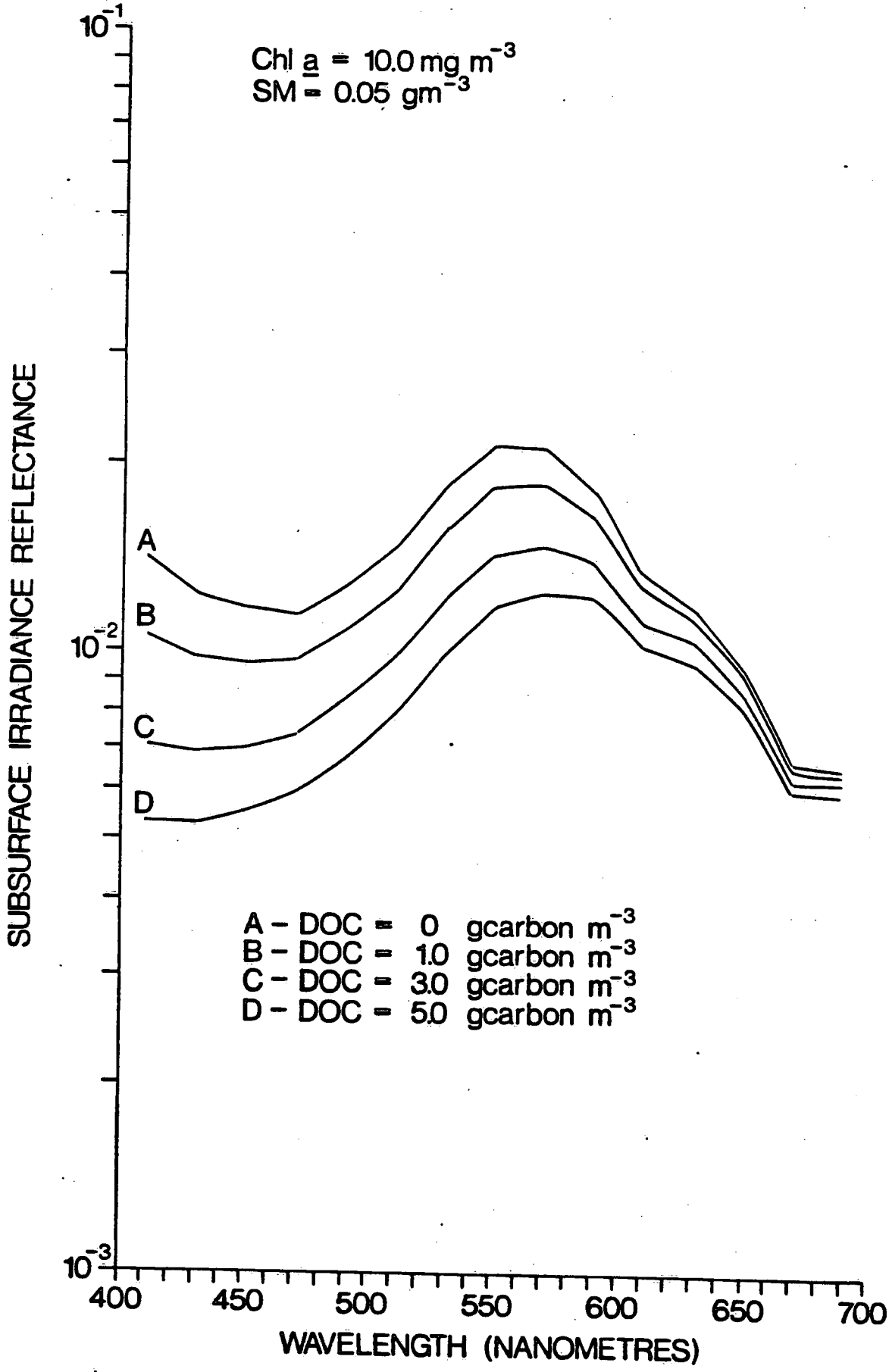
Chl a = 10.0 mg m^{-3}
SM = 0.05 gm^{-3}
SUBSURFACE IRRADIANCE REFLECTANCE
10^{-1}
10^{-2}
10^{-3}
A
B
C
D
A – DOC = 0 gcarbon m^{-3}
B – DOC = 1.0 gcarbon m^{-3}
C – DOC = 3.0 gcarbon m^{-3}
D – DOC = 5.0 gcarbon m^{-3}
400
450
500
550
600
650
700
WAVELENGTH (NANOMETRES)

FIG. 16

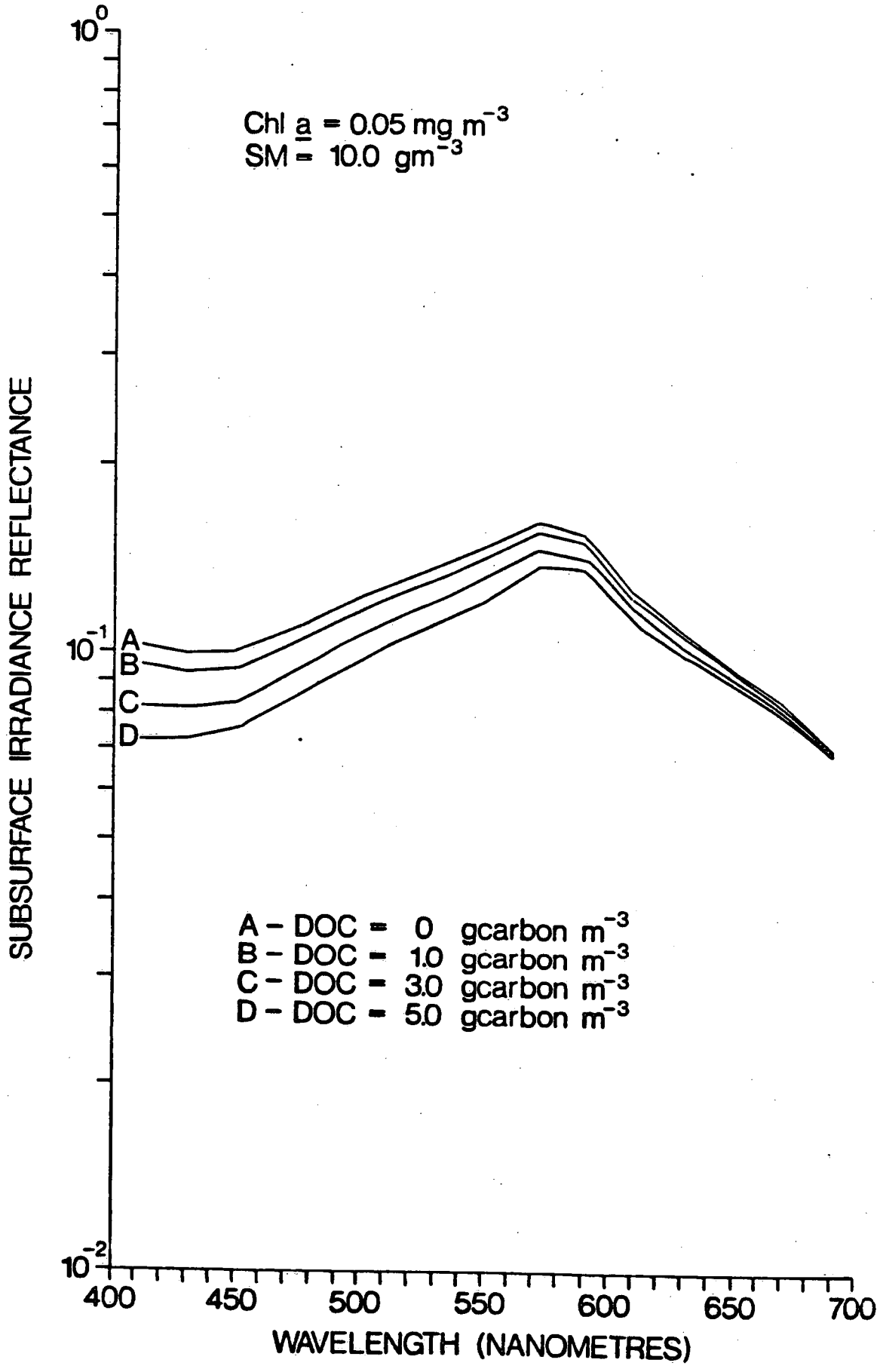
Chl a = 0.05 mg m^{-3}
SM = 10.0 gm^{-3}
SUBSURFACE IRRADIANCE REFLECTANCE
10^{0}
10^{-1}
10^{-2}
A
B
C
D
A – DOC = 0 gcarbon m^{-3}
B – DOC = 1.0 gcarbon m^{-3}
C – DOC = 3.0 gcarbon m^{-3}
D – DOC = 5.0 gcarbon m^{-3}
400
450
500
550
600
650
700
WAVELENGTH (NANOMETRES)

FIG. 17

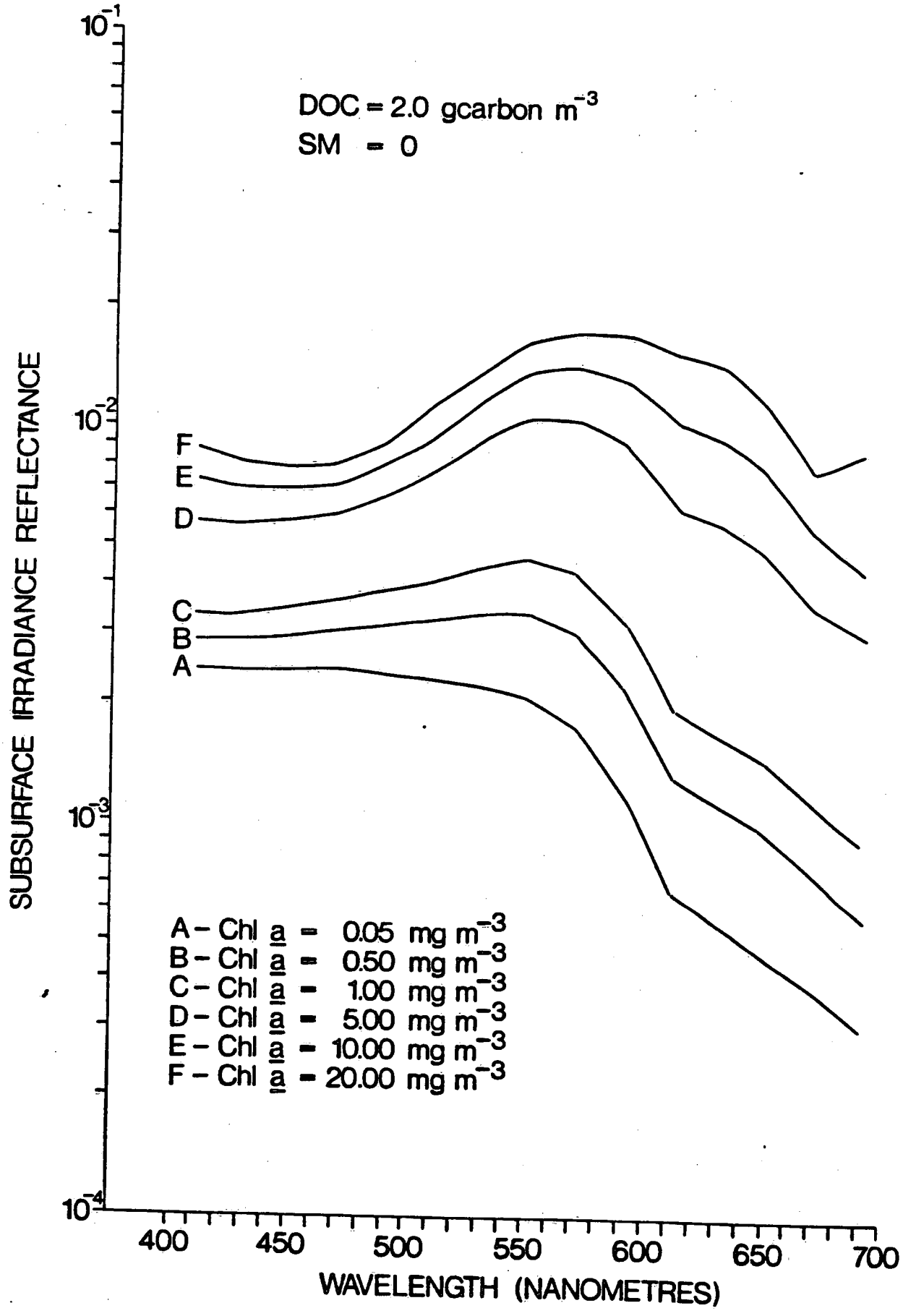
DOC = 2.0 gcarbon m^{-3}
SM = 0
SUBSURFACE IRRADIANCE REFLECTANCE
10^{-1}
10^{-2}
10^{-3}
10^{-4}
F
E
D
C
B
A
A – Chl a = 0.05 mg m^{-3}
B – Chl a = 0.50 mg m^{-3}
C – Chl a = 1.00 mg m^{-3}
D – Chl a = 5.00 mg m^{-3}
E – Chl a = 10.00 mg m^{-3}
F – Chl a = 20.00 mg m^{-3}
400
450
500
550
600
650
700
WAVELENGTH (NANOMETRES)

FIG. 18

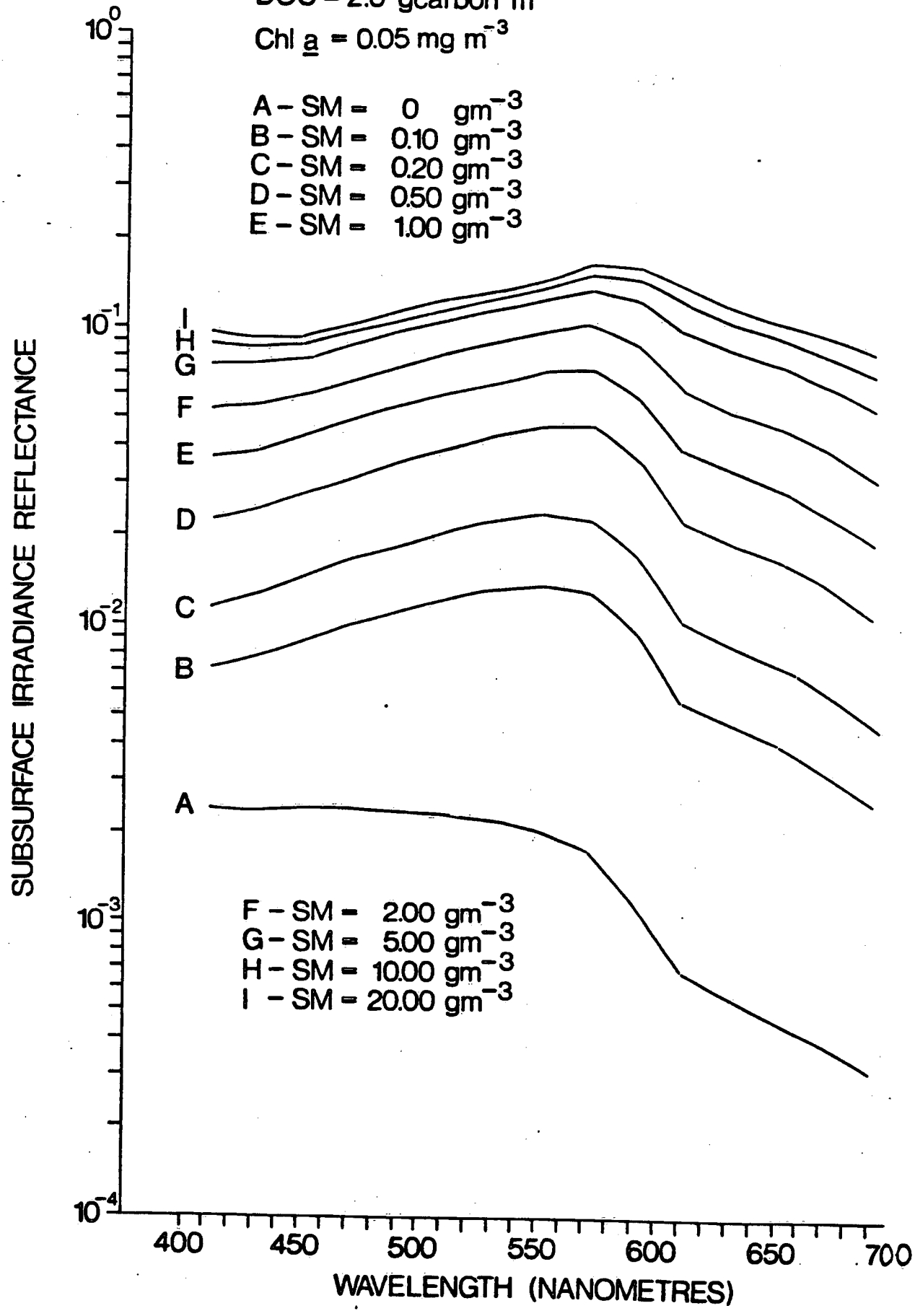
DOC = 2.0 gcarbon m^{-3}
Chl a = 0.05 mg m^{-3}
A – SM = 0 gm^{-3}
B – SM = 0.10 gm^{-3}
C – SM = 0.20 gm^{-3}
D – SM = 0.50 gm^{-3}
E – SM = 1.00 gm^{-3}
F – SM = 2.00 gm^{-3}
G – SM = 5.00 gm^{-3}
H – SM = 10.00 gm^{-3}
I – SM = 20.00 gm^{-3}
SUBSURFACE IRRADIANCE REFLECTANCE
10^{0}
10^{-1}
10^{-2}
10^{-3}
10^{-4}
400
450
500
550
600
650
700
WAVELENGTH (NANOMETRES)

FIG. 19

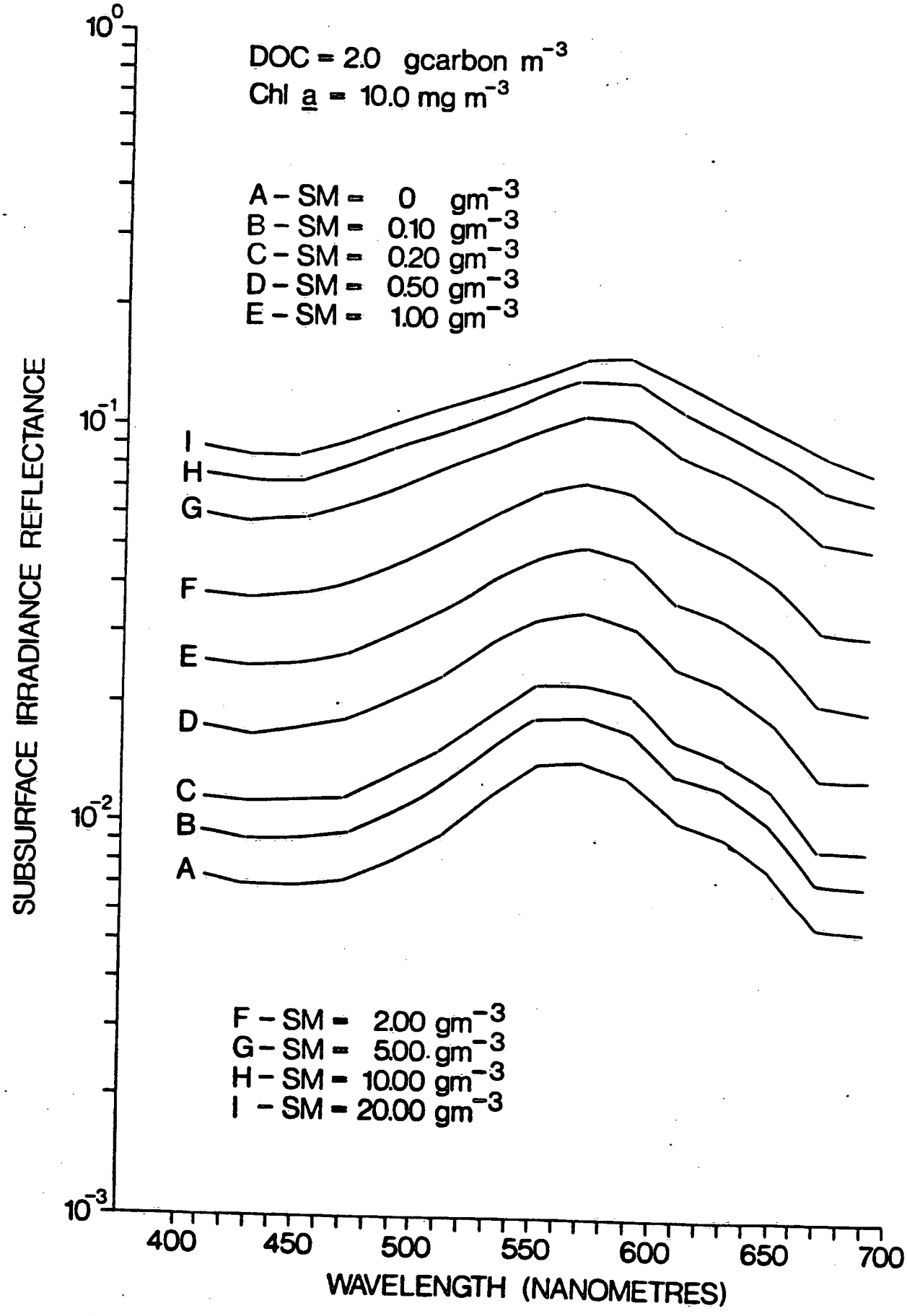
DOC = 2.0 gcarbon m^{-3}
Chl a = 10.0 mg m^{-3}
A – SM = 0 gm^{-3}
B – SM = 0.10 gm^{-3}
C – SM = 0.20 gm^{-3}
D – SM = 0.50 gm^{-3}
E – SM = 1.00 gm^{-3}
F – SM = 2.00 gm^{-3}
G – SM = 5.00 gm^{-3}
H – SM = 10.00 gm^{-3}
I – SM = 20.00 gm^{-3}
SUBSURFACE IRRADIANCE REFLECTANCE
10^{0}
10^{-1}
10^{-2}
10^{-3}
400
450
500
550
600
650
700
WAVELENGTH (NANOMETRES)

FIG. 20

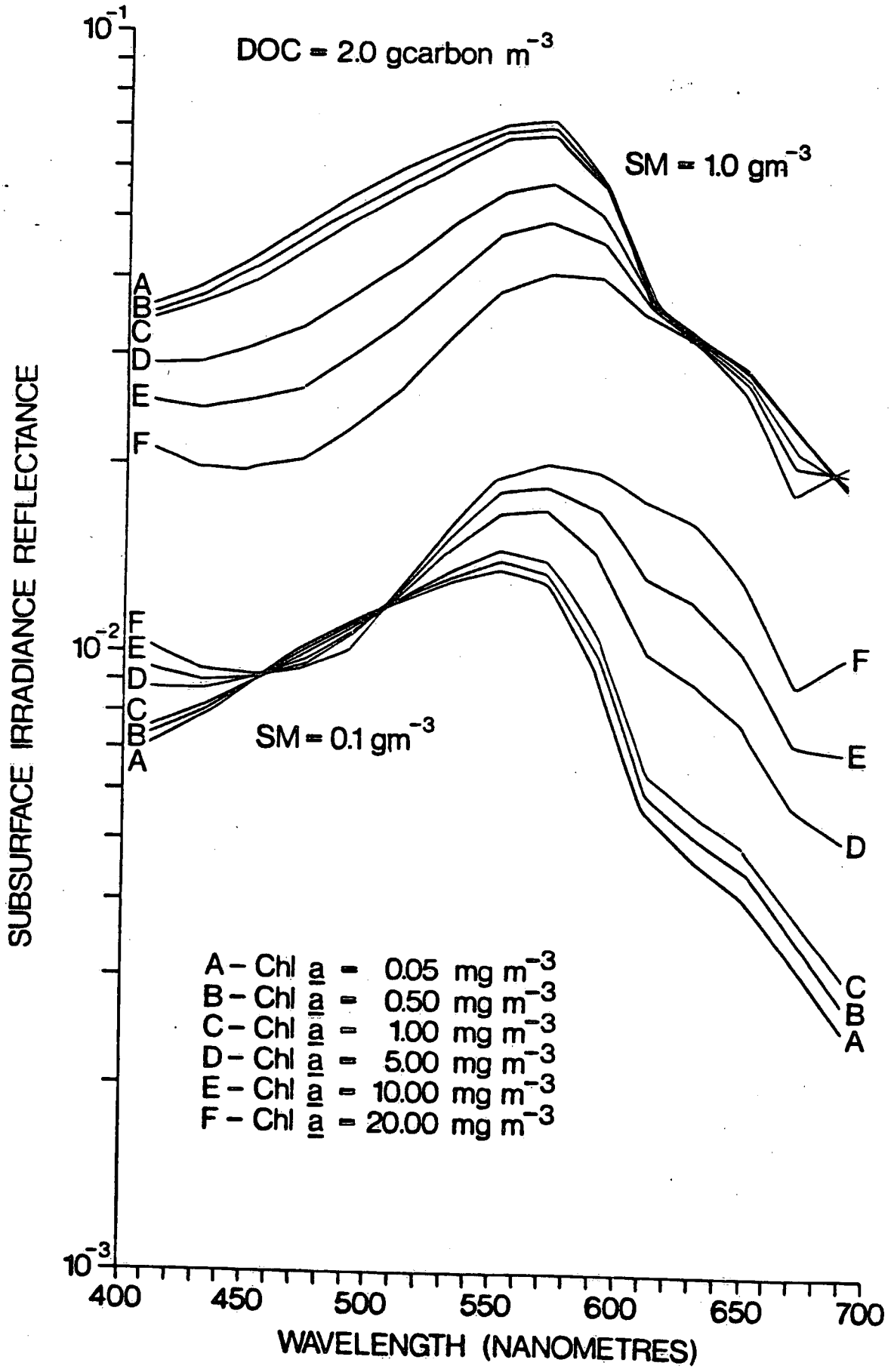
DOC = 2.0 gcarbon m^{-3}
SM = 1.0 gm^{-3}
SM = 0.1 gm^{-3}
SUBSURFACE IRRADIANCE REFLECTANCE
10^{-1}
10^{-2}
10^{-3}
A
B
C
D
E
F
A – Chl a = 0.05 mg m^{-3}
B – Chl a = 0.50 mg m^{-3}
C – Chl a = 1.00 mg m^{-3}
D – Chl a = 5.00 mg m^{-3}
E – Chl a = 10.00 mg m^{-3}
F – Chl a = 20.00 mg m^{-3}
400
450
500
550
600
650
700
WAVELENGTH (NANOMETRES)

FIG. 21

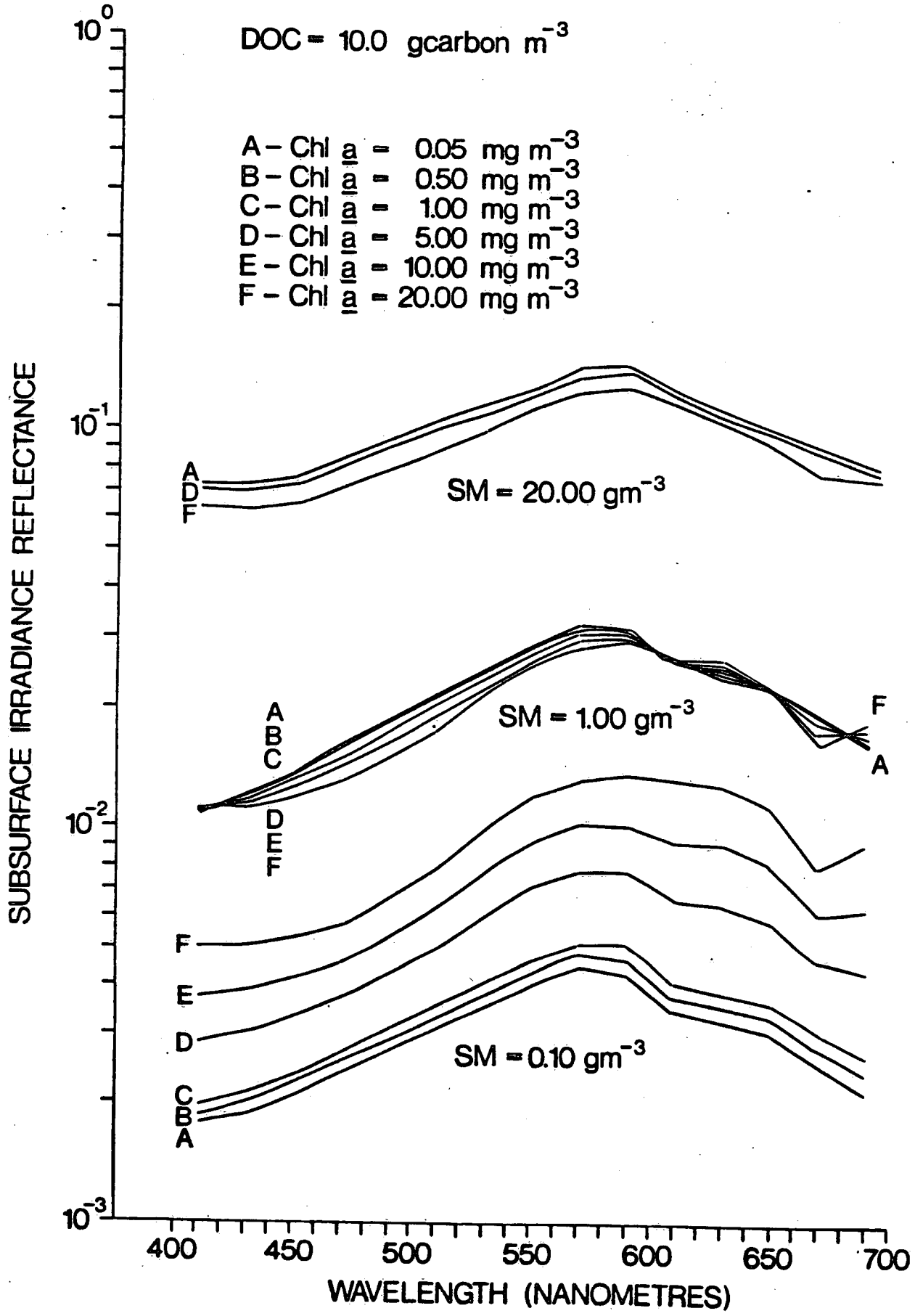
DOC = 10.0 gcarbon m^{-3}
A – Chl a = 0.05 mg m^{-3}
B – Chl a = 0.50 mg m^{-3}
C – Chl a = 1.00 mg m^{-3}
D – Chl a = 5.00 mg m^{-3}
E – Chl a = 10.00 mg m^{-3}
F – Chl a = 20.00 mg m^{-3}
SUBSURFACE IRRADIANCE REFLECTANCE
10^{0}
10^{-1}
10^{-2}
10^{-3}
SM = 20.00 gm^{-3}
SM = 1.00 gm^{-3}
SM = 0.10 gm^{-3}
400
450
500
550
600
650
700
WAVELENGTH (NANOMETRES)

FIG 22

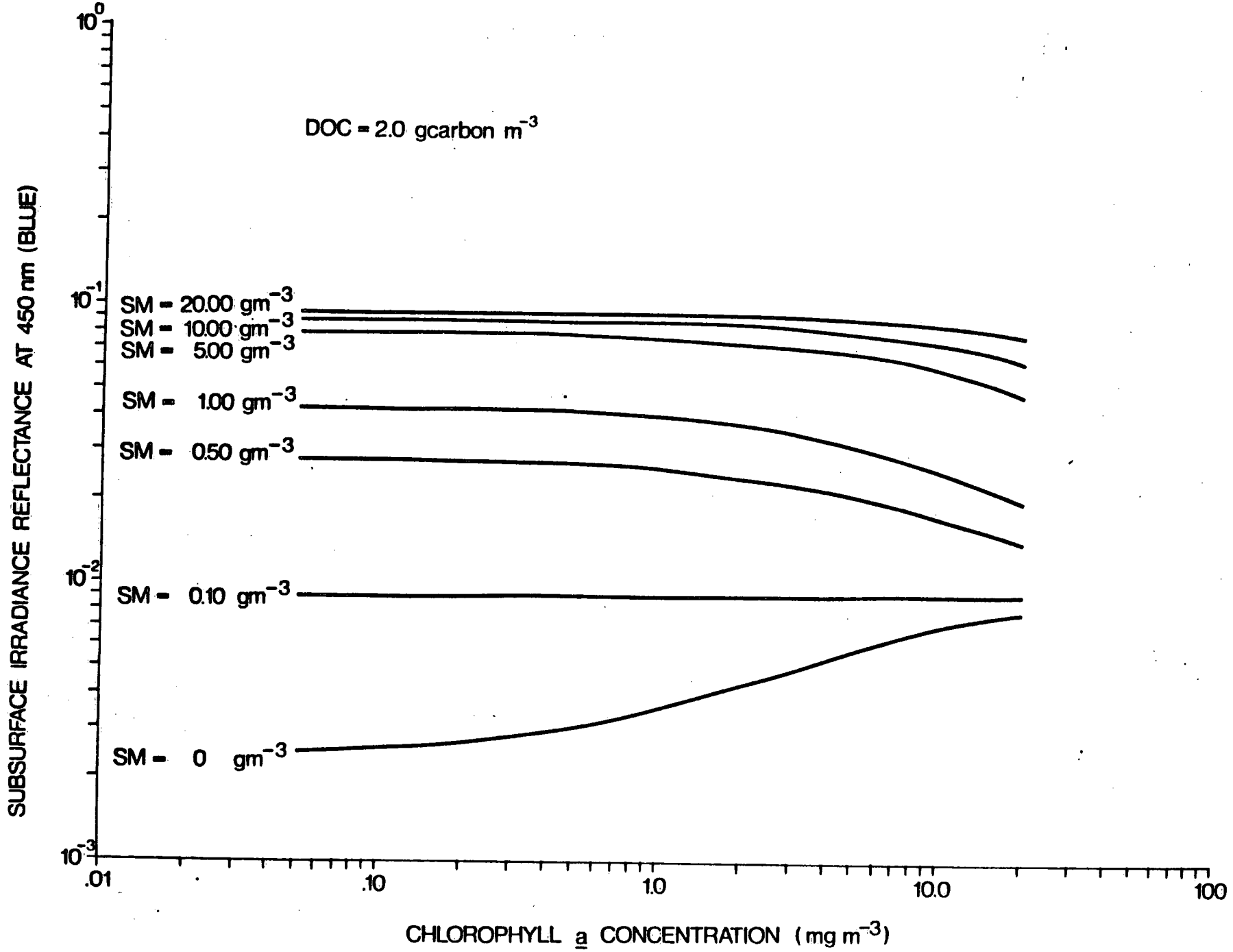
DOC = 2.0 gcarbon m^{-3}
SM = 20.00 gm^{-3}
SM = 10.00 gm^{-3}
SM = 5.00 gm^{-3}
SM = 1.00 gm^{-3}
SM = 0.50 gm^{-3}
SM = 0.10 gm^{-3}
SM = 0 gm^{-3}
SUBSURFACE IRRADIANCE REFLECTANCE AT 450 nm (BLUE)
10^{0}
10^{-1}
10^{-2}
10^{-3}
.01
.10
1.0
10.0
100
CHLOROPHYLL a CONCENTRATION (mg m^{-3})

FIG. 23

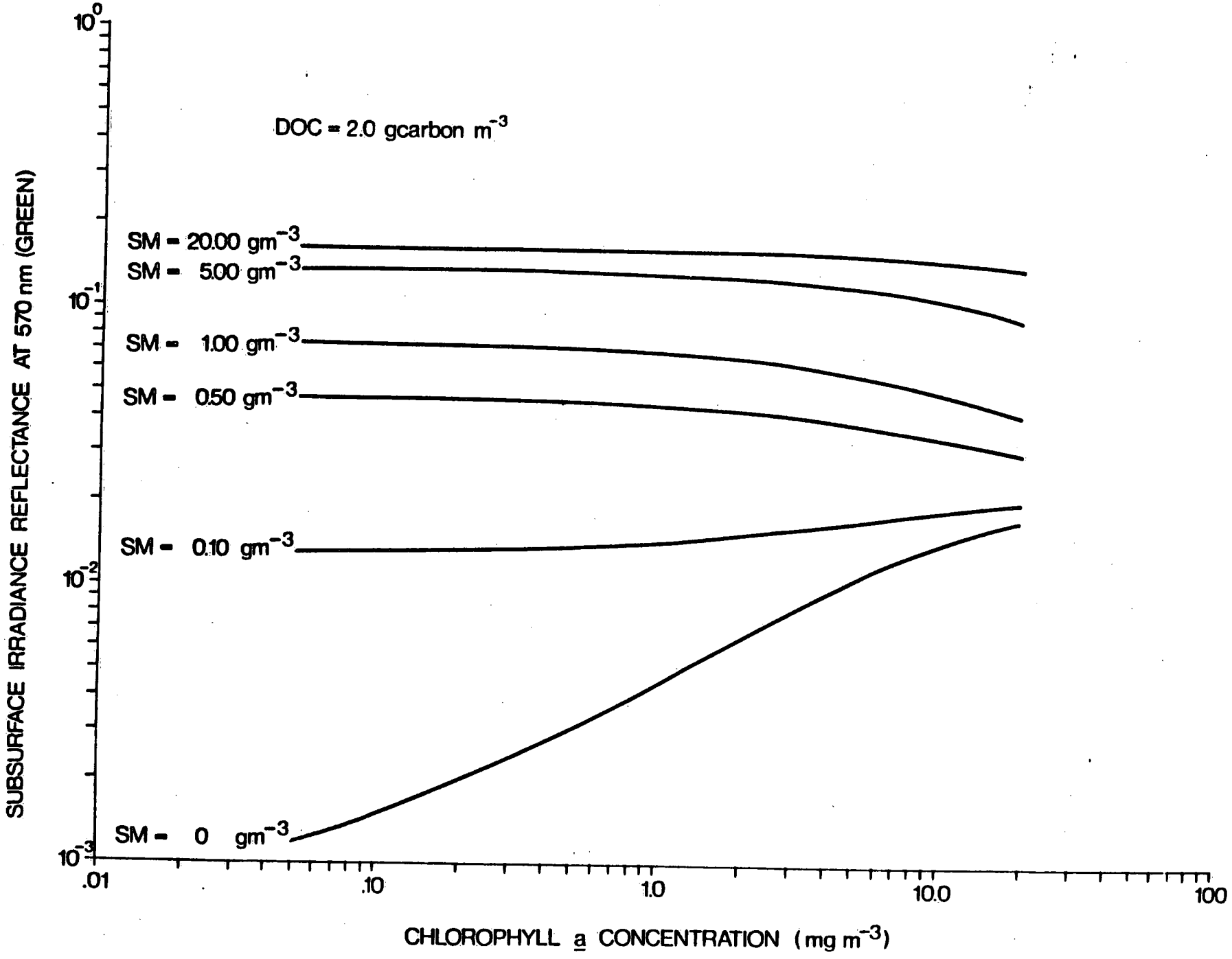
DOC = 2.0 gcarbon m^{-3}
SM = 20.00 gm^{-3}
SM = 5.00 gm^{-3}
SM = 1.00 gm^{-3}
SM = 0.50 gm^{-3}
SM = 0.10 gm^{-3}
SM = 0 gm^{-3}
SUBSURFACE IRRADIANCE REFLECTANCE AT 570 nm (GREEN)
10^{0}
10^{-1}
10^{-2}
10^{-3}
.01
.10
1.0
10.0
100
CHLOROPHYLL a CONCENTRATION (mg m^{-3})

FIG. 24

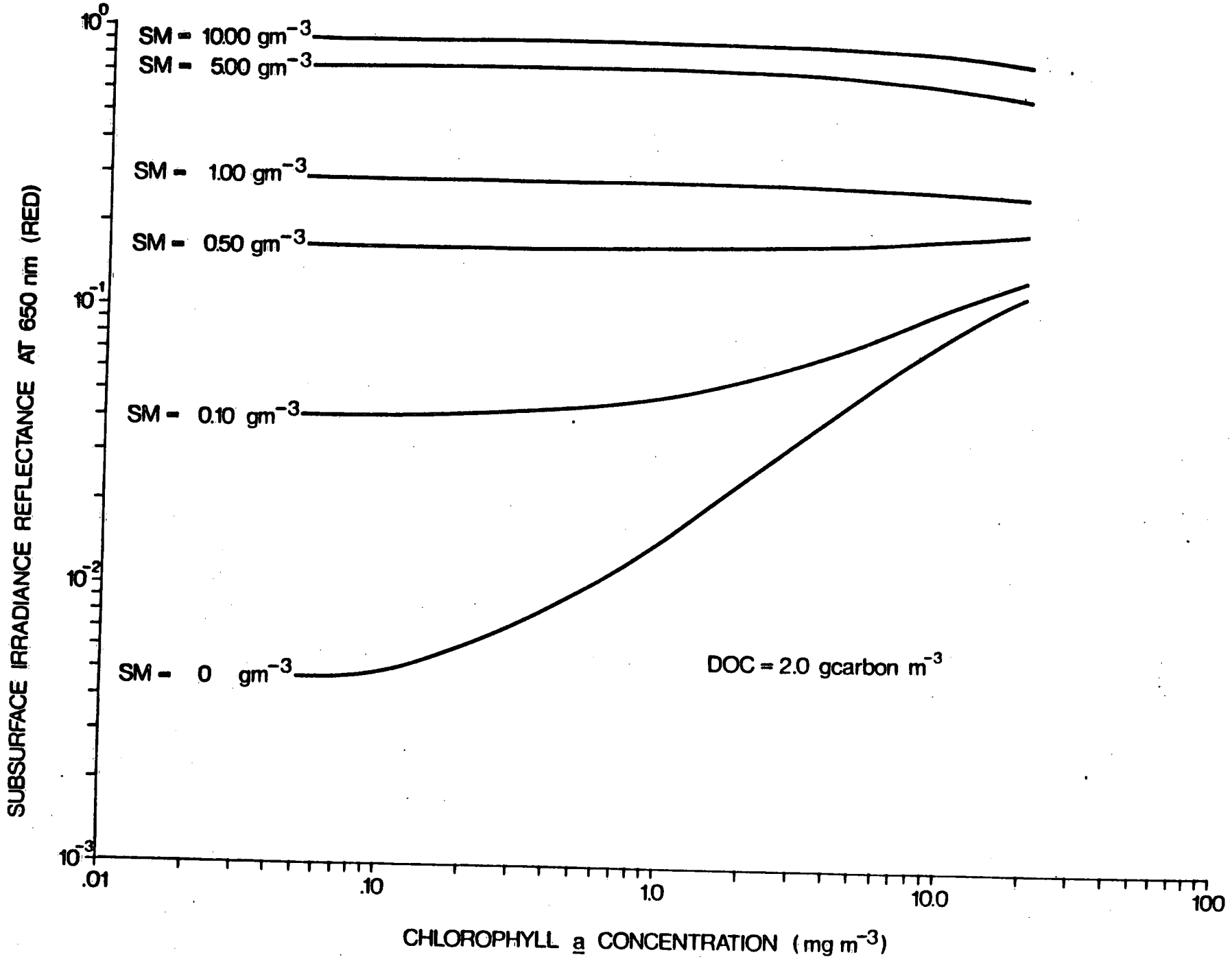
SM = 10.00 gm^{-3}
SM = 5.00 gm^{-3}
SM = 1.00 gm^{-3}
SM = 0.50 gm^{-3}
SM = 0.10 gm^{-3}
SM = 0 gm^{-3}
DOC = 2.0 gcarbon m^{-3}
SUBSURFACE IRRADIANCE REFLECTANCE AT 650 nm (RED)
10^{0}
10^{-1}
10^{-2}
10^{-3}
.01
.10
1.0
10.0
100
CHLOROPHYLL a CONCENTRATION (mg m^{-3})

FIG. 25

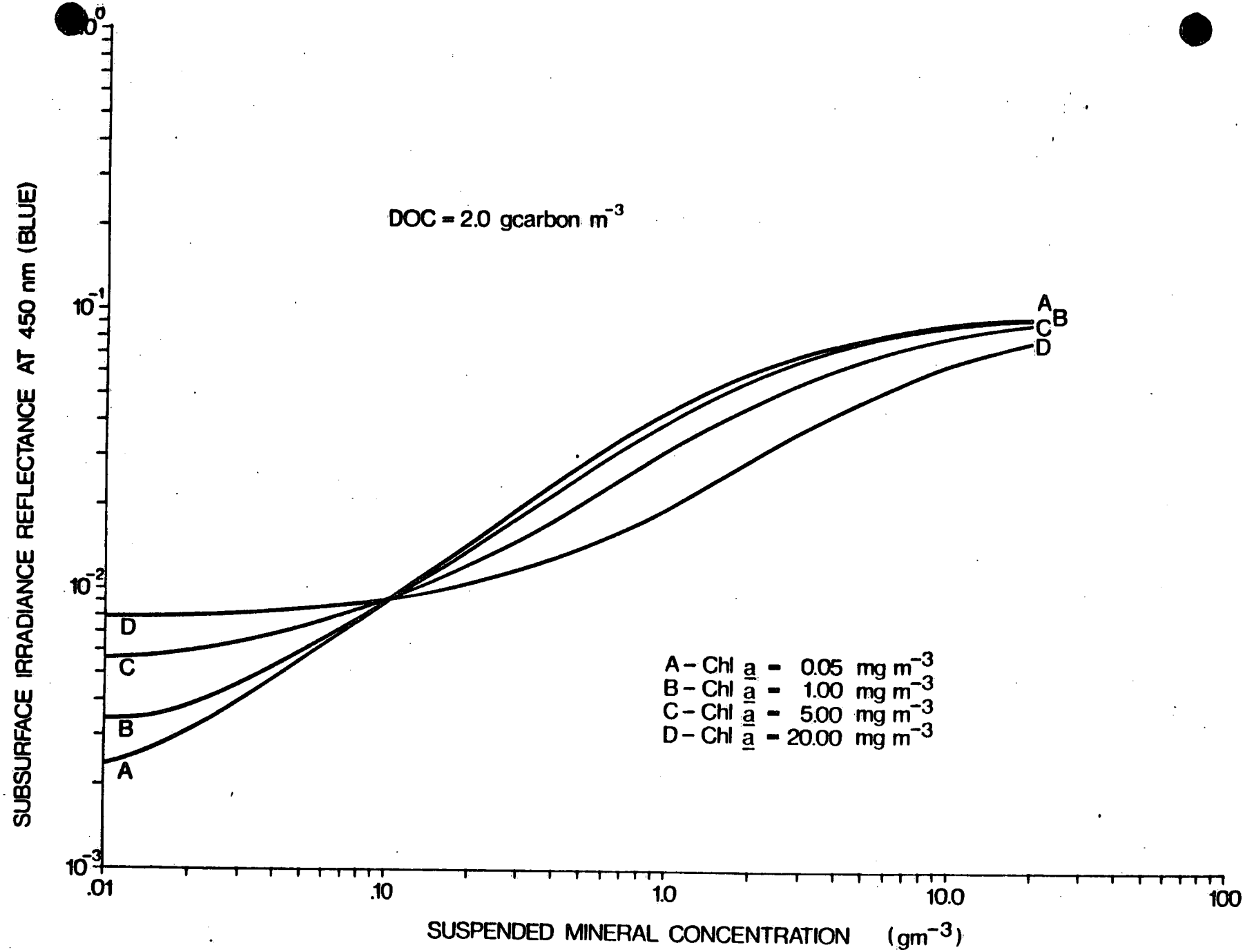
SUBSURFACE IRRADIANCE REFLECTANCE AT 450 nm (BLUE)
10^{0}
10^{-1}
10^{-2}
10^{-3}
DOC = 2.0 gcarbon m^{-3}
A
B
C
D
A – Chl a = 0.05 mg m^{-3}
B – Chl a = 1.00 mg m^{-3}
C – Chl a = 5.00 mg m^{-3}
D – Chl a = 20.00 mg m^{-3}
.01
.10
1.0
10.0
100
SUSPENDED MINERAL CONCENTRATION (gm^{-3})

FIG. 26

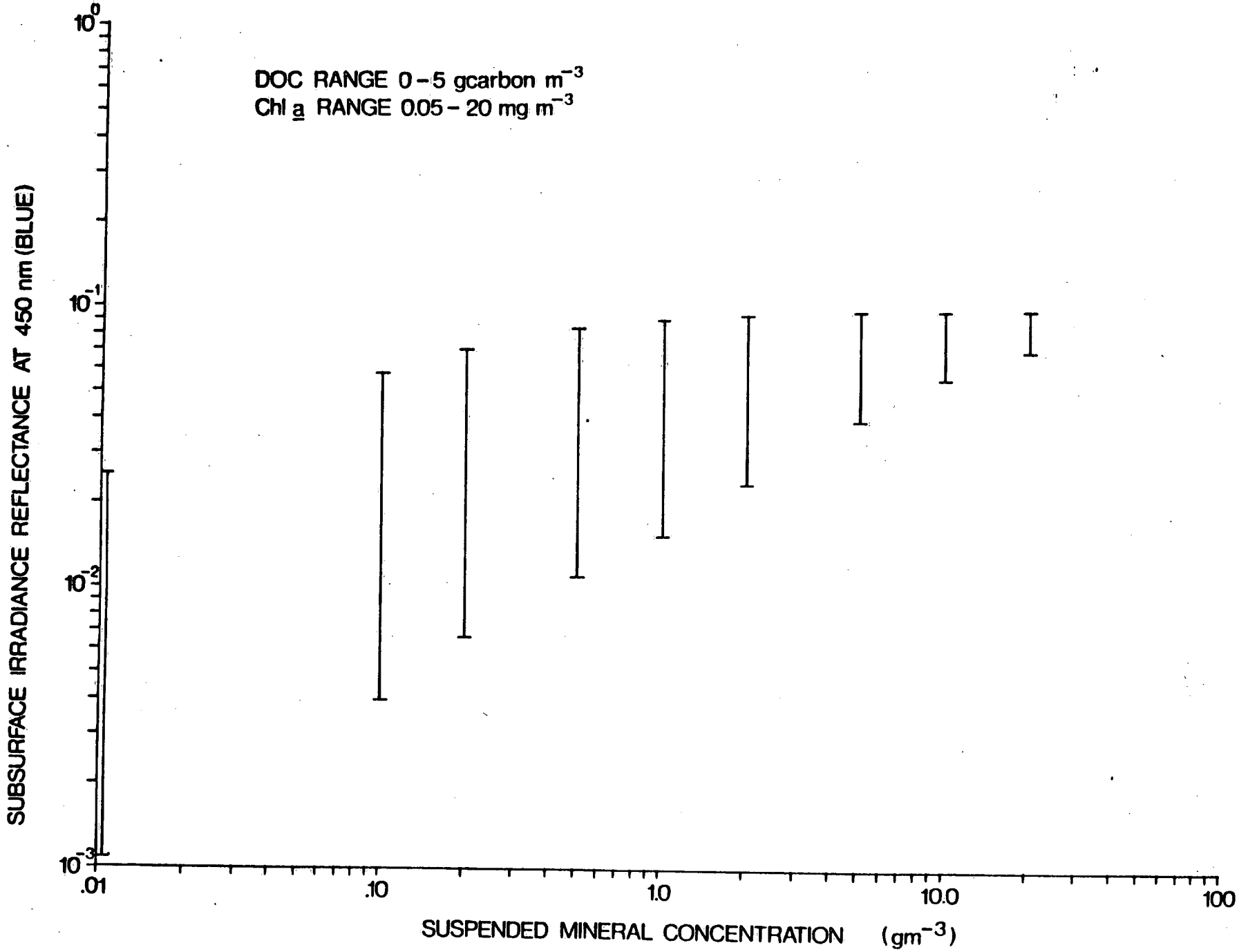
DOC RANGE 0 – 5 gcarbon m^{-3}
Chl a RANGE 0.05 – 20 mg m^{-3}
SUBSURFACE IRRADIANCE REFLECTANCE AT 450 nm (BLUE)
10^{0}
10^{-1}
10^{-2}
10^{-3}
.01
.10
1.0
10.0
100
SUSPENDED MINERAL CONCENTRATION (gm^{-3})

FIG. 27

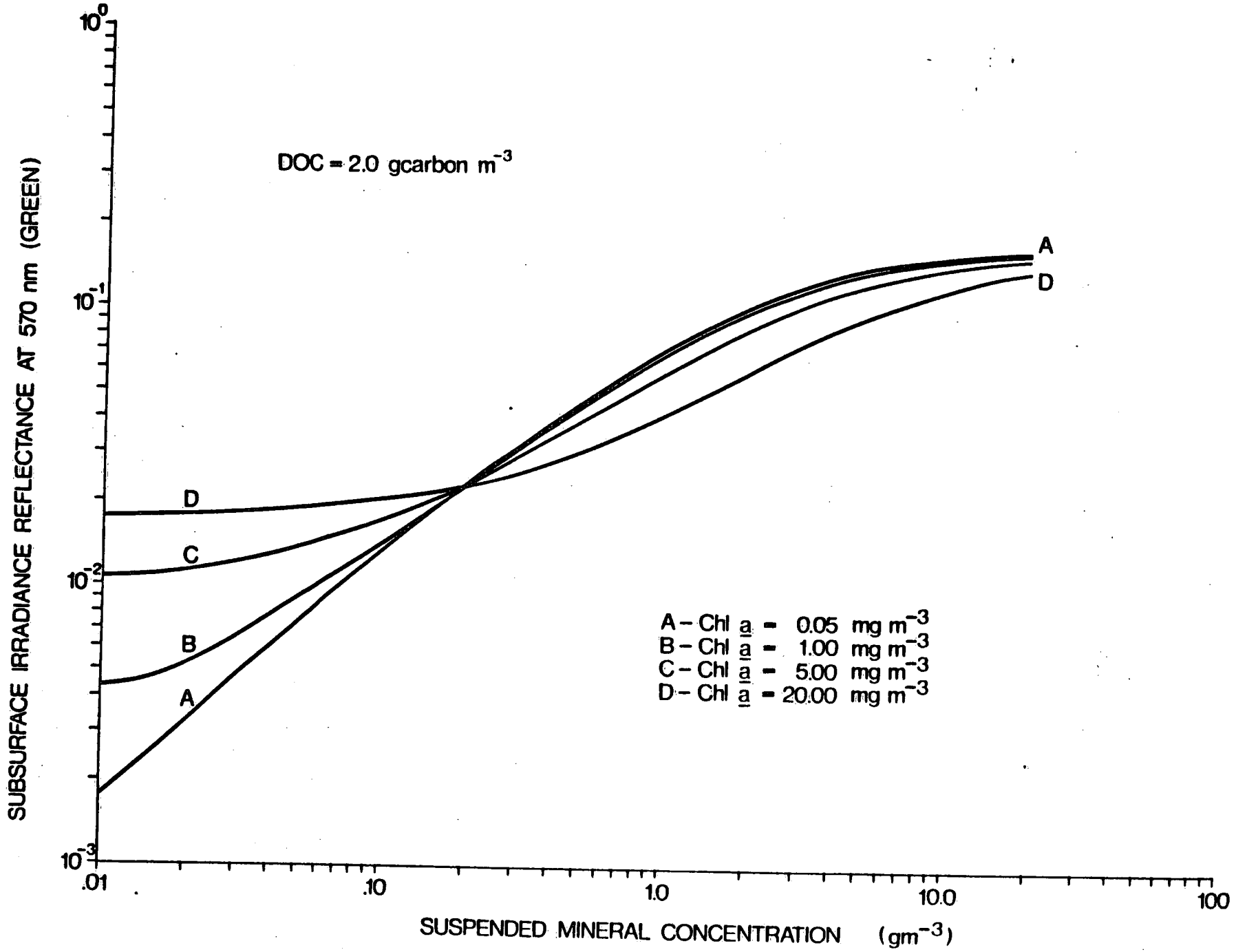
DOC = 2.0 gcarbon m^{-3}
SUBSURFACE IRRADIANCE REFLECTANCE AT 570 nm (GREEN)
10^{0}
10^{-1}
10^{-2}
10^{-3}
.01
.10
1.0
10.0
100
SUSPENDED MINERAL CONCENTRATION (gm^{-3})
A
D
D
C
B
A
A – Chl a = 0.05 mg m^{-3}
B – Chl a = 1.00 mg m^{-3}
C – Chl a = 5.00 mg m^{-3}
D – Chl a = 20.00 mg m^{-3}

FIG. 28

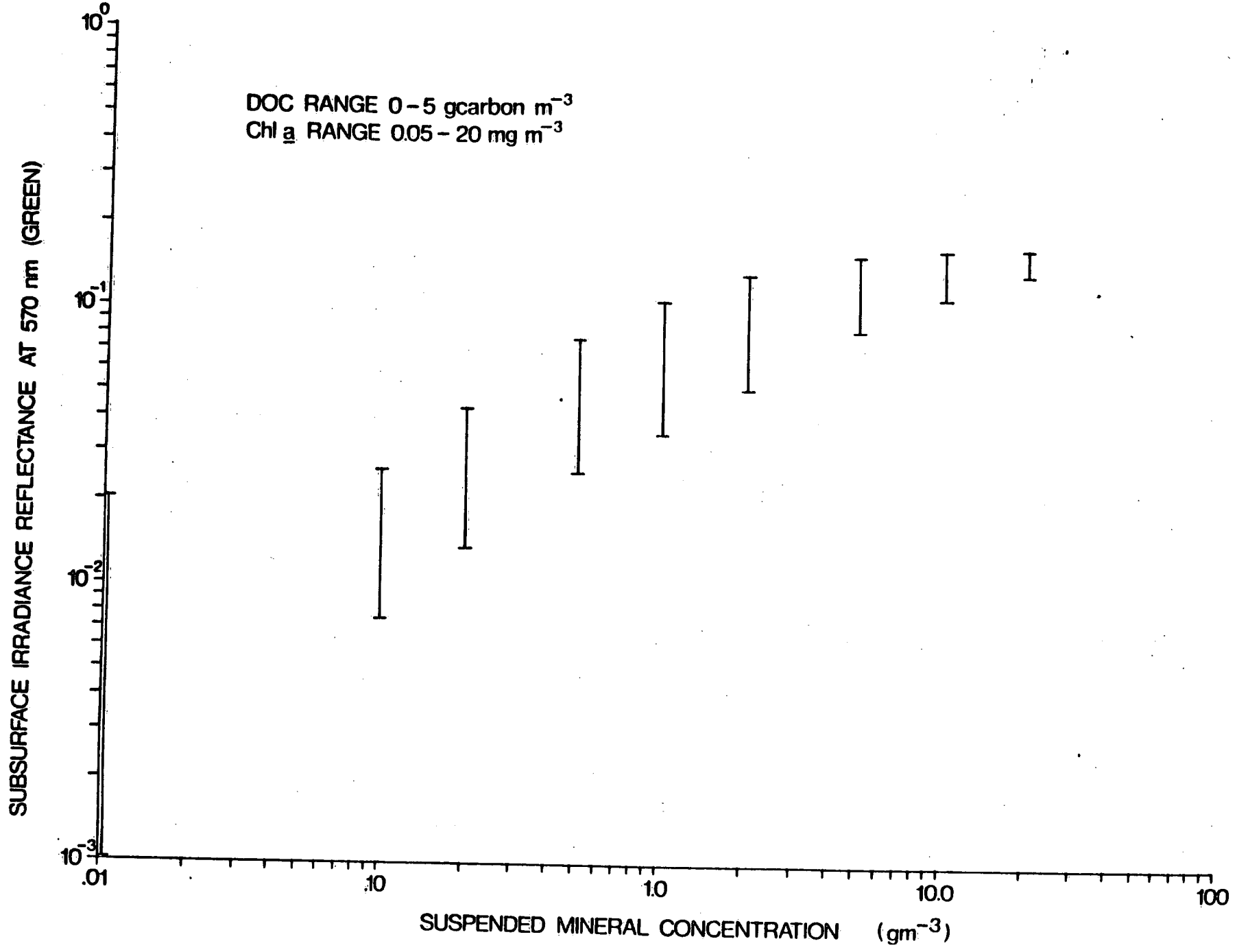
DOC RANGE 0 – 5 gcarbon m^{-3}
Chl a RANGE 0.05 – 20 mg m^{-3}
SUBSURFACE IRRADIANCE REFLECTANCE AT 570 nm (GREEN)
10^{0}
10^{-1}
10^{-2}
10^{-3}
.01
.10
1.0
10.0
100
SUSPENDED MINERAL CONCENTRATION (gm^{-3})

FIG. 29

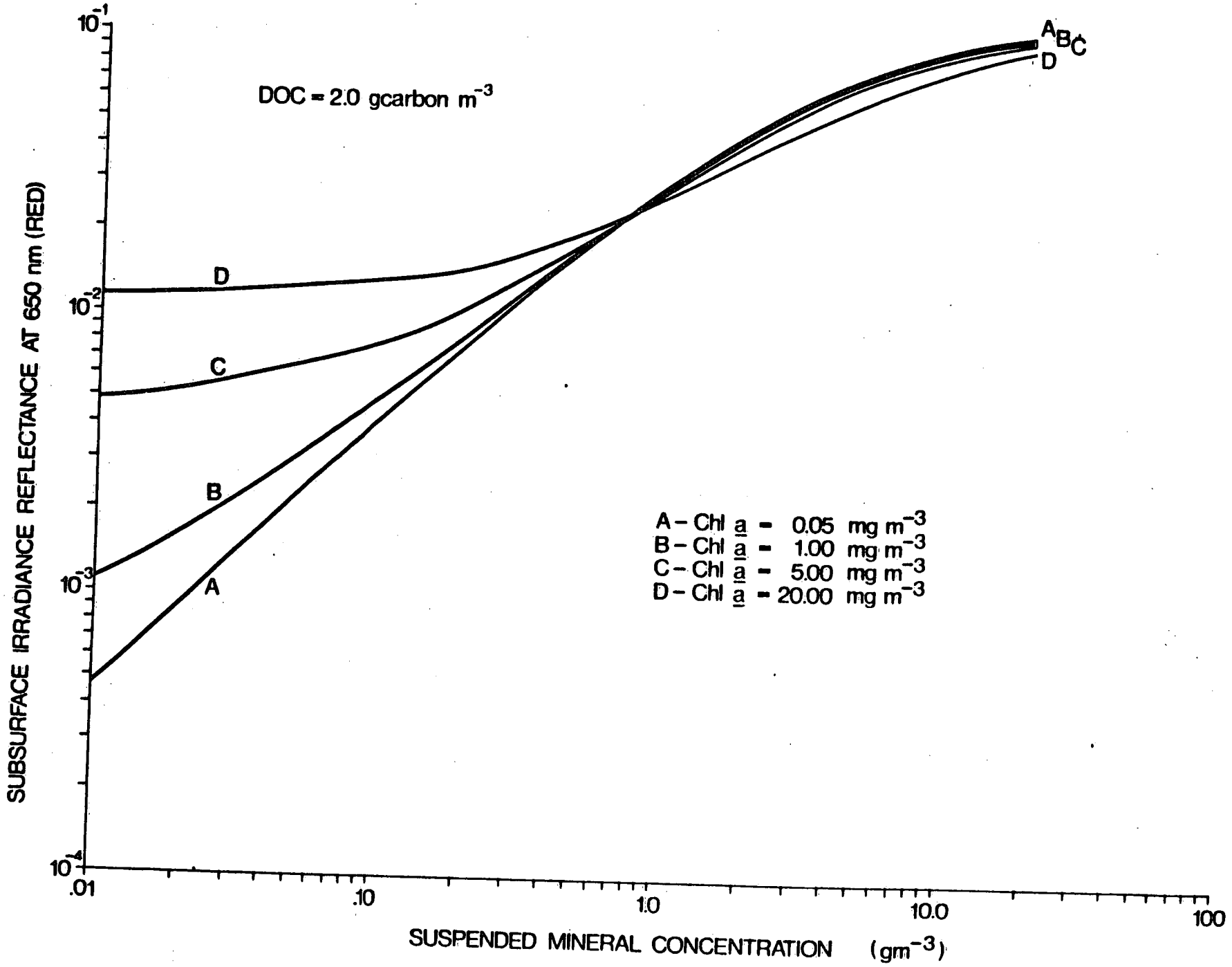
DOC = 2.0 gcarbon m^{-3}
A – Chl a = 0.05 mg m^{-3}
B – Chl a = 1.00 mg m^{-3}
C – Chl a = 5.00 mg m^{-3}
D – Chl a = 20.00 mg m^{-3}
A
B
C
D
SUBSURFACE IRRADIANCE REFLECTANCE AT 650 nm (RED)
10^{-1}
10^{-2}
10^{-3}
10^{-4}
.01
.10
1.0
10.0
100
SUSPENDED MINERAL CONCENTRATION (gm^{-3})

FIG. 30

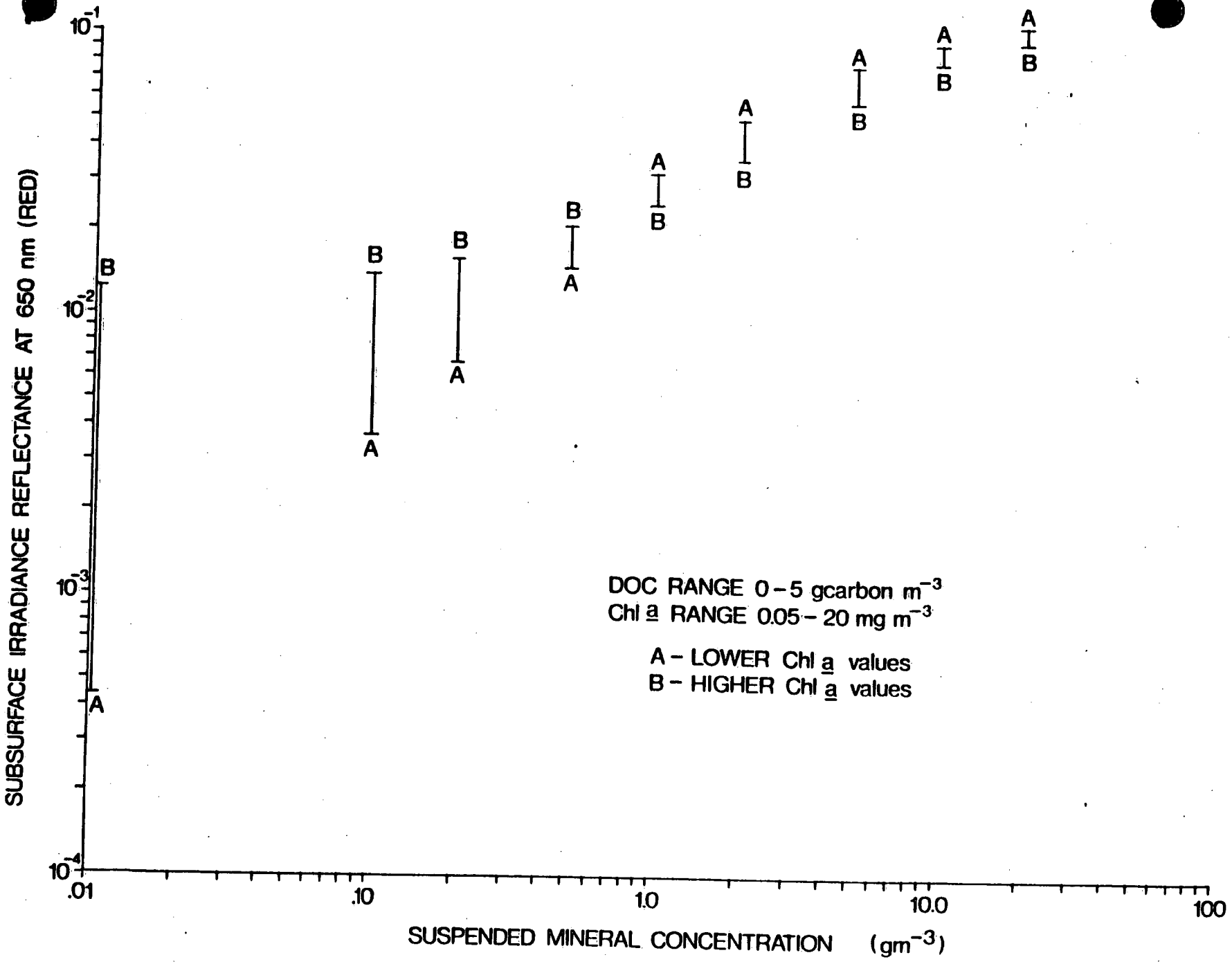
SUBSURFACE IRRADIANCE REFLECTANCE AT 650 nm (RED)
10^{-1}
10^{-2}
10^{-3}
10^{-4}
.01
.10
1.0
10.0
100
SUSPENDED MINERAL CONCENTRATION (gm^{-3})
DOC RANGE 0 – 5 gcarbon m^{-3}
Chl a RANGE 0.05 – 20 mg m^{-3}
A – LOWER Chl a values
B – HIGHER Chl a values

FIG. 31

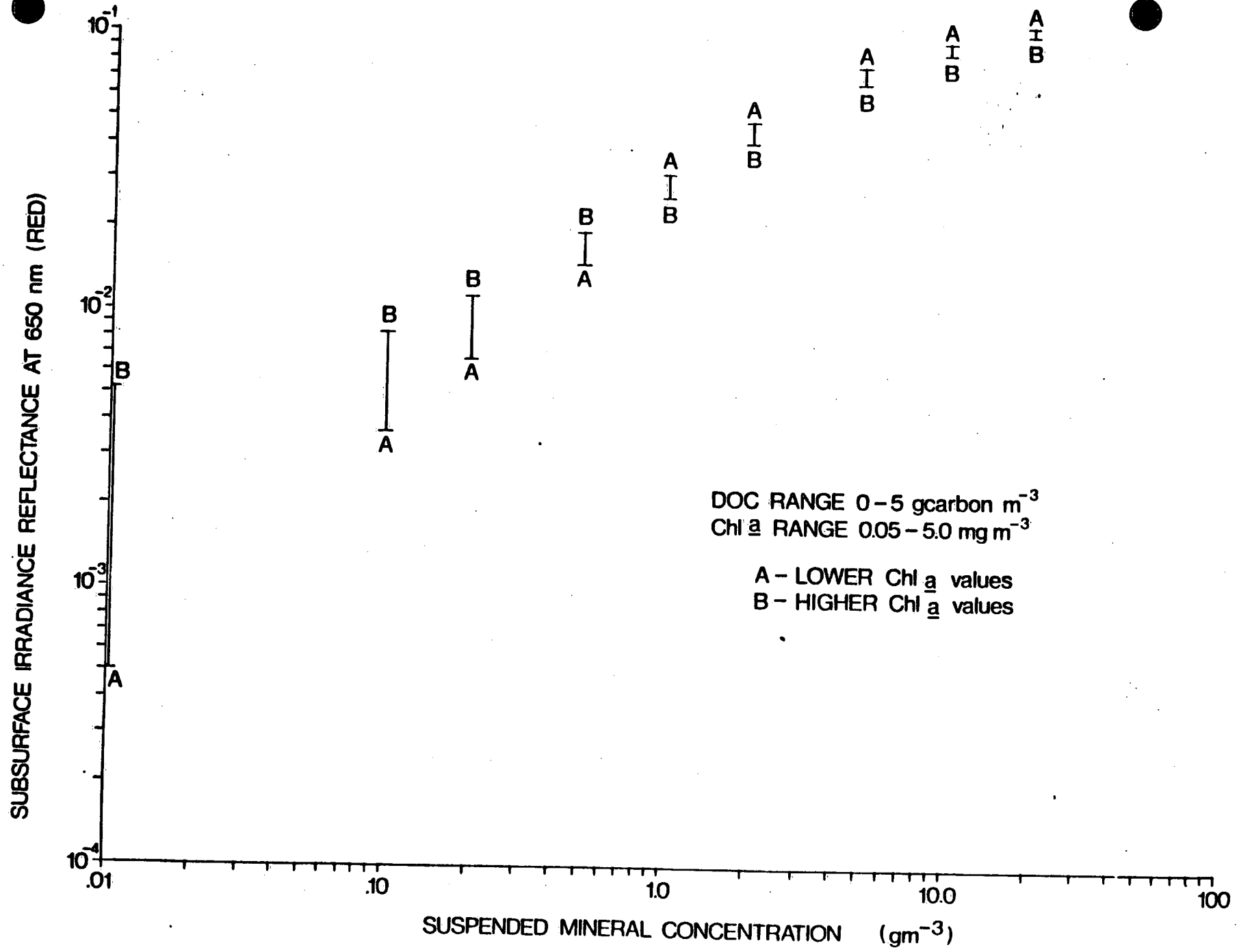
SUBSURFACE IRRADIANCE REFLECTANCE AT 650 nm (RED)
10^{-1}
10^{-2}
10^{-3}
10^{-4}
.01
.10
1.0
10.0
100
SUSPENDED MINERAL CONCENTRATION (gm^{-3})
DOC RANGE 0 – 5 gcarbon m^{-3}
Chl a RANGE 0.05 – 5.0 mg m^{-3}
A – LOWER Chl a values
B – HIGHER Chl a values

FIG. 32

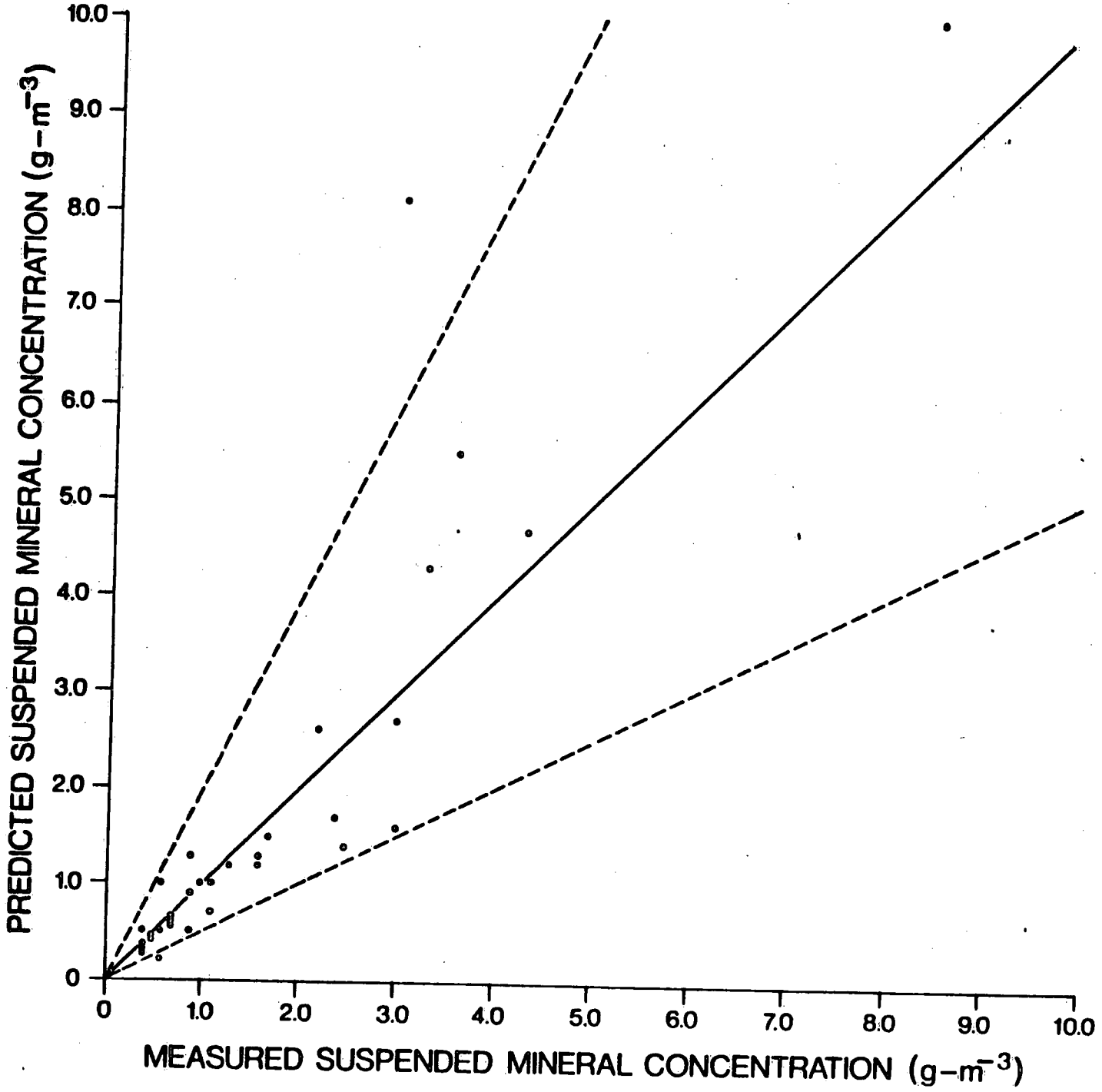
PREDICTED SUSPENDED MINERAL CONCENTRATION (g-m^{-3})
MEASURED SUSPENDED MINERAL CONCENTRATION (g-m^{-3})
0
1.0
2.0
3.0
4.0
5.0
6.0
7.0
8.0
9.0
10.0

FIG. 33

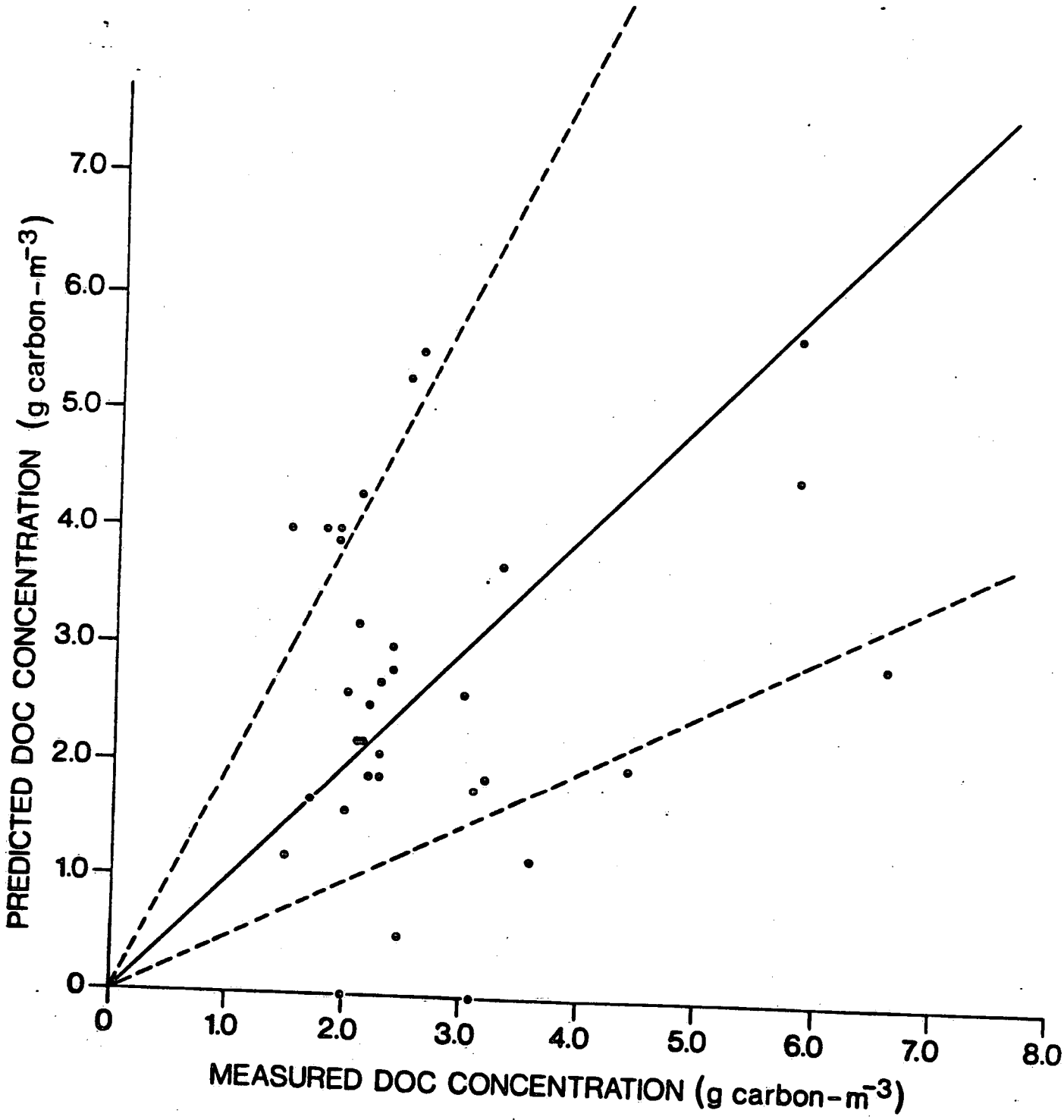
PREDICTED DOC CONCENTRATION (g carbon-m^{-3})
7.0
6.0
5.0
4.0
3.0
2.0
1.0
0
0
1.0
2.0
3.0
4.0
5.0
6.0
7.0
8.0
MEASURED DOC CONCENTRATION (g carbon-m^{-3})

FIG. 34

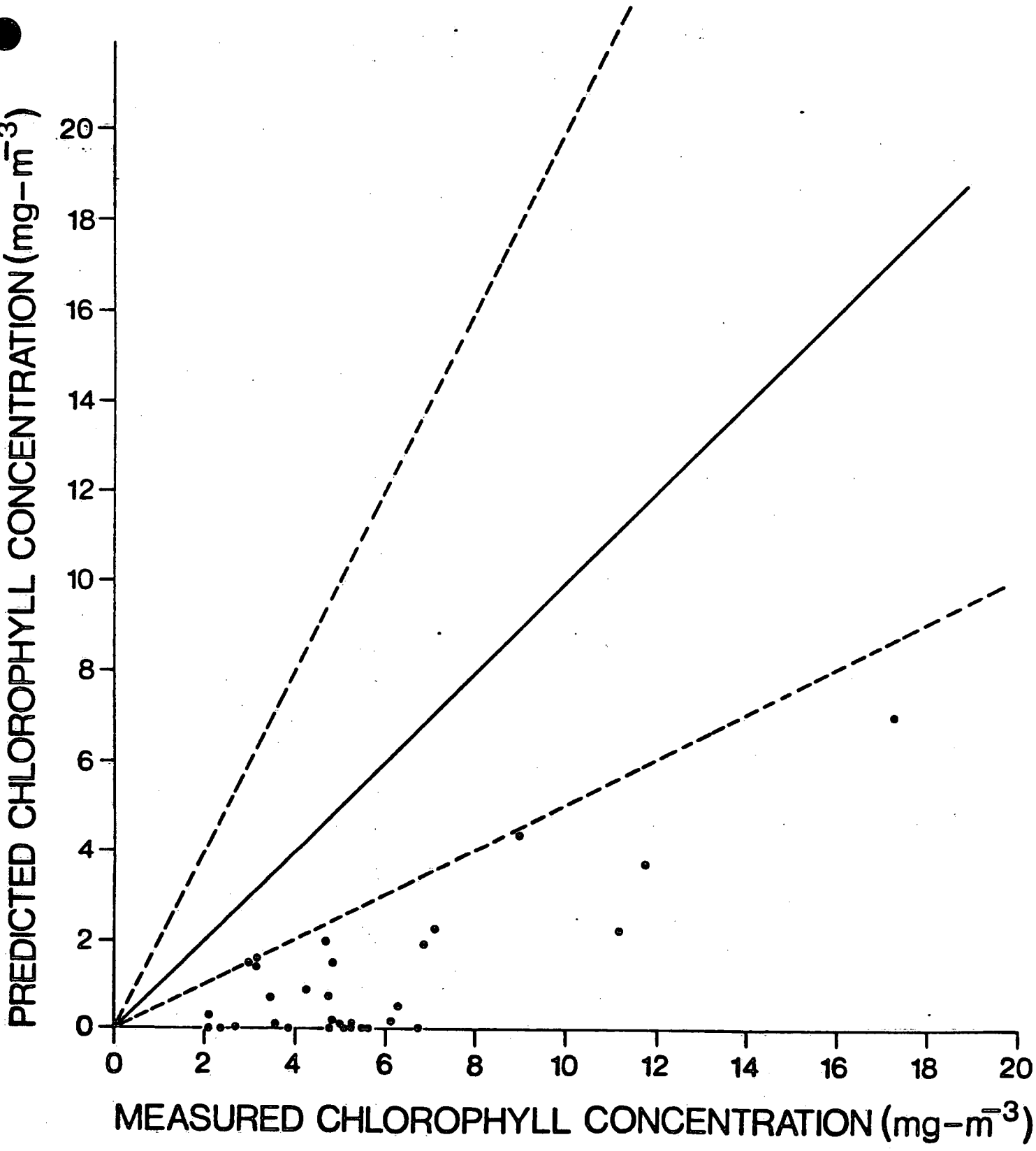
PREDICTED CHLOROPHYLL CONCENTRATION (mg-m^{-3})
MEASURED CHLOROPHYLL CONCENTRATION (mg-m^{-3})
0
2
4
6
8
10
12
14
16
18
20

FIG. 35

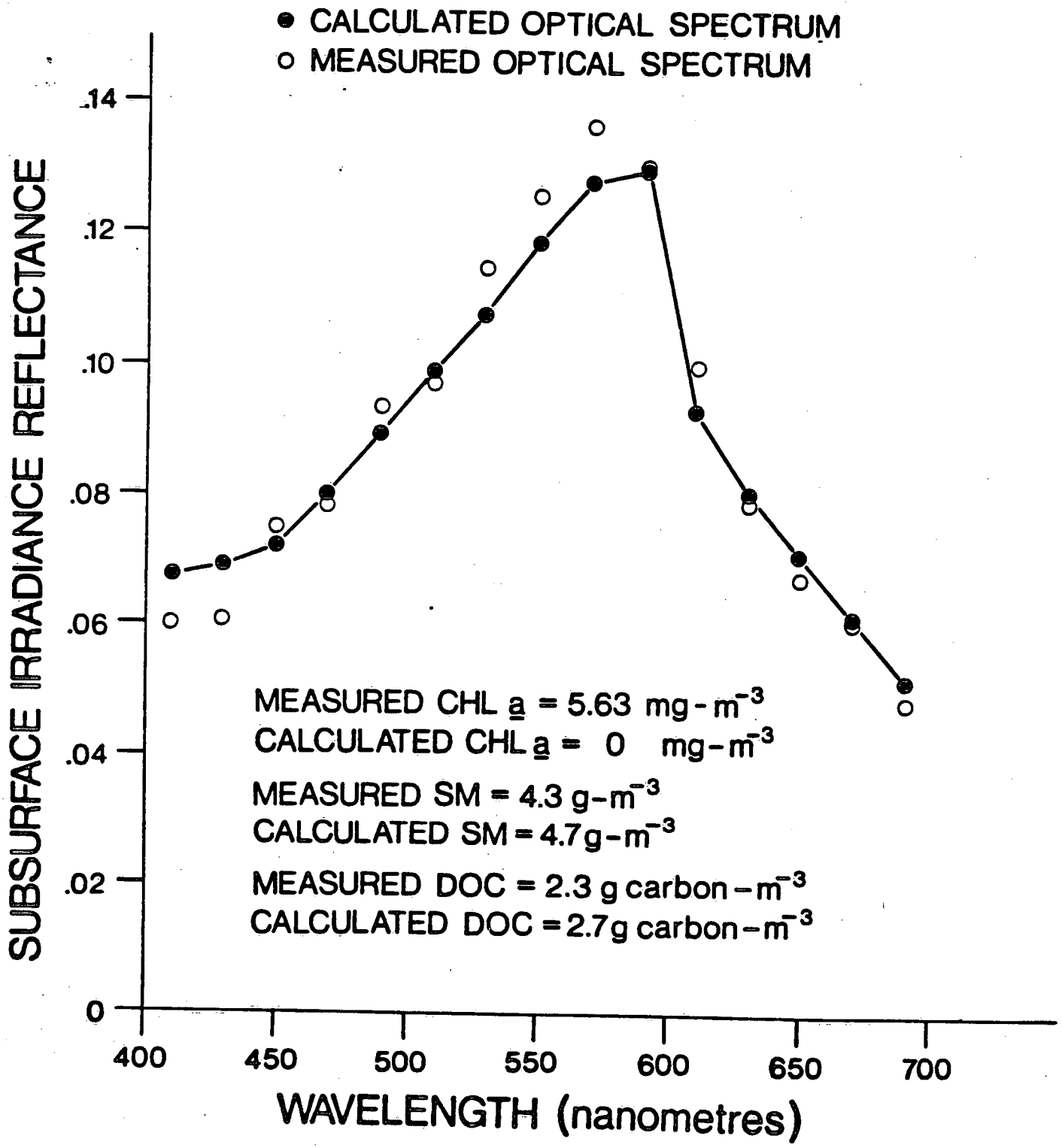
CALCULATED OPTICAL SPECTRUM
MEASURED OPTICAL SPECTRUM
SUBSURFACE IRRADIANCE REFLECTANCE
.14
.12
.10
.08
.06
.04
.02
0
400
450
500
550
600
650
700
WAVELENGTH (nanometres)
MEASURED CHL a = 5.63 mg-m^{-3}
CALCULATED CHL a = 0 mg-m^{-3}
MEASURED SM = 4.3 g-m^{-3}
CALCULATED SM = 4.7g-m^{-3}
MEASURED DOC = 2.3 g carbon-m^{-3}
CALCULATED DOC = 2.7g carbon-m^{-3}

FIG. 36

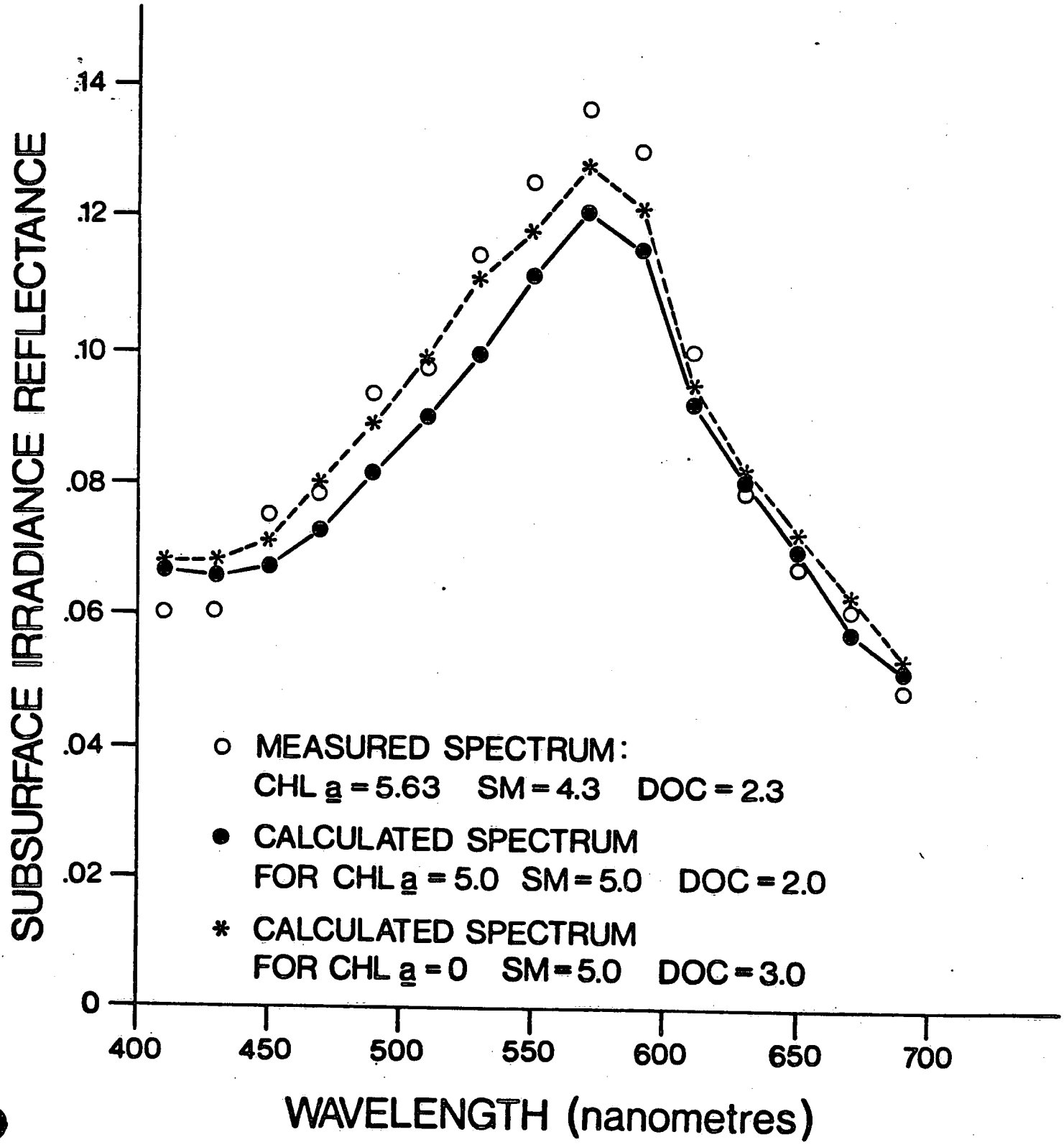
SUBSURFACE IRRADIANCE REFLECTANCE
.14
.12
.10
.08
.06
.04
.02
0
400
450
500
550
600
650
700
WAVELENGTH (nanometres)
o MEASURED SPECTRUM:
CHL a = 5.63 SM = 4.3 DOC = 2.3
● CALCULATED SPECTRUM
FOR CHL a = 5.0 SM = 5.0 DOC = 2.0
* CALCULATED SPECTRUM
FOR CHL a = 0 SM = 5.0 DOC = 3.0

FIG. 37

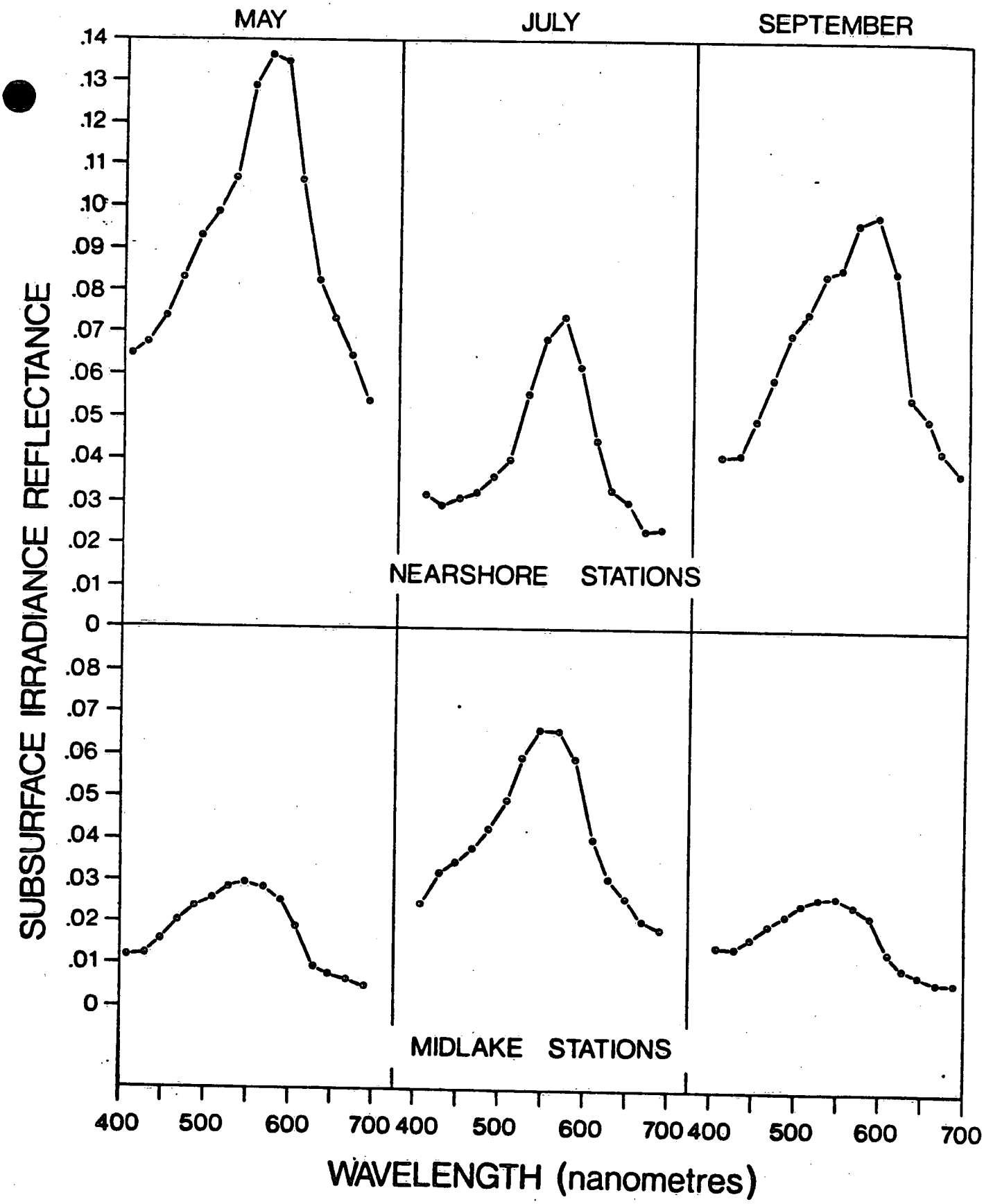
MAY
JULY
SEPTEMBER
.14
.13
.12
.11
.10
.09
.08
.07
.06
.05
.04
.03
.02
.01
0
NEARSHORE STATIONS
.08
.07
.06
.05
.04
.03
.02
.01
0
MIDLAKE STATIONS
SUBSURFACE IRRADIANCE REFLECTANCE
400
500
600
700
WAVELENGTH (nanometres)

FIG. 38

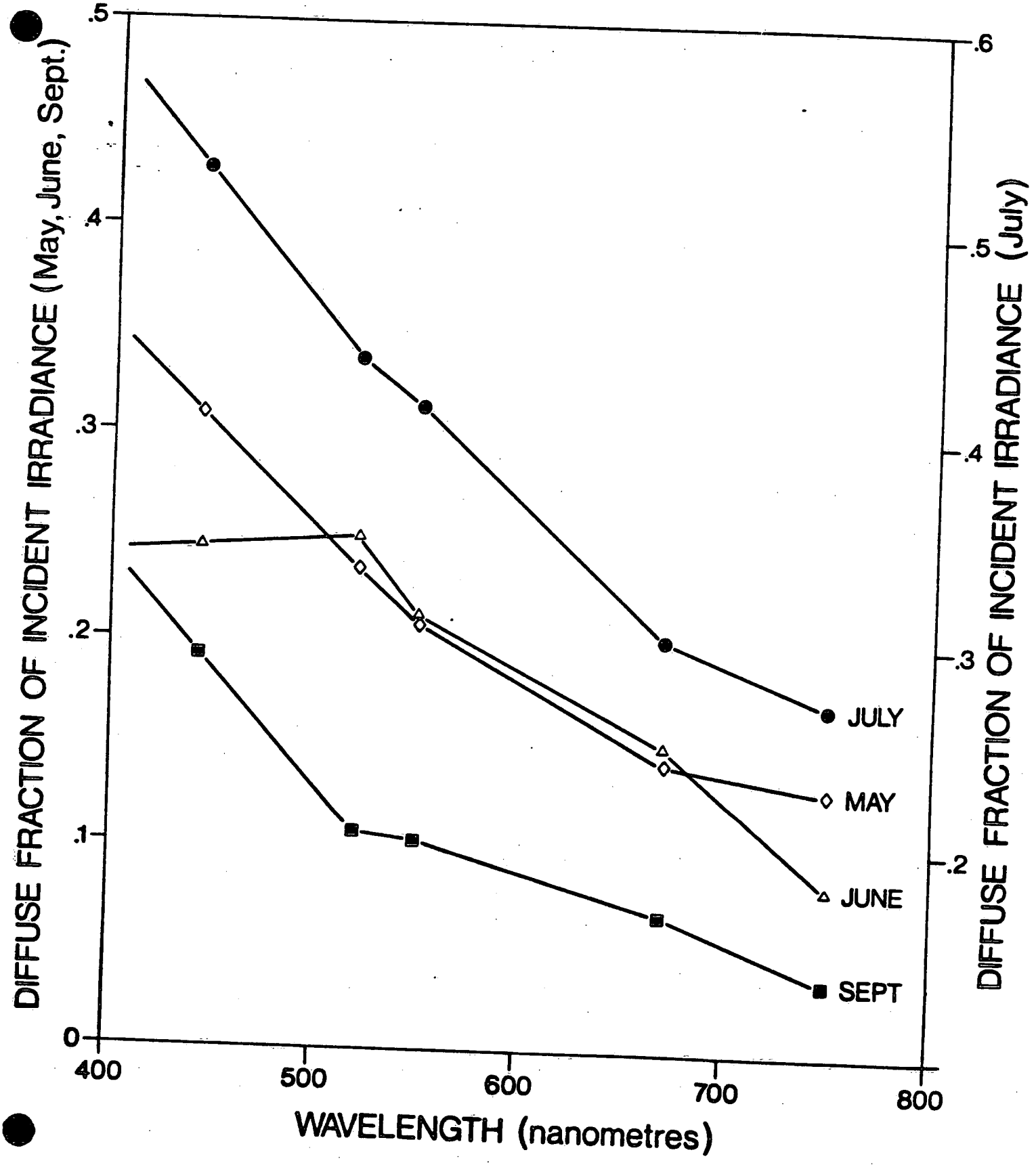
DIFFUSE FRACTION OF INCIDENT IRRADIANCE (May, June, Sept.)
DIFFUSE FRACTION OF INCIDENT IRRADIANCE (July)
WAVELENGTH (nanometres)
.5
.4
.3
.2
.1
0
.6
.5
.4
.3
.2
400
500
600
700
800
JULY
MAY
JUNE
SEPT

FIG. 39

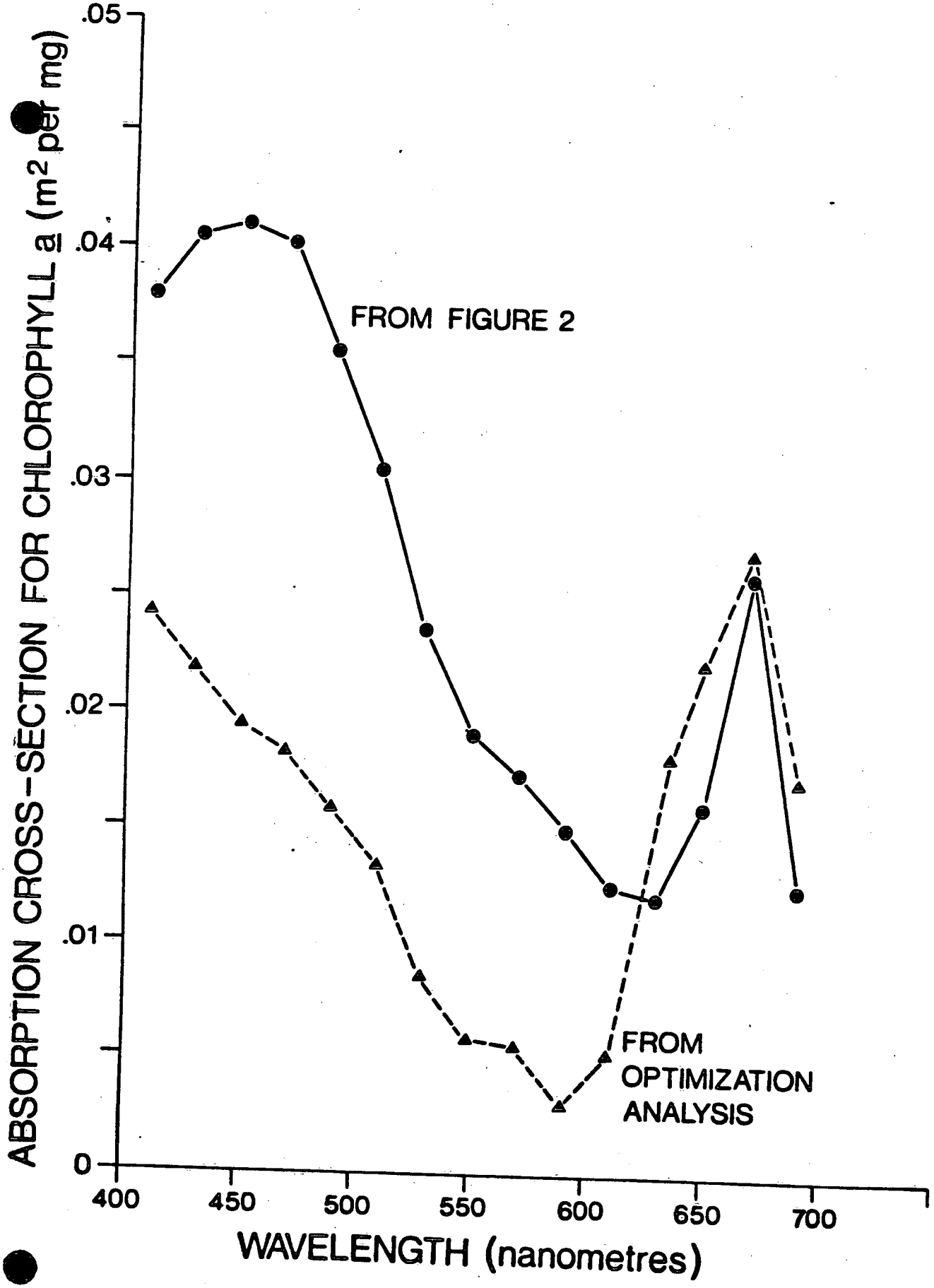
.05
.04
.03
.02
.01
0
ABSORPTION CROSS-SECTION FOR CHLOROPHYLL a (m² per mg)
FROM FIGURE 2
FROM OPTIMIZATION ANALYSIS
400
450
500
550
600
650
700
WAVELENGTH (nanometres)

FIG. 40

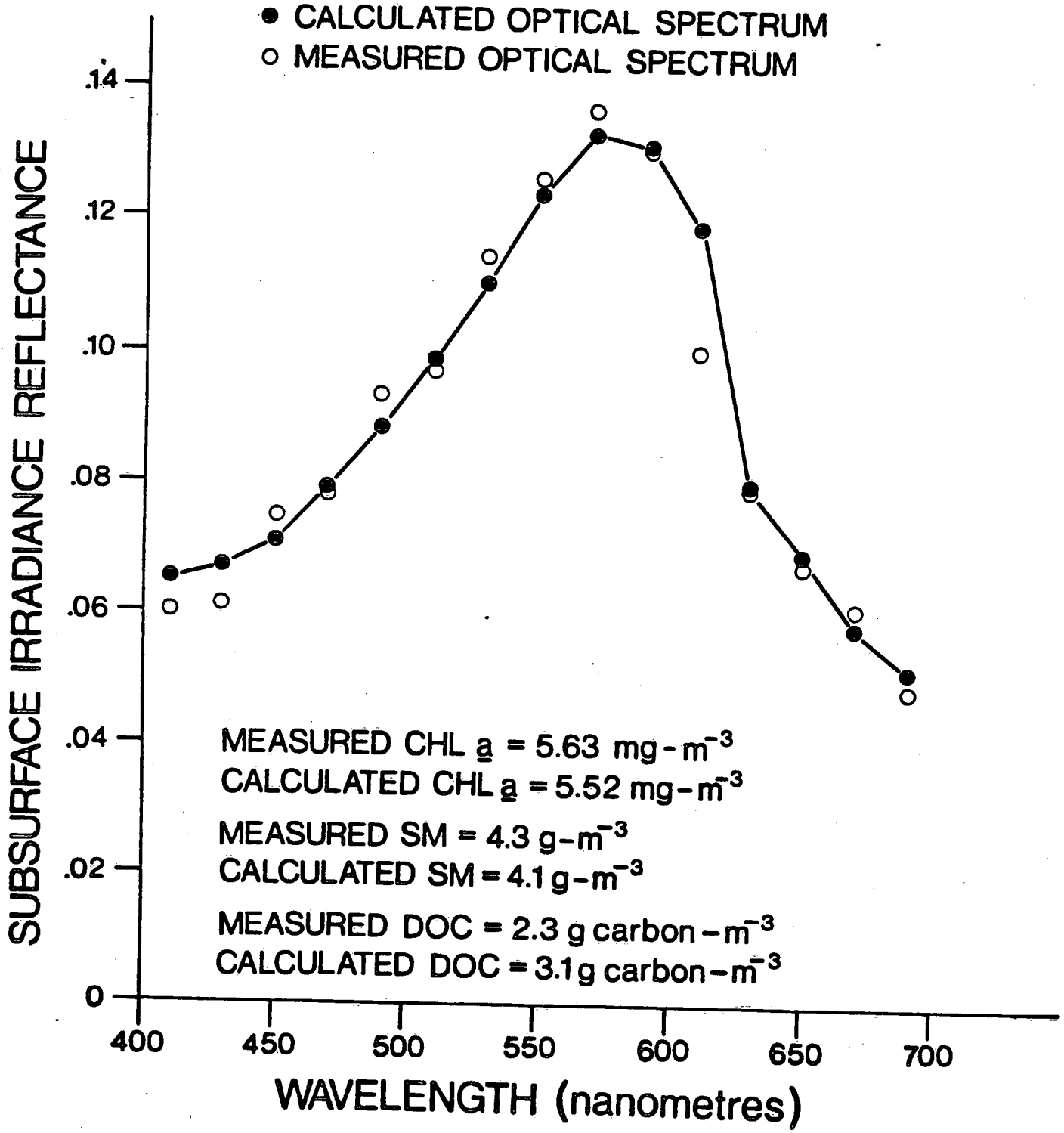
CALCULATED OPTICAL SPECTRUM
MEASURED OPTICAL SPECTRUM
SUBSURFACE IRRADIANCE REFLECTANCE
.14
.12
.10
.08
.06
.04
.02
0
400
450
500
550
600
650
700
WAVELENGTH (nanometres)
MEASURED CHL a = 5.63 mg-m⁻³
CALCULATED CHL a = 5.52 mg-m⁻³
MEASURED SM = 4.3 g-m⁻³
CALCULATED SM = 4.1 g-m⁻³
MEASURED DOC = 2.3 g carbon-m⁻³
CALCULATED DOC = 3.1 g carbon-m⁻³

FIG. 41

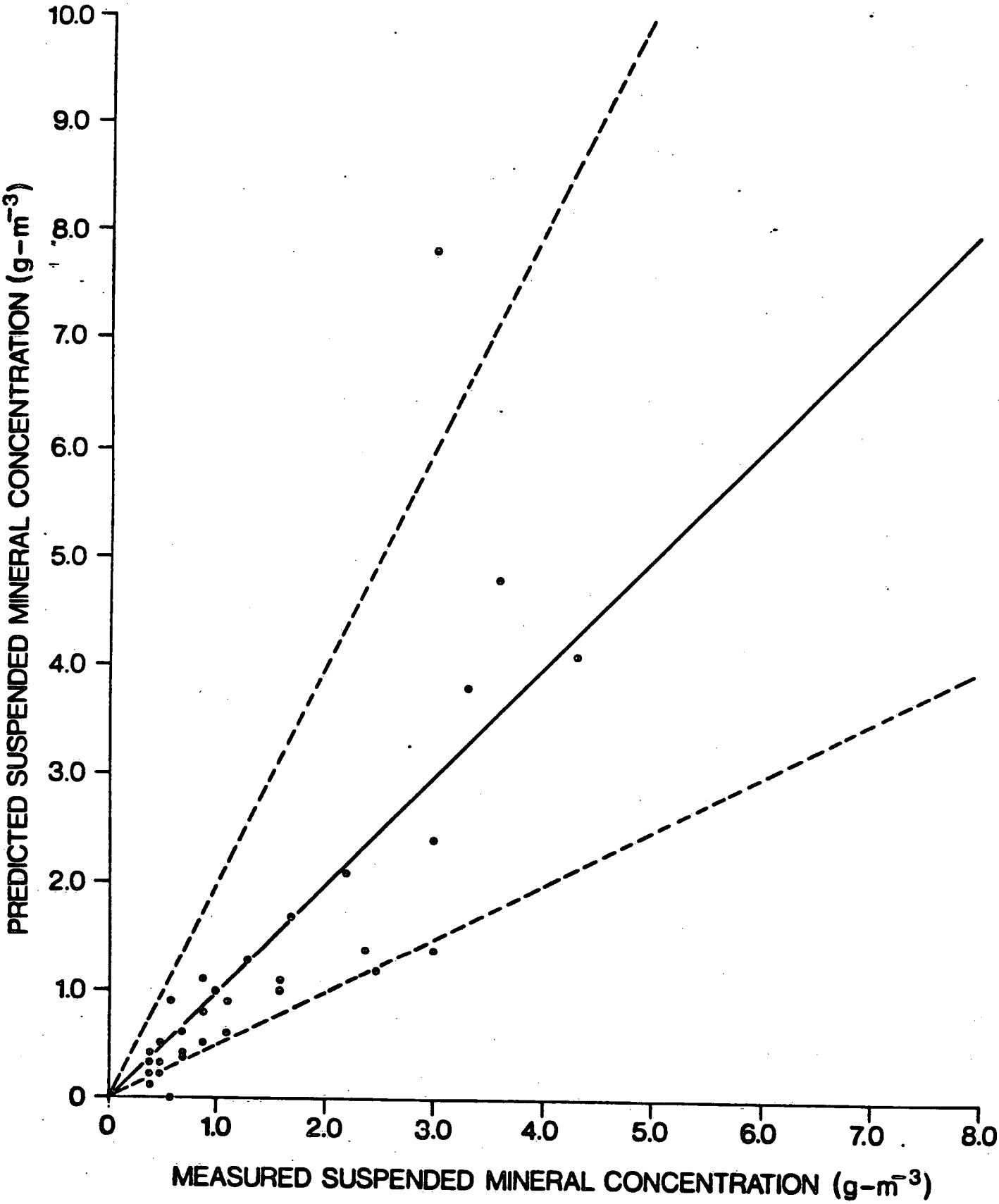
PREDICTED SUSPENDED MINERAL CONCENTRATION (g-m^{-3})
10.0
9.0
8.0
7.0
6.0
5.0
4.0
3.0
2.0
1.0
0
0
1.0
2.0
3.0
4.0
5.0
6.0
7.0
8.0
MEASURED SUSPENDED MINERAL CONCENTRATION (g-m^{-3})

FIG. 42

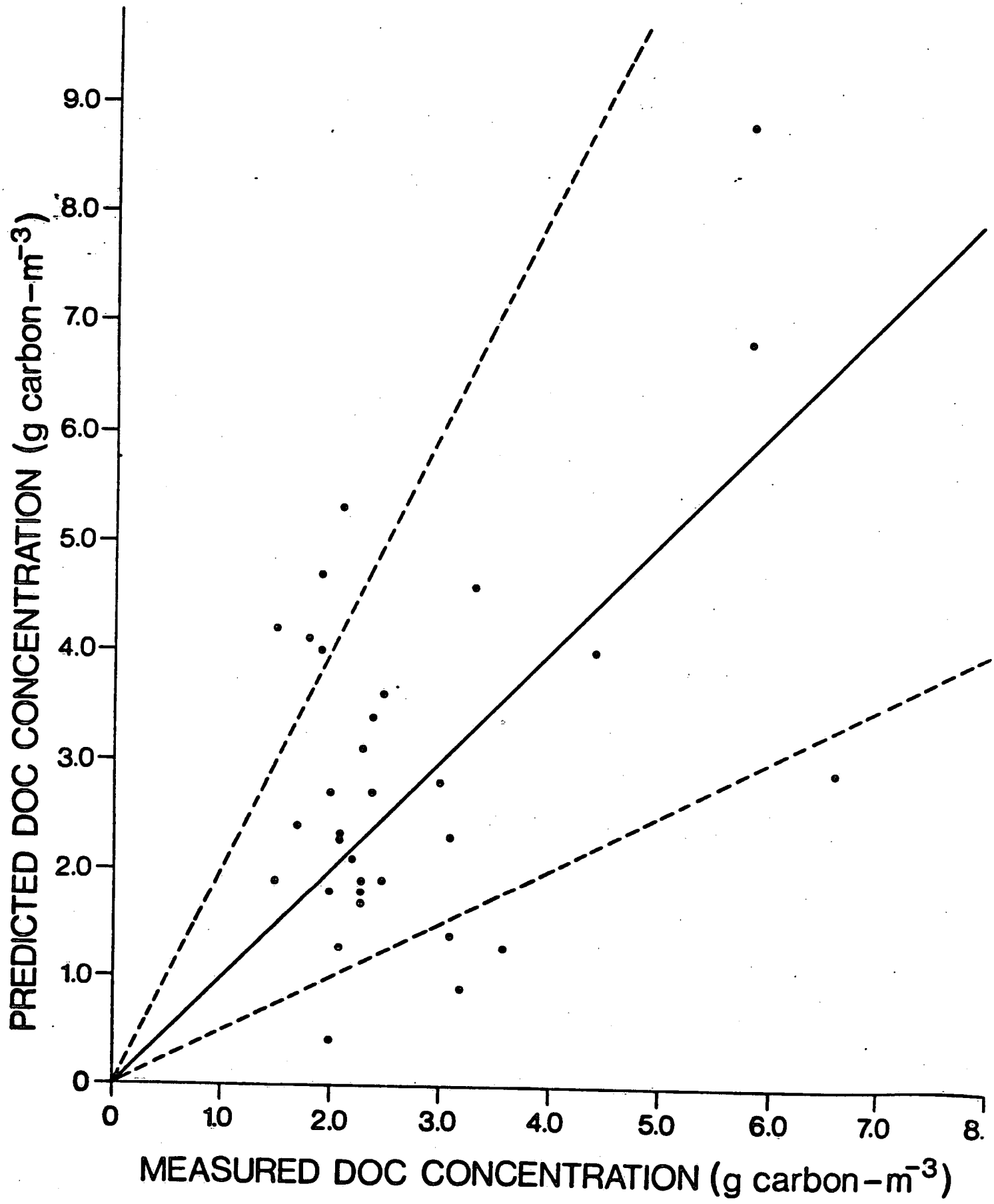
PREDICTED DOC CONCENTRATION (g carbon-m^{-3})
9.0
8.0
7.0
6.0
5.0
4.0
3.0
2.0
1.0
0
0
1.0
2.0
3.0
4.0
5.0
6.0
7.0
8.
MEASURED DOC CONCENTRATION (g carbon-m^{-3})

FIG. 43

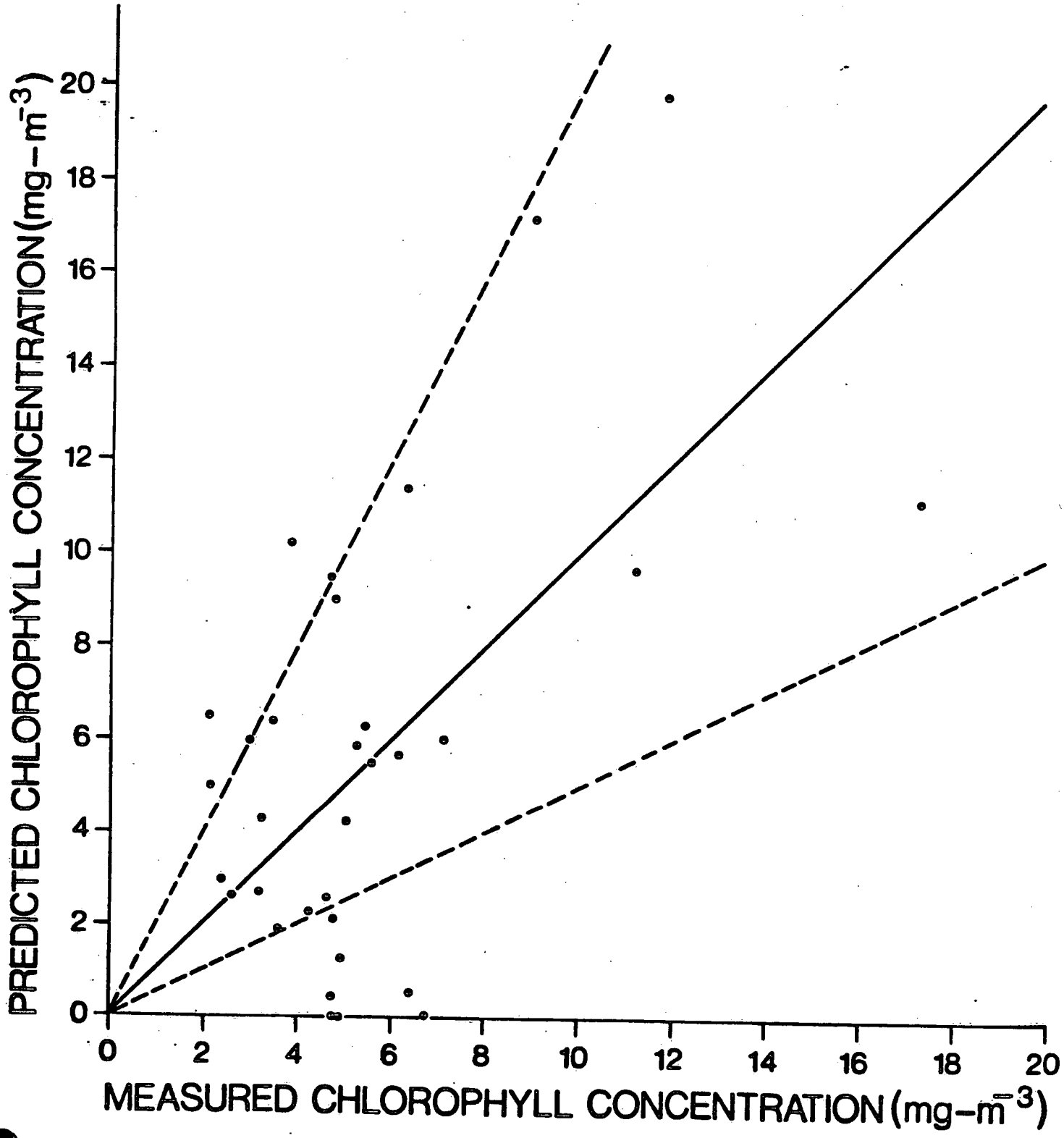
PREDICTED CHLOROPHYLL CONCENTRATION (mg-m^{-3})
MEASURED CHLOROPHYLL CONCENTRATION (mg-m^{-3})
0
2
4
6
8
10
12
14
16
18
20

FIG. 44

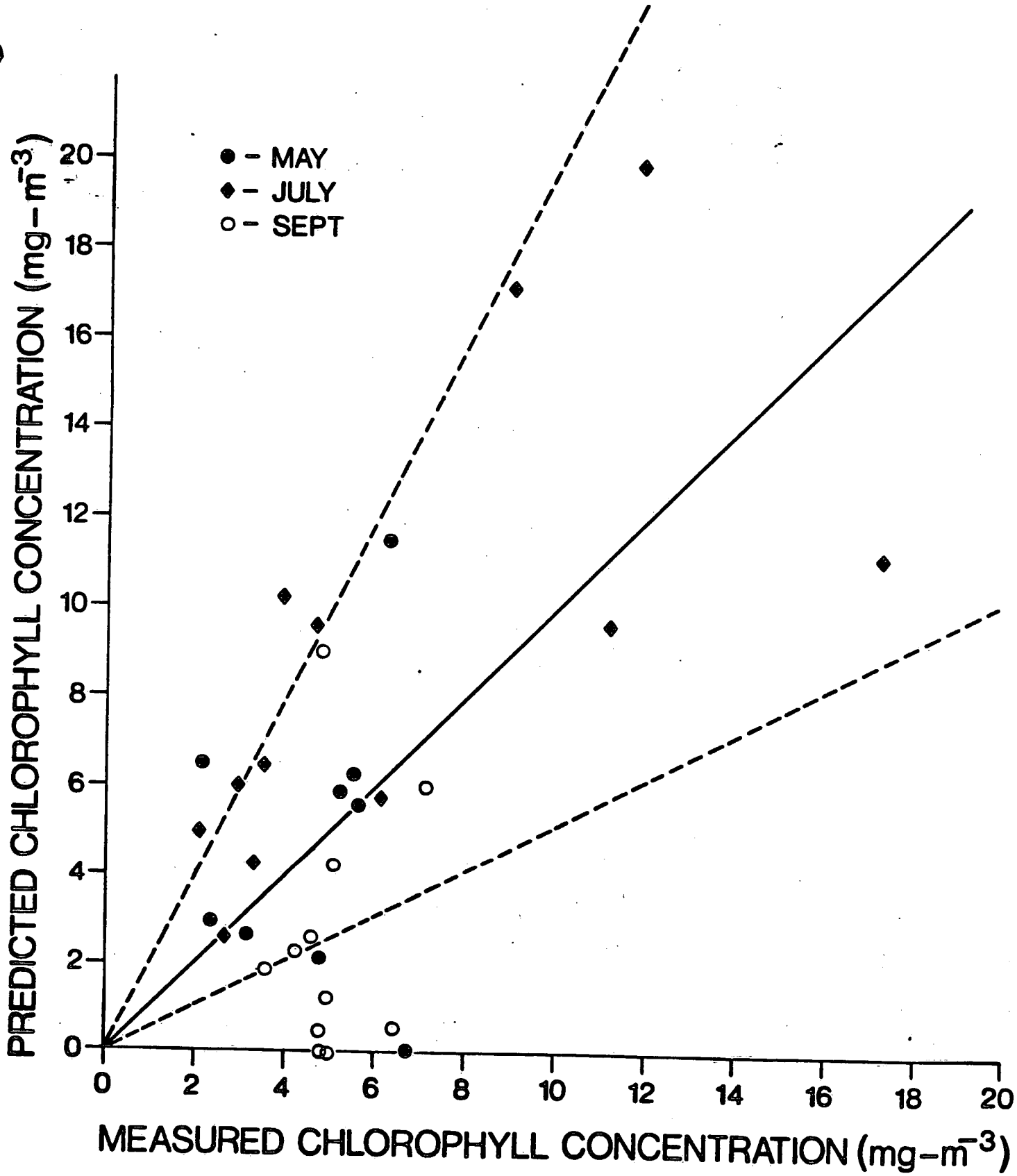
● – MAY
◆ – JULY
○ – SEPT
PREDICTED CHLOROPHYLL CONCENTRATION (mg-m^{-3})
MEASURED CHLOROPHYLL CONCENTRATION (mg-m^{-3})
0
2
4
6
8
10
12
14
16
18
20

FIG. 45

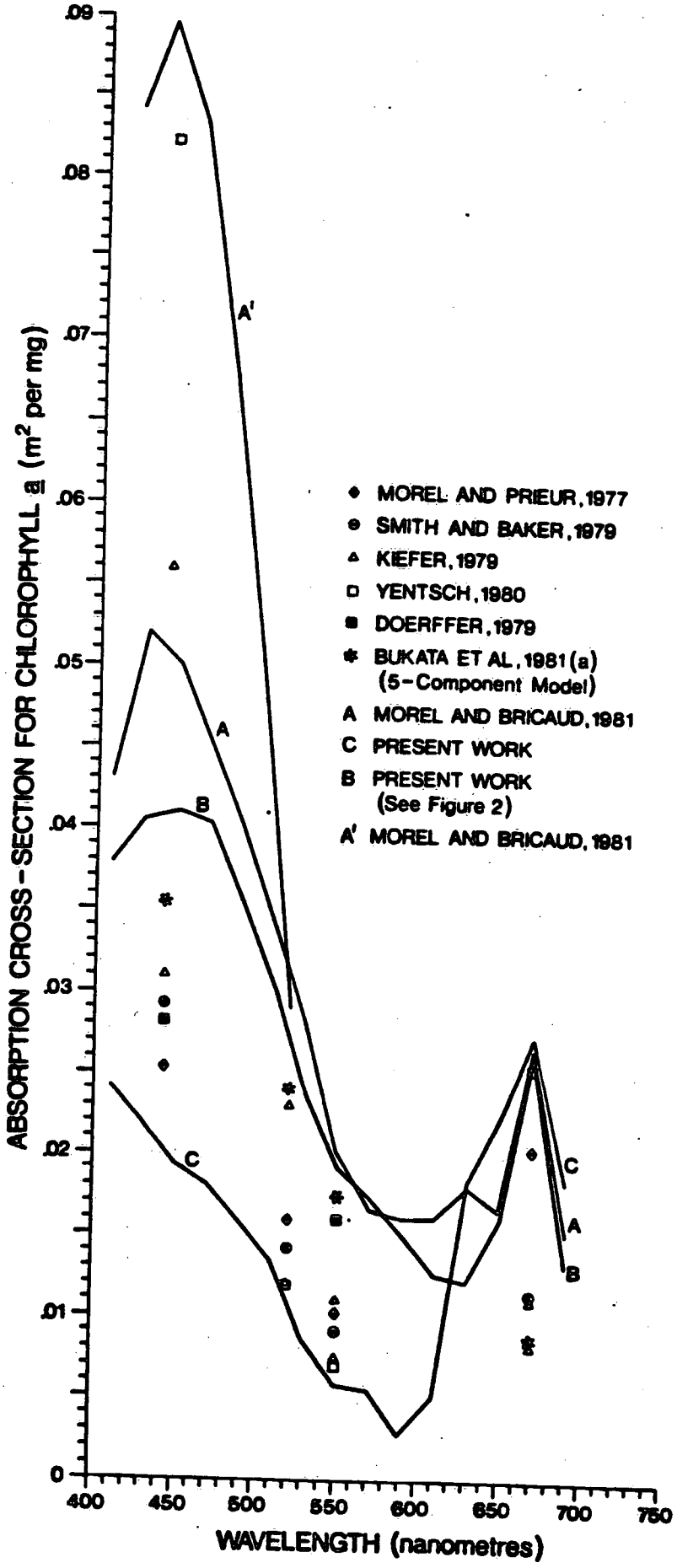
ABSORPTION CROSS-SECTION FOR CHLOROPHYLL a (m² per mg)
.09
.08
.07
.06
.05
.04
.03
.02
.01
0
400
450
500
550
600
650
700
750
WAVELENGTH (nanometres)
A'
A
B
C
MOREL AND PRIEUR, 1977
SMITH AND BAKER, 1979
KIEFER, 1979
YENTSCH, 1980
DOERFFER, 1979
BUKATA ET AL., 1981 (a) (5-Component Model)
A MOREL AND BRICAUD, 1981
C PRESENT WORK
B PRESENT WORK (See Figure 2)
A' MOREL AND BRICAUD, 1981

FIG. 46

9747